Czech Technical University in Prague

Faculty of Nuclear Sciences and Physical Engineering

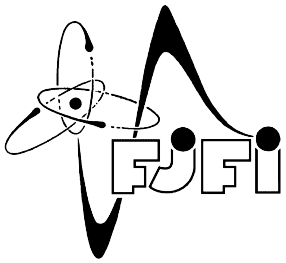

Doctoral Thesis

Electromagnetic Production of Kaons

Author:

Ing. Dalibor Skoupil

Supervisor:

RNDr. Petr Bydžovský, CSc.

Prague

2016

Bibliografický záznam

Autor:	Ing. Dalibor Skoupil, České vysoké učení technické v Praze, Fakulta jaderná a fyzikálně inženýrská, Katedra fyziky
Název práce:	Elektromagnetická produkce kaonů
Studijní program:	Aplikace přírodních věd
Studijní obor:	Jaderné inženýrství
Školitel:	RNDr. Petr Bydžovský, CSc., Ústav jaderné fyziky, Akademie věd České republiky
Akademický rok:	2015/16
Počet stran:	140
Klíčová slova:	kaon, hyperon, fotoprodukce, elektroprodukce, nukleonové rezonance, izobarický model, model Regge-plus-resonance

Bibliographic Entry

Author:	Ing. Dalibor Skoupil, Czech Technical University in Prague, Faculty of Nuclear Sciences and Physical Engineering, Department of Physics

Title of Dissertation:	Electromagnetic Production of Kaons
Degree Programme:	Application of Natural Sciences
Field of Study:	Nuclear Engineering
Supervisor:	RNDr. Petr Bydžovský, CSc., Nuclear Physics Institute, Czech Academy of Sciences
Academic Year:	2015/16
Number of Pages:	140
Keywords:	kaon, hyperon, photoproduction, electroproduction, nucleon resonances, isobar model, Regge-plus-resonance model

Abstrakt

Cílem této práce je poskytnout přehled o reakci fotoprodukce podivnosti a zpravit čtenáře o posledním vývoji v této problematice. Fotoprodukce kaonů na protonech je studována jak v rezonanční oblasti, kde je používán izobarický model a hybridní model Regge-plus-resonance, tak i nad touto oblastí s využitím modelu Regge-plus-resonance. Nukleonové rezonance se spinem 3/2 a 5/2 a hyperonové rezonance se spinem 3/2, které hrají důležitou úlohu při popisu dat, mohly být nově zahrnuty v našich modelech díky zavedení konzistentního popisu formulovaného V. Pascalutsou. Odhalili jsme, že hyperonové rezonance se spinem 1/2 a 3/2 spolu s Bornovskými členy značně přispívají k části amplitudy tvořící pozadí. Volné parametry v našich modelech byly určeny fitem na experimentální data pocházející zejména z kolaborací CLAS, LEPS a GRAAL, přičemž jsme vybrali dvě verze izobarického modelu, BS1 a BS2, a jednu verzi modelu Regge-plus-resonance. Všechny modely popisují rozumně experimentální data v kinematických oblastech, kde byly fitovány volné parametry modelů. Navzdory tomu, že fotoprodukce kaonů se odehrává v tzv. třetí rezonanční oblasti, kde existuje mnoho rezonančních stavů, celkový počet rezonancí zahnrutých v jednotlivých modelech (15 či 16 v izobarických modelech BS1 a BS2 a 10 ve fitu s modelem Regge-plus-resonance) je srovnatelný s množstvím rezonancí zahnrutých v jiných modelech. Sada vybraných nukleonových rezonancí se navíc částečně překrývá se sadou nukleonových rezonancí, které byly identifikovány v Bayesianské analýze za pomoci modelu Regge-plus-resonance.

Kandidát je spoluautorem vypočetního kódu k modelu Regge-plus-resonance, se kterým provedl řadu fitovacích procedur ke stanovení jeho volných parametrů a vybral dvě varianty vhodné k diskusi a dalším výpočtům. Následně se stal spoluautorem nových amplitud pro izobarický model a model Regge-plus-resonance, do kterých byla nově zahrnuta výměna baryonových rezonancí s vyšším spinem v konzistentním formalismu, a při fitování volných parametrů pomohl vybráním vhodných rezonancí sestavit nové izobarické modely BS1 a BS2 a nový fit s modelem Regge-plus-resonance a diskutoval vlastnosti těchto modelů.

Abstract

The aim of this work is to provide a deep overview of the strangeness photoproduction reaction and report on recent progress in this field. The kaon photoproduction on the proton is studied either in the resonance region, using an isobar model, or in the resonance region and beyond, exploiting a hybrid Regge-plus-resonace framework. The higher-spin nucleon, spin-3/2 and spin-5/2, and hyperon, spin-3/2, resonances have been included in the model utilizing the consistent formalism by Pascalutsa and they were found to play an important role in data description. The spin-1/2 and spin-3/2 hyperon resonances in combination with the Born terms were revealed to contribute significantly to the background part of the amplitude. The free parameters of the models were fitted to new experimental data from CLAS, LEPS, and GRAAL collaborations, and two versions of the isobar model, BS1 and BS2, and one version of the Regge-plus-resonance model were chosen. All models provide a reasonable overall description of the data in the kinematic regions where the free parameters were adjusted. Even though the kaon photoproduction takes place in the third-resonance region with many resonant states, the total number of included resonances, 15, 16, and 10 in the BS1, BS2, and RPR models, respectively, is quite moderate and it is comparable with amounts of resonances in other models. The sets of chosen nucleon resonances, moreover, overlaps well with the set of the most probable contributing states determined in the Bayesian analysis with the Regge-plus-resonance model.

The candidate is a coauthor of a computational code for the Regge-plus-resonance model, which was exploited to determine the free parameters of the model, two variants of which were then discussed and may be used for further calculations. Subsequently, the candidate helped derive the new amplitude for isobar and Regge-plus-resonance models, including the exchange of high-spin baryon resonances in the consistent formalism. In the following fitting procedures of both models, the candidate chose the resonances appropriate for a reasonable data description, which led to the creation of new isobar models BS1 and BS2 and the new RPR fit, and discussed the properties of these new fits.

Prohlášení

Prohlašuji, že jsem svou dizertační práci vypracoval samostatně a použil jsem pouze podklady uvedené v přiloženém seznamu literatury.

Nemám závažný důvod proti užití tohoto školního díla ve smyslu §60 Zákona č.121/2000 Sb., o právu autorském, o právech souvisejících s právem autorským a o změně některých zákonů (autorský zákon).

V Řeži dne _____ _____

Ing. Dalibor Skoupil

Acknowledgement

I would like to thank my supervisor RNDr. Petr Bydžovský, CSc. for his willingness, his continuous support during my doctoral study and during the work on this thesis and for many useful hints which helped me understand the topic of strangeness production. Moreover, I strongly appreciate his time spent on reading this work and I am grateful for many factual corrections proposed by him.

What is more, I would like to thank all the people in my surroundings for their support and assistance; particularly those who gave me occasional but very beneficial pieces of advice in many different topics more or less connected to physics, which make me open my eyes and perceive the world in its entirety.

List of Abbreviations

ABBHHM	Aachen-Berlin-Bonn-Hamburg-Heidelberg-München
CEBAF	Continuous Electrom Beam Accelerator Facility
CGLN	Chew, Goldberger, Low and Nambu
CLAS	CEBAF Large Acceptance Spectrometer
CQM	Constituent Quark Model
DESY	Deutsches Elektronen-Synchrotron
ELSA	Elektronen-Stretcher Anlage
EM	Electromagnetic
FWHM	Full Width in Half Maximum
GRAAL	GRenoble Anneau Accelerateur Laser
KM	Kaon-MAID
LEPS	Laser Electron Photon Experiment at SPring-8
MAMI	Mainzer Miktrotron
PDG	Particle Data Group
QCD	Quantum Chromodynamics
QED	Quantum Electrodynamics
R-S	Rarita-Schwinger
RPR	Regge-plus-resonance
SAPHIR	Spectrometer Arrangement for Photon Induced Reactions
SL	Saclay-Lyon
SLAC	Stanford Linear Accelerator Center

Contents

Preface

In this work, we deal with the production of kaons on nucleons in the energy range of several GeV. This process is suitable for gathering important information about baryons and their resonance spectrum and interactions in hyperon-nucleon systems arising from QCD. The models based on the tree-level approximation of perturbation theory of the effective hadron Lagrangian are a suitable tool for investigation of this process. The free parameters in the Lagrangian are determined by fitting observable quantities, such as cross section, polarization, *etc.*, on the experimental data.

As it is strongly believed that the electromagnetic particle production will bring much deeper insight into the structure of hadrons, it is an important and very promising field of study. Although there are many ways of studying the particle production, the most challenging processes are kaon photo- and electroproduction, since the electromagnetic part of the process is well understood.

Models for kaon photo- and electroproduction are either based on quark degrees of freedom or one takes hadrons as basic building blocks. We deal with the latter class of models and we have constructed a new isobar model for $K^+\Lambda$ photoproduction off the proton. Moreover, we have created our version of Regge-plus-resonance model where the background part of the amplitude is given in a much less complicated way in comparison with isobar models. Therefore, the plurality of models we deal with gives us a unique opportunity to study and understand the reaction dynamics.

The work is organized as follows. In the first chapter, properties of nuclei with non zero strangeness are briefly revealed and the strangeness production process is presented along with a short overview of history of its investigation either experimentally or theoretically. In the second chapter, the formalism which we use is outlined with kinematics and observables. The two subsequent chapters deal with properties of isobar and Regge-plus-resonance models which we use in our work and a discussion of many important features of both models can be found therein. In the fifth chapter, the procedure of fitting the free parameters is described in detail and in chapter six we discuss results of our work and compare the outcomes with experimental data. The seventh chapter summarizes our achievements and shows perspectives for the future work on this modern and very interesting field of physics. This work is replenished with four appendices providing detailed information on contributions to the invariant amplitude, Regge trajectories and propagators, and gauge invariance and showing experimental data which are at hand.

Since we want to increase the readibility of this work, we do not include many technicalities to the body of this work. However, an interested reader may find a vast majority of formulae in the appendices.

Chapter 1

Introduction

In the past century, the community of physicists made not a step but a great leap towards the theory of everything. They were successful in describing three out of four forces of nature: gravity, electromagnetism, and weak force. The recent detection of gravitational waves confirmed predictions of the general theory of relativity and brought a brand new perception of the universe. Quantum Electrodynamics (QED), a tool used to describe the electromagnetic interaction, became the most accurate physics theory in its predictions. Moreover, it was showed that the electromagnetic and weak interaction can be viewed as only one force and it was dubbed electroweak force.

Quantum Chromodynamics (QCD), the theory behind the strong interaction which is responsible for keeping nuclei together, is as effective as QED when it is used to depict the behaviour of quarks (the building blocks of which the nucleons are made of) and gluons (the mediators of the strong force) at very high energies. A reason for this is a phenomenon called asymptotic freedom: the coupling constant α_s of QCD decreases as the interaction energy increases. Unfortunately, in the low-energy region due to the large value of α_s, it is not possible to use perturbation theory in QCD and the problems simply become extremely difficult to solve.

Basically, there are two ways to get out of this problem: one can either use lattice QCD or insert appropriate effective degrees of freedom. The former approach allows to compute numerically the analytically incalculable problems of QCD in discretised space-time. Alternatively, the latter approach makes use of the fact that hadrons present themselves as objects with different properties depending on whether they are observed at low- or hard-energy scale. This contrast has led to the creation of hadrodynamics where the low-energy phenomena of the strong interaction are described with the help of mesons and baryons. Since both mesons and baryons are objects with internal structure in QCD, unlike the quarks and gluons, their inner structure is parametrized by means of a form factor. In this work, we employ the effective degrees of freedom.

During last decades, production of pseudoscalar mesons on nucleons revealed as a suitable tool for studying baryons and their resonant states and it is strongly believed that the analysis of the production processes can bring a deeper insight into this field of study. Production of the Λ and Σ hyperons on nucleons and nuclei induced by the electron beam provides supplemental information about properties of baryons and their behaviour in nuclei. Besides the study of the reaction mechanism, a correct description of the elementary production on nucleons is important for minimizing uncertainties in calculations of the excitation spectra for electroproduction of hypernuclei. What is more, photoproduction of kaons on nucleons offers new possibilities to study electromagnetic and strong interactions, which are not available in pion or η meson photoproducion. This is caused by a new degree of freedom, strangeness, which shifts the internal symmetry of the process considered from SU(2) to SU(3). Due to the problematic behaviour of the QCD in the low-energy region, strangeness photoproduction requires a hadrodynamical approach where the hadrons are described by effective fields.

There is another issue which makes the kaon photoproduction worth of studying. Constituent quark model (CQM) [24] predicts far more excited nucleon states around 2 GeV than what was observed in the pion production experiments or πN scattering. These states have been, therefore, called "missing resonances" and they are supposed to play an important role in the pionless channels where they have higher branching ratio.

All this makes the strangeness production one of the most promising field of study for the experimentalists as well as for the theoreticians.

1.1 Basic Properties of Hypernuclei

The strange quark, that introduces an SU(3)-flavour dimension to the traditional nuclear physics, comprises, in combination with u and d quarks, various strange hadrons. The strange hadrons, hyperons, are not affected by the Pauli principle and can, therefore, penetrate deep inside the nucleus, creating a hypernucleus - a long-lived multibaryonic system (10^{-10} s) with non zero strangeness. Among hypernuclei, the most studied and well-known are Λ hypernuclei where a Λ hyperon replaces a nucleon of the nucleus (similarly two Λ hyperons might engage with a nuclear core, forming the so-called double Λ hypernuclei). Whereas Λ hypernuclei are stable at the nuclear time scale (10^{-23} s to 10^{-20} s), Σ-hypernuclear excitations are relatively narrow with widths at the order of a few MeV and the strong conversion $\Sigma N \rightarrow \Lambda N$ reaction which occurs in nuclei makes these nuclear states very difficult to observe [15, 42].

A survey of hypernucleus production mechanism and structure provides us with indications on the still highly ambiguous interactions of two hyperons (Y-Y) or a hyperon and a nucleon (Y-N), which can shed light on the role of strange quarks in the dynamics of the low- and intermediate-energy baryonic systems, as well as effective field theory approaches encoding the basic ingredients of QCD at low energies. This is of paramount importance in modern physics since neither Y-N nor Y-Y strong interaction can be fully determined from the scattering experiments (only the central part is determined in this way, while no information is gathered for the spin-dependent part). Furthermore, hypernucleus weak decay is the only tool which can shed light on the strangeness-changing weak baryon interactions [15].

Hypernuclear experimental studies have been performed by hadron-induced reactions, (K^-, π^-) or (π^+, K^+), with limited energy resolution. The experimental knowledge can be improved utilizing the electroproduction of strangeness, which is characterized by a large momentum transfer ($q \geq 350\,\mathrm{MeV}/c$) and strong spin-flip terms even at zero kaon production angles. Moreover, virtual photons can excite both natural and unnatural parity, low and high-spin hypernuclear states, including also the states with a deeply bound Λ hyperon. In the hadron-induced reactions, the elementary production of the Λ hyperon happens on the neutron, whereas in the case of electromagnetic production, the production of $K^+\Lambda$ occurs on the proton, which makes it possible to investigate hypernuclei not available in other reactions, *e.g.* ${}^{12}_{\Lambda}\mathrm{B}$. A comparison of the spectra of

mirror hypernuclei can then provide useful information on the charge asymmetry of forces between hyperon and nucleon [43].

The models on strong and weak interactions have a direct connection with astrophysics as they can serve as inputs when one scrutinizes the composition and macroscopic properties (*e.g.* mass and radius) of compact stars (such as supernovae and neutron stars), their stability and thermal evolution [98]. What is more, interactions embracing hyperons are also pertinent in the physics of heavy-ion collisions whose main purpose is the examination of the nuclear equation of state, the possible phase transition from hadronic matter to a quark-gluon plasma and the modification of hadron properties in dense strong interacting matter.

Since the hypernuclei can provide us with very useful information on distinct fields of contemporary physics, it is of paramount importance to study their production. In order to do that, it is essential to have a reliable elementary operator at hand, which can be further used in the electromagnetic production of strangeness on nuclei, *i.e.* study the $\Lambda-N$ interactions and hypernuclei physics. In this work, we deal with an elementary process of strangeness production, namely with production of $K^+\Lambda$ particles. Nonetheless, the extension of models describing elementary production towards production of hypernuclei can be accomplished straightforwardly.

1.2 Strangeness Production Processes

There are several ways of producing the strangeness and the information can therefore be gathered from a wide variety of experiments. The production of particles with non zero strangeness in the final state can be achieved through experiments involving meson-nucleon initial states, with the help of reactions with hadron beams, *e.g.* $n(\pi^+, K^+)\Lambda$ and $n(K^-, \pi^-)\Lambda$, or in the photo- and electroproduction reactions.

The two-body reactions that lead to a great deal of experimental information on production of Λ hyperons are the following:

1. The strangeness exchange reaction

$$K^- + N \to \Lambda + \pi,$$

where the strangeness is transferred from the incident meson to the baryon in the final state. This process is exploited mainly in the $K^- + n \to \Lambda + \pi^-$ charge state

and its cross section is at the order of mb. However, the luminosity of this process is low and, therefore, the production role of this reaction is small.

2. The pion induced process

$$\pi^+ + n \rightarrow K^+ + \Lambda,$$

known as a strangeness creation, proceeds by the generation of a $s\bar{s}$ pair by the incident meson.

3. The electromagnetic production of strangeness, where a strange quark-antiquark pair has to be produced, has much lower cross section in comparison with other processes mentioned: it is at the order of hundreds of nb (the luminosity can be, however, increased significantly using a high intensity electron beam, *e.g.* CEBAF in the Jefferson Lab, USA). On the other hand, the inclusion of a strange quark-antiquark pair in the reaction opens up an additional degree of freedom and it is believed that some of the "missing resonances" have a specific strong coupling into these "strange channels". In the electroproduction process

$$e + p \rightarrow e' + K^+ + \Lambda$$

the virtual photon has, besides the transverse polarization component, also a longitudinal part and, therefore, offers the possibility of varying the energy and momentum transfers independently [32]. The electroproduction process can be formally reduced to an investigation of the binary process of a photoproduction by virtual photons

$$\gamma_V + p \rightarrow K^+ + \Lambda,$$

as the electromagnetic coupling constant is small enough to justify the one-photon approximation.

Although the largest count rates are obtained in the hadronic processes, the use of an electromagnetic probe is still advantageous, as the electromagnetic ingredients in the reaction amplitude can be directly expressed in the context of the Quantum Electrodynamics, the well-established theory of electromagnetic interactions. Therefore, gathering information about the nucleon spectrum is far easier from the electromagnetically induced reactions than from the reactions induced by hadrons.

Theoretical approaches to the electromagnetic production of strangeness can be, in general, divided into two distinct categories. In parton-based models, the quark-gluon structure of the interacting hadrons is explicitly included in the reaction dynamics. As the strange quarks are absent in the initial state, the production process is forced to make a connection to the quark sea. In these models, resonances are implicitly included as excited states and, therefore, the number of free parameters is relatively small. A further merit of this approach is a natural description of the internal structure of hadrons, which has to be modelled phenomenologically utilizing form factors in the isobar models. However, the quark models for the electromagnetic production of kaons are overly complicated for their further use in calculations of hypernucleus electroproduction and, apart from the region of very high energies, where QCD processes can be solved perturbatively, quarks and gluons do not represent the ideal building blocks in hadron reaction models.

On the other hand, hadrodynamical approaches consider the interacting hadrons as the basic degrees of freedom of the effective field theory. In such an approach, the hadrons are treated as effective particles with specific properties. In the lowest order, the reaction mechanism proceeds through the exchange of intermediate states (*i.e.* resonances).

In the sequel of this section, we will summarize the basic properties of various approaches exploited for the study of photo- and electroproduction of strangeness.

Constituent Quark Model

In its long history, the Constituent Quark Model (CQM) has gathered a number of achievements. In the framework of this model, the spectra of mesons and baryons, as well as their strong, electromagnetic, and weak decays have been treated.

This model is in a closer connection with QCD than other models based on the hadronic degrees of freedom. It needs a smaller number of parameters to describe the data; in fact, it contains only a few coupling constants which are related together and there is no need to introduce the resonances, since they emerge naturally from the model as excited states of the system. The quark models, therefore, presume explicitly the extended structure of hadrons, which was found to be important for a reasonable description of the photoproduction data. In the quark model, we usually restrict the description to the non relativistic one.

The survey of nucleon spectroscopy has arrived at a very important topic that points at the subtle interplay between CQM and QCD. By definition, the CQM depicts the nucleon as a bound state of three constituent quarks, and has predicted a substantial number of "missing" light baryons that have not been experimentally proven so far. On the one hand, the constituent quarks might not represent the proper degrees of freedom, and the quark-diquark models, which contain fewer degrees of freedom, may be more convenient for the description of baryons. On the other hand, these missing states in fact do exist but manifest themselves in different reaction channels [24].

In addition, the concept of chiral symmetry can be exploited to include pseudoscalar mesons as the Goldstone bosons in the phenomenological quark model [122, 123], creating a chiral quark model. This model makes use of the low-energy QCD Lagrangian and the resonances in the s and u channels are treated in the framework of the quark model; the t-channel contributions are limited by the duality hypothesis, which reduces the number of free parameters even further and, in principle, there is only one parameter of each isospin channel [123].

Chiral Perturbation Theory

The concepts of chiral symmetry may be utilized to build up a chiral effective meson-baryon Lagrangian in the gauge-invariant chiral unitary model [14]. The chiral effective Lagrangian is exploited to derive the interaction kernel in the Bethe-Salpeter equation which then generates resonances dynamically. Thus, the importance of particular resonances can be studied without their explicit inclusion [14].

Attempts were also made to calculate the kaon-hyperon photoproduction process in the threshold region in the framework of the chiral perturbation theory [105]. However, as it is limited to energies from threshold to approximately 100 MeV only, this approach cannot describe physics higher in the resonance region. Contributions originating from resonances with spin higher than 3/2, therefore, cannot be reproduced as the majority of these states lie beyond the energy region where Chiral Perturbation Theory works.

Coupled-Channel Analysis

Generally, the meson-baryon rescattering processes among hadrons in the final state, so-called final-state interactions, connect various channels of the production process. For

instance, the reaction channels $\gamma p \to K^+\Lambda$ and $\gamma p \to \pi^+ n$ are, due to the final-state interaction, coupled together and one should include both of them in order not to break the condition of unitarity. Although the single-channel models, such as the isobar model, describe the available experimental data well, the coupled-channel effects caused by the intermediate states, such as πN, are ignored. However, the sequence $\gamma N \to \pi N \to KY$ may be substantial in kaon photoproduction, as the $\gamma N \to \pi N$ amplitudes are much larger than the direct amplitudes $\gamma N \to KY$ [26].

In the coupled-channel models [8, 62, 99], the rescattering effects in the meson-baryon final-state system are included, since their contribution may induce changes at the level of 20% on total cross sections [26]. Among existing studies of kaon photoproduction, the effects of coupled channels have been examined within two different approaches. Kaiser *et al.* [68] applied a coupled-channel approach with chiral SU(3) dynamics to study pion- and photon-induced meson production near the KY threshold. On the contrary, Feuster and Mosel [39] used a K-matrix method to investigate photon- and meson-induced reactions, including $\gamma p \to K^+\Lambda$. Moreover, Chiang *et al.* presented another coupled-channel model and discussed the significance of coupled-channel effects [26].

Unfortunately, the models face the problem of missing experimental information on some transition amplitudes, *e.g.* $K^+\Lambda \to K^+\Lambda$. These unknowns have to be parametrized somehow and then fitted to data from all considered channels.

1.3 Historical Background

The commencement of both theoretical and experimental study of kaon photo- and electroproduction was given in the year 1957 when Caltech [38] and Cornell [102] laboratories published the $p(\gamma, K^+)\Lambda$ cross-section data gathered at their electron synchrotrons. There were a number of data collected on the kaon photoproduction (Caltech, Cornell, *etc.*) but only a few experiments were carried out on the electroproduction (DESY, Cambridge).

The modelling of kaon photoproduction processes started in 1960s by the pioneering works of Kuo [63] and Thom [109] who wrote a kaon photoproduction operator using Feynman diagrams for the Born terms and partial-wave amplitudes for the resonances. For the sake of the limited electron energies available at that time, only the kinematical region close to threshold (*i.e.* from threshold up to photon lab energy of 1.4 GeV) could be probed.

Further theoretical work by Adelseck *et al.* [2] was ignited through subsequent experiments in the 1970s and 1980s which were performed in Bonn [13], Tokyo [41] and in the USA. Adelseck *et al.* identified a number of changes from the earlier operator obtained by Thom when less data were available and their model laid the corner stone of a wide-spread theoretical framework for electromagnetic strangeness production: the isobar model. Nonetheless, since the pioneering work of Thom, the isobar models were among the first models capable of describing the kaon photoproduction in the resonance region.

In the year 1998, the SAPHIR collaboration, working at the electron stretcher ring ELSA in Bonn, released the first experimental data of high precision for all three reaction channels on the proton target [110, 45], *i.e.*

$$\gamma + p \longrightarrow K^+ + \Lambda, \tag{1.1a}$$

$$\gamma + p \longrightarrow K^+ + \Sigma^0, \tag{1.1b}$$

$$\gamma + p \longrightarrow K^0 + \Sigma^+, \tag{1.1c}$$

covering the photon lab energy from the threshold up to 2 GeV. These data sets renewed the concern of the theoretical community for seeking the missing resonanes.

The reaction (1.1a) is by far the most studied one, both experimentally and theoretically, although a non negligible part of the existing data base suffers from inconsistencies within the reported accuracies. There are less investigations of the reaction (1.1b) and the process (1.1c) has up to the mid-nineties received very little attention because of experimental difficulties in identifying the particles in the final state.

There is much less experimental data available on the production processes off the neutron – owing to the weak binding of deuteron, it is ideally suited as an effective neutron target. To our knowledge, there are only two data sets for the $n(\gamma, K^+)\Sigma$ and $n(\gamma, K^0)\Lambda$ reaction channels available. The results of the LEPS collaboration [69], which have been gathered through a quasi-free kaon photoproduction off a deuterium target, include differential-cross-section and beam-asymmetry data at forward kaon angles, *i.e.* for $\cos\theta_K^{c.m.} \geq 0.65$ in the energy range $1.5\,\text{GeV} \leq E_\gamma^{lab} \leq 2.4\,\text{GeV}$. Moreover, using photons on a target of liquid deuterium, CLAS collaboration [6] produced a large set of $n(\gamma, K^+)\Sigma^-$ data on differential cross section for a broad energy range. A liquid deuterium target was exploited by Tsukada *et al.* [111] at the Laboratory of Nuclear Science of

Tohoku University in Japan as well in order to accomplish an investigation of $n(\gamma, K^0)\Lambda$ process, which may provide invaluable information on the strangeness photoproduction.

Over the last decade, the database for the $p(\gamma, K)Y$ process was replenished with high-precision data for $p(\gamma, K^+)\Lambda$ and $p(\gamma, K^+)\Sigma^0$ reactions from the CLAS [17, 82, 83], SAPHIR [44], LEPS [51, 108, 121], and GRAAL [66, 67] collaborations. Experiments at MAMI-C exploiting the Crystal Ball calorimeter [61] have provided us with several hundreds of differential-cross-section data on $K^+\Lambda$ and $K^+\Sigma^0$ photoproduction, revealing particularly the behaviour at backward kaon angles where the data had been scarce. Moreover, SAPHIR collaboration has provided another analysis of the $p(\gamma, K^0)\Sigma^+$ channel [64]. However, beyond the resonance region (*i.e.* for $E_\gamma^{lab} \geq 4\,\mathrm{GeV}$) a limited number of $p(\gamma, K^+)Y$ data are available. For the channel with $K^+\Lambda$ in the final state, 72 data exists, including 56 differential-cross-section data [16], 9 beam-asymmetry data [94], and 7 hyperon-polarization data [118]. The number of available data for $K^+\Sigma^0$ production is even smaller: there are 48 differential-cross-section data [16] and 9 beam-asymmetry data [94].

The electroproduction process was measured in the late seventies [19, 10, 11]. Additional experimental data on the electroproduction processes $p(e, e'K^+)\Lambda, \Sigma^0$ were provided at Jefferson Lab [25, 86, 7]. The present research of the electroproduction of strangeness plays an important role also at Mainz Microtron (MAMI). With the help of the Kaos spectrometer for kaon detection, they have performed cross-section measurements of the $p(e, e'K^+)\Lambda, \Sigma^0$ reactions at low-momentum transfers, which may be used to distinguish between effective-Lagrangian models for photo- and electroproduction of strangeness [4].

The theoreticians made a great deal of work in the last decades. In 1990, Adelseck and Saghai [3] made a profound analysis of the $p(\gamma, K^+)\Lambda$ differential-cross-section data up to 1.4 GeV, reproducing the differential and total cross section, hyperon polarization and polarized target data well. On the other hand, they used spin-1/2 nucleon and hyperon resonances only and some authors criticised that Adelseck and Saghai analyzed only cross-section data and their fit is, therefore, not sensitive to the relative magnitudes and phases of the transversity amplitudes [120].

Few years later, while extending their photoproduction model parametrization beyond the photon lab energy E_γ^{lab} of 1.4 GeV, Williams *et al.* [119] found baryon resonances with

spin higher than 1/2 to be necessary to describe the photoproduction data in this energy region. Moreover, they also extended the use of duality as they represented high-spin s- and u-channel resonances with a few low-lying t-channel resonances. The restriction to a small number of N^*'s, however, can reproduce only gross features of the data as the details are given mainly by an interplay between many resonant states. Another approach was published by Mart *et al.* [76], discussing the constraints on coupling constants through photoproduction of Σ mesons.

Subsequently, David *et al.* [32] followed the work of Adelseck and Saghai [3], extended it to higher energies and for the first time included nucleon resonances with spin up to 5/2. In order to achieve a set of resonances which contribute to the process with the highest probability, they evaluated a huge number of models, originating from various combinations of about 30 considered resonances, and generalized their approach to study simultaneously all photoproduction and radiative capture reactions (introduced via the crossing symmetry). Their model provided a first comprehensive description of both photo- and electroproduction of $K^+\Lambda$, $K^+\Sigma^0$, and $K^0\Sigma^+$ and was called Saclay-Lyon.

The work of SAPHIR collaboration [110], published in 1998, clearly envisaged that the total $p(\gamma, K^+)\Lambda$ cross-section data set is not characterized by a smooth energy dependence above the peak in the threshold region. On the contrary, the data displayed a structure at the total energy of approximately 1.9 GeV.

In a further study of kaon photoproduction, Mart and Bennhold [74] closely investigated the energy region of 1.9 GeV, where a broad peak in the cross-section data is seen, and exposed a "missing" $D_{13}(1875)$ resonance to be responsible for a creation of such a bump (we will come back to the concept of missing resonances later on). Another key feature in this model is the inclusion of a hadron form factor which introduces inner structures in hadron and helps reduce the overly strong contributions of Born terms. In addition, they have included energy-dependent widths along with partial branching fractions in the resonance propagators, which approximately account for unitarity corrections. This model is available for calculations online [75].

Since an unrealistically large contribution of the Born terms manifested to be a serious shortcoming of isobar models, another model, with three variants for treating contributions of background terms, was created at the University of Ghent [57].

A lot of work on the photo- and electroproduction of both $K^+\Lambda$ and $K^+\Sigma^0$ [79] from protons as well as on photoproduction of kaons on deuterons has been done by Maxwell. In the case of photoproduction of $K^+\Lambda$ on protons, he has studied model dependencies in these reactions, exploring the treatment of the spin-3/2 resonance propagator and the prescription exploited for the widths of resonances [80]. He has also examined the effects of relaxing the SU(3)-symmetry constraints on the Born contributions [93]. Moreover, he has investigated the electroproduction of $K^+\Lambda$ on proton, discussing constraints on electromagnetic form factors incorporated at the photon vertices in order to extend the photoproduction process to electroproduction [81].

Last but not least, there came a Regge approach, suitable for a study of high-energy region, replenished with nucleon states in order to give predictions of the resonance region as well. The idea of modelling the high-energy amplitude by means of Regge-trajectory exchanges in the t channel was proposed by Levy *et al.* [65]. Subsequently, Guidal *et al.* [46, 47, 48] exploited the same techniques to study the forward kaon photoproduction, criticising the work of Levy *et al.* for using the notion of (over)absorption to explain the experimental data, which leads to gauge-invariance violation and creates dips in the differential cross section at larger values of $-t$ which are not observed in the experiments. Further work, particularly the extension of the model towards the resonance region through inclusion of N^* states, has been done by researchers at the University of Ghent. Their approach, dubbed Regge-plus-resonance model, treats background terms in a completely different way in comparison with the isobar model [29].

Since this should be only an overview of the historical path that led us to this work, the interested reader may find much more detailed description of various models in Sections 3.1 and 4.2.

Chapter 2

Formalism

2.1 Kinematics

In the one-photon-exchange approximation, the electroproduction reaction can be considered as the electron scattering on the target proton through the exchange of a single virtual photon, resulting in the kaon, hyperon, and scattered electron in the final state. The dynamics can be in this case separated into a lepton and hadron part of the process. The lepton part occurs on a so-called lepton plane which is determined by the direction of electron propagation before and after the scattering. The hadron plane, where the hadron part takes place, is set by the direction of propagation of the photon and kaon. The planes are tilted with respect to each other by an angle φ_K. This situation is schematically depicted in Figure 2.1. Whereas the lepton part of the electroproduction reaction is usually depicted in the laboratory frame with a stationary nucleon, the hadron part of the process is considered in the center-of-mass frame. For photoproduction, the photon is on shell and there is thus no lepton plane, which leads to a significant simplification.

The kinematic quantities which are involved in the photoproduction reaction,

$$\gamma_V(k) + p(p) \longrightarrow K^+(p_K) + \Lambda(p_\Lambda), \tag{2.1}$$

are shown in the Figure 2.1. In the case of photoproduction, we work in the center-of-mass

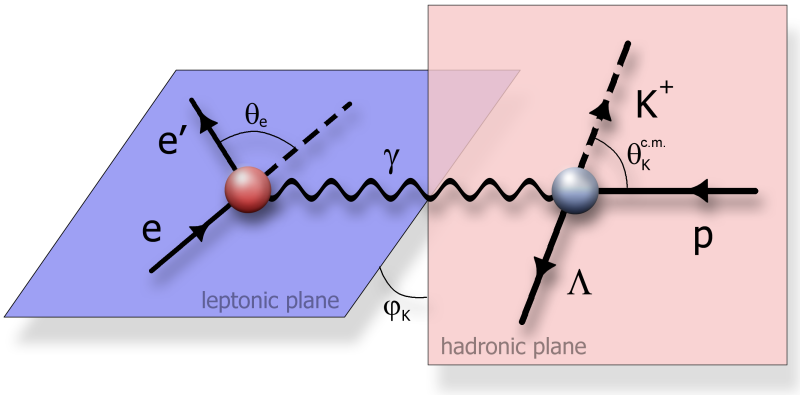

Figure 2.1: A definition of reference frames for leptonic and hadronic part of the $p(e,e'K)Y$ process is shown together with kinematic variables. The photoproduction reaction occurs only at the hadronic plane.

frame and the four-momenta are given as

$$\begin{aligned} k &= (E^*_\gamma, \vec{k}^*), \qquad p_K = (E^*_K, \vec{p}^*_K) \\ p &= (E^*_p, -\vec{k}^*), \quad p_\Lambda = (E^*_Y, -\vec{p}^*_K), \end{aligned} \tag{2.2}$$

where $E^*_i = \sqrt{m_i^2 + |\vec{p}^*_i|^2}$ for $i \equiv p, K, \Lambda$ and $E^*_\gamma = |\vec{k}^*|$. All of these momenta can form Mandelstam variables

$$s = (p+k)^2 = (p_K + p_\Lambda)^2 \tag{2.3a}$$

$$t = (p_K - k)^2 = (p_\Lambda - p)^2 \tag{2.3b}$$

$$u = (p_\Lambda - k)^2 = (p_K - p)^2, \tag{2.3c}$$

which in the photoproduction fulfil the following relation

$$s + t + u = m_p^2 + m_K^2 + m_\Lambda^2. \tag{2.4}$$

From the energy-conservation relation,

$$E^*_\gamma + \sqrt{m_p^2 + E^{*2}_\gamma} = \sqrt{m_K^2 + |\vec{p}^*_K|^2} + \sqrt{m_\Lambda^2 + |\vec{p}^*_K|^2}, \tag{2.5}$$

it is easy to see that the kaon momentum $|\vec{p}^*_K|$ is defined as a function of the incoming photon energy E^*_γ. The reaction dynamics, therefore, depends only on the center-of-mass kaon scattering angle $\theta^{c.m.}_K$ (see Figure 2.1) and the energy of incoming photon. Since the incoming photon energy is measured in the laboratory frame, the experimental outcomes are commonly delivered as a function of E^{lab}_γ rather than E^*_γ.

2.2 Observables

In the electroproduction

$$e(k_1) + p(p) \to e(k_2) + K^+(p_K) + \Lambda(p_\Lambda),$$

the transition amplitude in the one-photon exchange approximation is a product of the matrix elements of the hadron $\mathbb{J}^\mu$ and lepton $l_\mu = e\,\bar{u}(k_2)\gamma_\mu u(k_1)$ currents mediated by the photon propagator

$$M_{fi} = \frac{1}{k^2}\, l_\mu\, \mathbb{J}^\mu(k^2, s, t, u)\,, \tag{2.6}$$

where $k = k_1 - k_2$ is the four-momentum of virtual photon and s, t, and u are the Mandelstam variables defined in (2.3). The conservation of the hadron and lepton currents implies $\mathbb{J}^\mu k_\mu = l^\mu k_\mu = 0$. The matrix element of the hadron current can be therefore decomposed into the linear combination of six covariant gauge-invariant contributions

$$\mathbb{J}^\mu \varepsilon_\mu = \sum_{j=1}^{6} \mathcal{A}_j(k^2, s, t, u)\; \bar{u}(p_\Lambda)\, \gamma_5\, \mathcal{M}_j\, u(p)\,, \tag{2.7}$$

where $\mathcal{M}_j$ are explicitly gauge-invariant operators

$$\mathcal{M}_1 = (\not{k}\not{\varepsilon} - \not{\varepsilon}\not{k})/2, \tag{2.8a}$$

$$\mathcal{M}_2 = p\cdot\varepsilon\, k\cdot p\, k\cdot\varepsilon/k^2, \tag{2.8b}$$

$$\mathcal{M}_3 = p_\Lambda\cdot\varepsilon\, k\cdot p_\Lambda\, k\cdot\varepsilon/k^2, \tag{2.8c}$$

$$\mathcal{M}_4 = \not{\varepsilon} k\cdot p - \not{k} p\cdot\varepsilon, \tag{2.8d}$$

$$\mathcal{M}_5 = \not{\varepsilon} k\cdot p_\Lambda - \not{k} p_\Lambda\cdot\varepsilon, \tag{2.8e}$$

$$\mathcal{M}_6 = \not{k} k\cdot\varepsilon - \not{\varepsilon} k^2, \tag{2.8f}$$

and ε_μ is the polarization vector of the virtual photon. The $\mathcal{M}_1$ operator can be recast to the form $\mathcal{M}_1 = \not{k}\not{\varepsilon} - k\cdot\varepsilon = k\cdot\varepsilon - \not{\varepsilon}\not{k}$, which may be convenient for casting the amplitude to the compact form of Equation (2.7). The scalar amplitudes $\mathcal{A}_j(k^2, s, t, u)$ contain contributions from the considered tree-level Feynman diagrams. Their expressions for various types of particle exchanges are given in Appendix A. In the photoproduction case ($k^2 = 0$), there are only four terms in the decomposition (2.7) [3].

In the calculations which involve also a non relativistic input, *e.g.* the calculation of the hypernucleus production cross sections [23] with non relativistic wave functions

of the nucleus and hypernucleus, one also needs a more convenient representation of the Lorentz invariant matrix element (2.7) in terms of the two-component-spinor amplitudes known as the Chew, Goldberger, Low, and Nambu (CGLN) amplitudes [3, 32, 104]. These amplitudes are, however, also widely used in calculations of observables in the elementary process. In the c.m. frame, the Lorentz invariant matrix element (2.7) can be written as

$$\mathbb{J}^{\mu}\varepsilon_{\mu} = \chi_{\Lambda}^{+}\,\mathcal{F}\,\chi_{p} \tag{2.9}$$

where χ_p and χ_Λ are the Pauli spinors and

$$\begin{aligned}\mathcal{F} = {} & f_1\,\vec{\sigma}\cdot\vec{\varepsilon} - \mathtt{i} f_2\,\vec{\sigma}\cdot\hat{\vec{p}}_K\,\vec{\sigma}\cdot(\hat{\vec{k}}\times\vec{\varepsilon}) + f_3\,\vec{\sigma}\cdot\hat{\vec{k}}\,\hat{\vec{p}}_K\cdot\vec{\varepsilon} \\ & + f_4\,\vec{\sigma}\cdot\hat{\vec{p}}_K\,\hat{\vec{p}}_K\cdot\vec{\varepsilon} + f_5\,\vec{\sigma}\cdot\hat{\vec{k}}\,\hat{\vec{k}}\cdot\vec{\varepsilon} + f_6\,\vec{\sigma}\cdot\hat{\vec{p}}_K\,\hat{\vec{k}}\cdot\vec{\varepsilon}.\end{aligned} \tag{2.10}$$

Here $\hat{\vec{k}} = \vec{k}/|\vec{k}|$, $\hat{\vec{p}}_K = \vec{p}_K/|\vec{p}_K|$, $\vec{\sigma}$ are the Pauli matrices, and $\vec{\varepsilon}$ is the spatial component of the virtual-photon polarization vector. The CGLN amplitudes, $f_i(k^2, s, t, u)$, are expressed via the scalar amplitudes A_j

$$f_1 = N^*[-(W-m_p)\mathcal{A}_1 + k\cdot p\,\mathcal{A}_4 + k\cdot p_\Lambda\,\mathcal{A}_5 - k^2\mathcal{A}_6], \tag{2.11a}$$

$$f_2 = N^*\frac{|\vec{k}||\vec{p}_K|}{(E_\Lambda^*+m_\Lambda)(E_p^*+m_p)}[(W+m_p)\mathcal{A}_1 + k\cdot p\,\mathcal{A}_4 + k\cdot p_\Lambda\,\mathcal{A}_5 - k^2\mathcal{A}_6], \tag{2.11b}$$

$$f_3 = -N^*\frac{|\vec{k}||\vec{p}_K|}{E_p^*+m_p}[\mathcal{A}_3 + (W+m_p)\mathcal{A}_5], \tag{2.11c}$$

$$f_4 = N^*\frac{|\vec{p}_K|^2}{E_\Lambda^*+m_\Lambda}[\mathcal{A}_3 - (W-m_p)\mathcal{A}_5], \tag{2.11d}$$

$$f_5 = N^*\frac{|\vec{k}|^2}{E_p^*+m_p}\left[\mathcal{A}_1 - \frac{1}{k^2}[(k^2+k\cdot p)\mathcal{A}_2 + k\cdot p_\Lambda\,\mathcal{A}_3] - (W+m_p)(\mathcal{A}_4+\mathcal{A}_6)\right], \tag{2.11e}$$

$$\begin{aligned}f_6 = {} & N^*\frac{E_\gamma^*|\vec{k}||p_K|}{(E_\Lambda^*+m_\Lambda)(E_p^*+m_p)}\left\{\mathcal{A}_1 - m_p\mathcal{A}_4 + \frac{k\cdot p_\Lambda}{E_\gamma^*}\mathcal{A}_5\right. \\ & \left. + \frac{(E_p^*+m_p)}{E_\gamma^* k^2}[(k^2+k\cdot p)\mathcal{A}_2 + k\cdot p_\Lambda\,\mathcal{A}_3] - (W+m_p)\mathcal{A}_6\right\},\end{aligned} \tag{2.11f}$$

where $W = \sqrt{s}$ and E_p^*, E_Λ^*, E_K^*, and E_γ^* are the c.m. energies of the proton, hyperon, kaon and photon, respectively. The normalization factor reads

$$N^* = \sqrt{\frac{(E_\Lambda^*+m_\Lambda)(E_p^*+m_p)}{4m_\Lambda m_p}}. \tag{2.12}$$

The triple-differential cross section for electroproduction of unpolarized hyperon with unpolarized electron beam and target is obtained as

$$\frac{\mathrm{d}^3\sigma}{\mathrm{d}E_{e'}\mathrm{d}\Omega_{e'}\mathrm{d}\Omega_K^{\mathrm{c.m.}}} = \Gamma\left[\sigma_T + \varepsilon\sigma_L + \varepsilon\sigma_{TT}\cos 2\varphi_K + \sqrt{2\varepsilon_L(\varepsilon+1)}\sigma_{LT}\cos\varphi_K\right], \tag{2.13}$$

where φ_K, Γ, ε and ε_L are the angle between the lepton and hadron planes, the virtual-photon flux factor, and the transverse and longitudinal photon polarization parameters, respectively [104]. The response functions σ_T and σ_L describe the cross sections for the unpolarized and longitudinally polarized photon beam, respectively, while σ_{TT} stands for the asymmetry of a transversally polarized photon beam. The last term containing σ_{LT} describes the interference effects between the longitudinal and transverse components of the photon beam. Note that σ_T and σ_{TT} correspond to the cross section and beam asymmetry in the photoproduction process, respectively. The response functions in terms of the CGLN amplitudes read as follows

$$\begin{aligned}\sigma_T =& C\,\mathtt{Re}\Big\{|f_1|^2+|f_2|^2-2f_1f_2^*\cos\theta_K \\ &+\sin^2\theta_K\left[\frac{1}{2}(|f_3|^2+|f_4|^2)+f_1f_4^*+f_2f_3^*+f_3f_4^*\cos\theta_K\right]\Big\},\end{aligned} \tag{2.14a}$$

$$\sigma_L = C\,\mathtt{Re}\left\{|\tilde{f}_5|^2+|\tilde{f}_6|^2+2\tilde{f}_5\tilde{f}_6^*\cos\theta_K\right\}, \tag{2.14b}$$

$$\sigma_{TT} = C\,\mathtt{Re}\left\{\frac{1}{2}(|f_3|^2+|f_4|^2)+f_1f_4^*+f_2f_3^*+f_4f_3^*\cos\theta_K\right\}\sin^2\theta_K,, \tag{2.14c}$$

$$\sigma_{LT} = -C\,\mathtt{Re}\left\{(f_1+f_4)\tilde{f}_6^*+(f_2+f_3)\tilde{f}_5^*+(f_3\tilde{f}_6^*+f_4\tilde{f}_5^*)\cos\theta_K\right\}\sin\theta_K, \tag{2.14d}$$

where we have defined the linear combinations

$$\tilde{f}_5 = f_1+f_3\cos\theta_K+f_5, \tag{2.15}$$

$$\tilde{f}_6 = f_4\cos\theta_K+f_6 \tag{2.16}$$

and the normalization factor C is given as

$$C=(\hbar c)^2\frac{\alpha}{4\pi}\frac{m_\Lambda|\vec{p}_K|}{|\vec{k}|W}. \tag{2.17}$$

The general expression for the electroproduction cross section considering all three possible types of polarization can be found in Ref. [70]. Here we give the single-polarization observables P, Σ, and T and the double-polarization observables C_x, C_z, O_x, and O_z which we use in the analysis and which in terms of the CGLN amplitudes read

$$P=-\mathtt{Im}[2f_1^*f_2+f_1^*f_3-f_2^*f_4-(f_2^*f_3-f_1^*f_4)\cos\theta_K-f_3^*f_4\sin^2\theta_K]\sin\theta_K, \tag{2.18}$$

$$\Sigma=-\mathtt{Re}[(|f_3|^2+|f_4|^2)/2+f_2^*f_3+f_1^*f_4+f_3^*f_4\cos\theta_K]\sin^2\theta_K, \tag{2.19}$$

$$T=\mathtt{Im}[f_1^*f_3-f_2^*f_4+\cos\theta_K(f_1^*f_4-f_2^*f_3)-f_3^*f_4\sin^2\theta_K]\sin\theta_K, \tag{2.20}$$

$$C_x = -\mathtt{Re}[-|f_1|^2 + |f_2|^2 + f_2^* f_3 - f_1^* f_4 + (f_2^* f_4 - f_1^* f_3)\cos\theta_K]\sin\theta_K, \tag{2.21}$$

$$C_z = -\mathtt{Re}[-2f_1^* f_2 + \cos\theta_K(|f_1|^2 + |f_2|^2) - \sin^2\theta_K(f_1^* f_3 + f_2^* f_4)], \tag{2.22}$$

$$O_x = \mathtt{Im}[f_2^* f_3 - f_1^* f_4 + \cos\theta_K(f_2^* f_4 - f_1^* f_3)]\sin\theta_K, \tag{2.23}$$

$$O_z = -\mathtt{Im}[f_1^* f_3 + f_2^* f_4]\sin^2\theta_K, \tag{2.24}$$

where P, Σ and T stands for hyperon polarization, beam asymmetry (see also Equation (2.14c)) and target polarization, respectively.

In the laboratory frame, the CGLN amplitudes read

$$F_1 = N\bigg[-\frac{(k\cdot p_\Lambda) + k_0 m_\Lambda}{E_\Lambda + m_\Lambda}\mathcal{A}_1 + k_0 m_p \mathcal{A}_4 + (k\cdot p_\Lambda)\mathcal{A}_5 - k^2\mathcal{A}_6\bigg], \tag{2.25a}$$

$$F_2 = N\frac{|\vec{k}||\vec{p}_K|}{E_\Lambda + m_\Lambda}\mathcal{A}_1, \tag{2.25b}$$

$$F_3 = N\frac{|\vec{k}||\vec{p}_K|}{E_\Lambda + m_\Lambda}[\mathcal{A}_1 - \mathcal{A}_3 - (E_\Lambda + m_\Lambda - k_0)\mathcal{A}_5], \tag{2.25c}$$

$$F_4 = N\frac{|\vec{p}_K|^2}{E_\Lambda + m_\Lambda}[\mathcal{A}_3 - k_0\mathcal{A}_5], \tag{2.25d}$$

$$\begin{aligned} F_5 = -N\frac{|\vec{k}|^2}{E_\Lambda + m_\Lambda}\bigg\{&\mathcal{A}_1 + \frac{1}{k^2}[m_p k_0 \mathcal{A}_2 + ((k\cdot p_\Lambda) - k^2)\mathcal{A}_3] \\ &+ (E_\Lambda + m_\Lambda - k_0)(\mathcal{A}_6 - \mathcal{A}_5)\bigg\}, \end{aligned} \tag{2.25e}$$

$$F_6 = N\frac{|\vec{k}||\vec{p}_K|}{E_\Lambda + m_\Lambda}\bigg\{\frac{1}{k^2}[m_p k_0 \mathcal{A}_2 + ((k\cdot p_\Lambda) - k^2)\mathcal{A}_3] + k_0(\mathcal{A}_5 - \mathcal{A}_6)\bigg\}, \tag{2.25f}$$

where all momenta are in the lab frame, E_Λ and k_0 are the energies of the Λ hyperon and virtual photon, respectively. The normalization factor N is

$$N = \sqrt{\frac{E_\Lambda + m_\Lambda}{2m_\Lambda}}.$$

Chapter 3

An Overview of the Isobar Model

In the isobar model, the starting point in modelling the photo- and electroproduction processes is a description in terms of hadron degrees of freedom. The amplitude is, thus, constructed from an effective meson-baryon Lagrangian as a sum of tree-level Feynman diagrams which represent the s-, t-, and u-channel exchanges of the hadrons in the ground state (the Born terms) and various resonances (the non-Born terms); see Figure 3.1. In this approach, we neglect the higher-order contributions which account for, *e.g.* the rescattering effects. It is only the exchange of nucleon resonances that makes a resonant structure in the observables. Since the corresponding poles of the other diagrams are far from the physical region, they contribute to the background part of the amplitude only and do not give rise to peaks in the energy dependence of the cross section. The isobar model works well in the near-threshold and resonant region involving photon lab energy from threshold up to approximately 2.5 GeV.

Unlike the pion or η-meson photoproduction, there exists no dominant resonance in photoproduction of kaons. Therefore, one has to take into account *a priori* more than 20 resonances with mass ≤ 2 GeV. This leads to a huge number of possible configurations of resonances which should be investigated [3, 32, 35], still resulting in a large number of models describing the data reasonably well (*i.e.* with a small χ^2). In order to reduce

this large number of models, one imposes constraints to acceptable values of the $K\Lambda N$ and $K\Sigma N$ coupling constants and relates them to the well-known πNN value by means of the SU(3) symmetry [3, 32, 57].

The SU(3) flavour symmetry, which governs the baryon and meson multiplets can be used to establish relations between various meson-baryon-baryon coupling constants connecting different processes (*e.g.* production of π, η and K). Furthermore, these relations allow one to connect the coupling constants of the up-down sector to the coupling constants of the strange sector. Using the convention of de Swart [107], in the case of the unbroken SU(3) symmetry one can derive relations for the $K\Lambda N$ and $K\Sigma N$ coupling constants

$$g_{K\Lambda N} = -\frac{1}{\sqrt{3}}(3-2\alpha_D)g_{\pi NN}, \tag{3.1a}$$

$$g_{K\Sigma N} = (2\alpha_D - 1)g_{\pi NN}, \tag{3.1b}$$

where α_D is the fraction of symmetric coupling in the πNN vertex. Taking the α_D value of 0.644 ± 0.006 and the experimental knowledge of $g^2_{\pi NN}/4\pi = 14.4$, the values for the $K\Lambda N$ and $K\Sigma N$ coupling constants can be determined. Due to the substantial difference between the mass of the proton and the mass of the Λ hyperon (which originates in interchanging an up quark with a strange quark), it is known that the SU(3) symmetry is not exact but it is violated at the level of 20%. Thus, the relations (3.1) are not exact and one obtains the following ranges for the coupling constants

$$-4.4 \leq \frac{g_{K\Lambda N}}{\sqrt{4\pi}} \leq -3.0, \quad 0.8 \leq \frac{g_{K\Sigma N}}{\sqrt{4\pi}} \leq 1.3. \tag{3.2}$$

In order to ensure regularity for the tree-level invariant amplitude in the physical region, the poles corresponding to the resonances are shifted to the complex plane, $m_R \to m_R - \mathtt{i}\Gamma_R/2$, introducing the decay width Γ_R which accounts for a finite lifetime of the resonant state. The Feynman propagator can then be written as

$$\frac{1}{\not{q} - m_R + \mathtt{i}\Gamma_R/2} = \frac{\not{q} + m_R - \mathtt{i}\Gamma_R/2}{q^2 - m_R^2 + \mathtt{i}m_R\Gamma_R + \Gamma_R^2/4},$$

and various approximations are assumed in various isobar models. In the Saclay-Lyon and Ghent models the following approximation is exploited

$$\frac{\not{q} + m_R}{q^2 - m_R^2 + \mathtt{i}m_R\Gamma_R}, \tag{3.3}$$

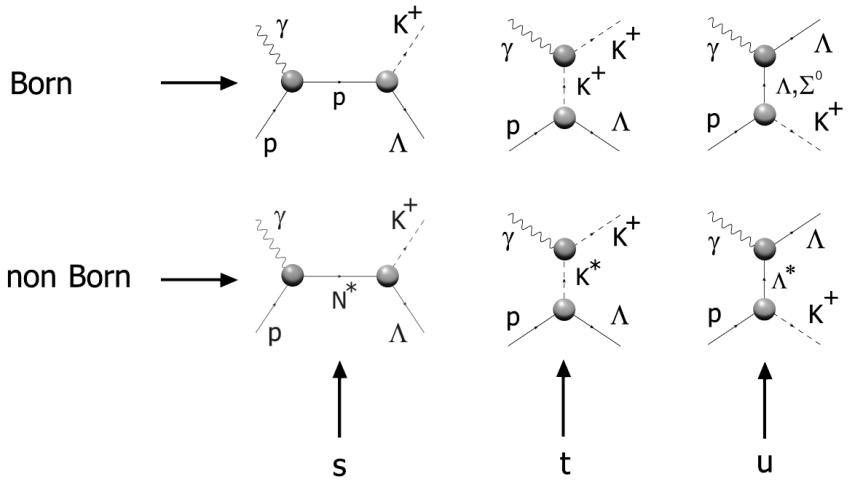

Figure 3.1: The tree-level contributions to the $p(\gamma, K^+)\Lambda$ amplitude are shown. The Born terms with an exchange of a hadron in its ground state and the non-Born terms with nucleon-, kaon-, and hyperon-resonance exchanges are shown in the upper and lower rows, respectively. The t- and u-channel diagrams and the s-channel Born term contribute to the background part since the energy-momentum conservation prevents their poles from being reached in the physical region. Only the s-channel non Born term produces resonant structures in the observables.

while in the Kaon-MAID model and in Ref. [104] the Feynman propagator reads

$$\frac{\not{q} + m_R - \mathrm{i}\Gamma_R/2}{q^2 - m_R^2 + \mathrm{i}m_R\Gamma_R}. \tag{3.4}$$

In the tree-level approximation, the decay widths can, to some extent, mimic dressing of the propagator. In most of the isobar models, the widths are assumed to be constant parameters, and the Breit-Wigner values suggested in the Particle Data Tables are used. In order to approximately account for unitarity corrections in the single-channel approach, the energy-dependent widths for the nucleon resonances were used in the Kaon-MAID model. The energy dependence of Γ_R is given by a possibility of a resonance to decay into various open channels. In this work, we use the approximation (3.4) with constant decay widths.

One of the characteristic features of the kaon photoproduction process described by an isobar model is too large a contribution of the Born terms to the cross sections which largerly overshoots the data. This non physically large strength of the Born terms has to be reduced in order to get a realistic description of the cross sections and other observables allowing an analysis of the resonant content of the amplitude. We can achieve

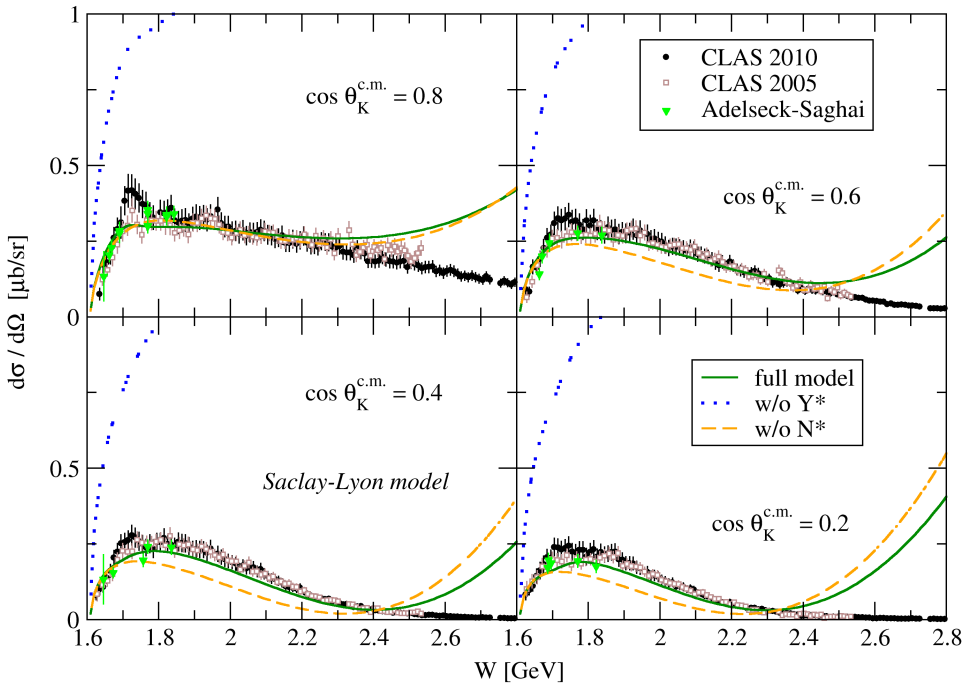

Figure 3.2: Cross-section prediction of SL model is shown in dependence on total energy W for various kaon angles $\theta_K^{c.m.}$ in the forward hemisphere. The solid, dotted, and dashed lines represent the full SL model and outcomes of SL model with no hyperon and nucleon resonances, respectively. The calculation with no hyperon resonances illustrates the requirement of reducing the Born terms; in SL model, the hyperon resonances are employed for this purpose.

this by introducing the form factors into the strong vertices (hadron form factors in this case) [74] or by exchanges of several hyperon resonances [32] or by a combination of both methods [57, 59]. In our model, we exploit both the implementation of hadron form factors and the exchange of hyperon resonances. Needless to say, the choice of the method strongly affects the dynamics of the model. Note that the problem with too large a contribution of Born terms is not present in the Regge-plus-resonance model [29, 30, 31] since in this approach the background is modelled in a different way (for a detailed description see Chapter 4).

Another ambiguity in construction of the gauge-invariant Lagrangian arises from a coupling in the $K\Lambda N$ vertex which can be either pseudoscalar- or pseudovector-like [52, 53]. While the former makes the total contribution of the Born terms gauge invariant, the use of the latter coupling requires introducing a contact term even with no hadron form

factors inserted. The role of these couplings was investigated in the threshold region [72] and it was concluded that both couplings can describe the $K\Lambda$ photoproduction data equally well. In this work, however, we have used the pseudoscalar coupling as in the most of isobar models.

3.1 Variants of the Isobar Model

Since the photoproduction process occurs in the so-called third-resonance region, where a plenty of resonances exist and none of them seems to be dominant in $K^+\Lambda$ photoproduction, there is a number of versions of the isobar model. The most successful in the data description and the most frequently cited are Saclay-Lyon, Kaon-MAID and Ghent models. Moreover, the latter one inspired the researchers at Ghent University to the development of a brand new approach coined Regge-plus-resonance model which is of interest in this work as well. In this section, the main ideas of aforementioned isobar models will be given. In all of them, the non consistent formalism for exchanges of high-spin fields, which leads to a propagation of lower-spin components (for details see Chapter 3.2), is used.

Saclay-Lyon model

Saclay-Lyon (SL) model [32] provided a first extensive description of photo- and electroproduction of $K^+\Lambda$, $K^+\Sigma^0$, and $K^0\Sigma^+$ in the energy range from threshold up to photon lab energy of 2.1 GeV as well as radiative kaon capture reactions. An astute reader may notice that David *et al.* show in their work some results beyond the energy of 2.1 GeV. However, the models were obtained by fitting the data up to roughly 2.1 GeV and, therefore, the outcomes beyond this energy region are merely predictions shown so as to investigate the behaviour of different models at higher energies.

In addition to Born terms (exchanges of the proton, K^+, Λ, and Σ particles in their ground state), this model includes the exchanges of vector ($K^*(890)$) and axial-vector ($K_1(1270)$) mesons in the t channel as well as exchanges of hyperon resonances ($\Lambda(1407)$, $\Lambda(1670)$, $\Lambda(1810)$, and $\Sigma(1660)$) in the u channel. The structures in the resonance region are modelled by the addition of nucleon resonances ($P_{11}(1440)$, $P_{13}(1720)$, and $F_{15}(1680)$) in the s channel. Moreover, the Saclay-Lyon model includes no hadron form factors and

their effects are, to some extent (*i.e.* helping reduce the large Born-term contributions), simulated by the presence of hyperon resonances, see Figure 3.2. Among the strangeness production models, the Saclay-Lyon model was the first one to include nucleon and Δ resonance contributions with spin up to 5/2 [34].

In the beginning, David *et al.* started with the set of spin-1/2 resonances chosen by Adelseck and Saghai in their analysis [3] and added resonances with higher spin. Subsequently, they performed an evaluation of a huge number of models taking into account various combinations of about 30 possible baryon resonant states and described the sensitivity of various observables on the inclusion or omission of particular resonances. The resulting model is the only configuration fulfilling the criteria of acceptably low χ^2's for all channels under study, agreement with the SU(3)-symmetry constraints for the two main coupling constants $g_{K\Lambda N}$ and $g_{K\Sigma N}$, predictivity power, and a simple reaction mechanism.

Cross-section predictions of SL model for kaon angles in the forward hemisphere are shown in Figure 3.2. The omission of hyperon resonances in the u channel leads to a gross overestimation of cross-section data, whereas the nucleon s-channel resonances subtly replenish contributions of other parts of the amplitude in order to give the full model.

Kaon-MAID model

Mart and Bennhold [74] have constructed an isobar model for kaon photoproduction called Kaon-MAID (KM) with calculational interface available online [75]. Since the amplitude of this model is not unitary by construction, the nucleon resonance propagator is replenished with an energy-dependent width which accounts for unitarity corrections. In order to regularize too large a contribution of Born terms, hadron form factors are implemented. This leads to a strong suppression of the electric part of the s-channel Born term which results in a bump in the cross-section prediction for small kaon angles, approximately for $\theta_K^{c.m.}$ of 30°, and the total energy higher than $W = 1.9\,\mathrm{GeV}$.

Besides the Born terms (exchanges of proton, K^+, Λ, and Σ particles in their ground state), the exchanges of vector ($K^*(890)$) and axial-vector ($K_1(1270)$) mesons in the t channel build up the background of Kaon-MAID model. The resonant part of the amplitude is modelled by exploiting the s-channel $S_{11}(1650)$, $P_{11}(1710)$, and $P_{13}(1720)$

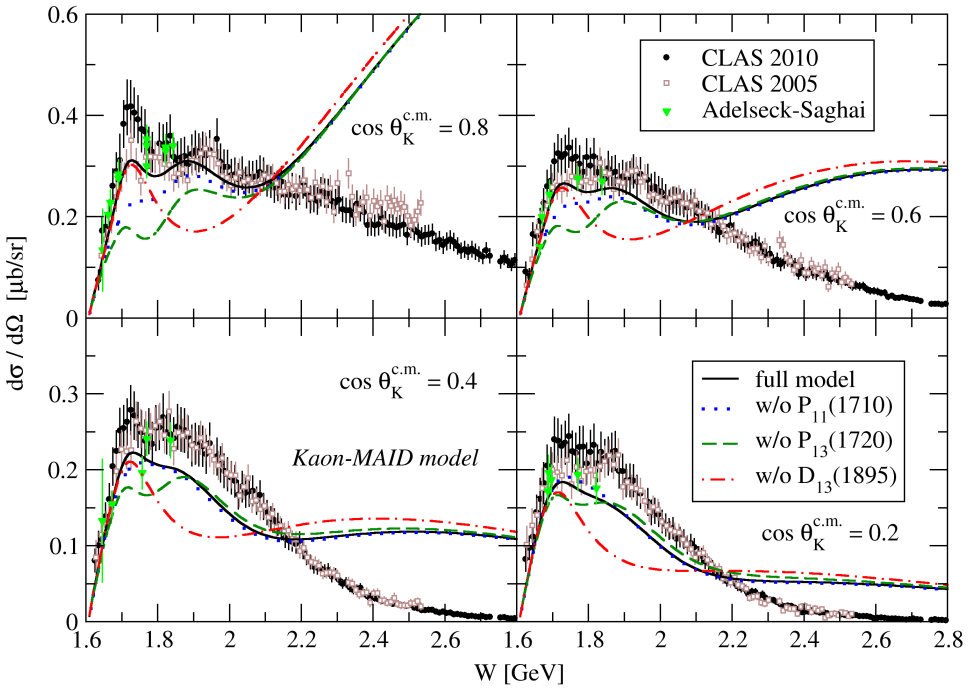

Figure 3.3: Cross-section prediction of KM model is shown for various kaon angles in the forward hemisphere. The solid, dotted, dashed, and dash-dotted lines represent the predictions of the full KM model and of the model with $P_{11}(1710)$, $P_{13}(1720)$, and $D_{13}(1895)$ resonances omitted. The importance of $D_{13}(1895)$ resonance for a satisfactory description of the peak around W of 1.9 GeV is demonstrated in this way.

nucleon resonances. Moreover, in order to describe the broad peak in the SAPHIR [110] cross-section data around 1.9 GeV, Mart and Bennhold performed a number of fits with several states predicted by the constituent quark model [24] in this energy region, allowing the fit to determine the mass, width and coupling constants of the resonances. While all of the examined resonances proved to reproduce the structure around the considered energy and reduced the χ^2 value, only the $D_{13}(1895)$ state was predicted to have also significant photocouplings [74]. Thus, they identified the structure seen in the data with the $D_{13}(1895)$ state predicted by the quark model and added this state to their model. However, the reproduction of the visual peak in the total cross-section should not be interpreted as a steadfast evidence for the occurence of the given missing resonance.

The behaviour of the KM model for various fixed kaon angles is shown in Figure 3.3 and its predictions are compared with several data sets. Note that the KM-model parameters were not adjusted to any of the CLAS data as these data were not available at the time

of formation of KM model. Apparently, the presence of nucleon resonances is important for the model in order to give a trustworthy correspondence with experimental data. Omitting a resonance leads to a drop in the cross-section prediction, which strongly suggests the importance of the resonance for the particular kinematic region. For instance, the KM model with no $P_{11}(1710)$ or $P_{13}(1720)$ is not able to capture the first peak in the cross section, while leaving out the $D_{13}(1895)$ resonance leads to a failure in reproducing the second peak of the cross-section data at W around 1.9 GeV, see Figure 3.3. Moreover, since this model was proposed in the energy range from the threshold up to the total energy W of 2.2 GeV, the cross sections diverge beyond this energy region, which is well apparent in Figure 3.3.

Ghent Isobar Model

In this work, close attention have been paid to the determination of the background part of the amplitude, which consists of Born terms and vector and axial-vector meson exchange in the t channel. Three different options of balancing the Born terms, which on their own predict the cross section being a few times the measured one, were investigated. As a first scheme, Janssen *et al.* [57] introduced hadron form factors which are a well-known tool for reducing the strength stemming from the Born terms. Considering the hadron form factors, the best fits were obtained with values of the cutoff parameter which approach an imposed underlimit of 0.4 GeV, making the hadron form factor extremely soft. Despite the good agreement with the data reached in this scheme, the magnitude of cutoff masses, being as small as the kaon mass, is doubtful [57].

A second variant was to introduce hyperon resonances in the u channel which interfere destructively with the Born terms and in this way reduce their contributions. In this option, considering the large value of coupling constants for $\Lambda(1800)$ and $\Lambda(1810)$ hyperon resonances included, Janssen *et al.* argued that these two hyperon resonaces may be interpreted as effective particles accounting for a larger set of hyperon resonances which participate in the process [57].

A third option was based on ignoring the limits for the main coupling constants, $g_{K\Lambda N}$ and $g_{K\Sigma N}$, which leads to smaller values of these coupling constants than what is expected on the basis of the broken SU(3) flavour symmetry. They showed that all techniques considered result in a fair agreement of the model calculations with the available

Nickname	Particle	Mass [MeV]	Width [MeV]	J^π	Status
K^*	$K^*(892)$	891.66	50.8	1^-	
K1	$K_1(1270)$	1272	90	1^+	
N1	$P_{11}(1440)$	1430	350	$1/2^+$	****
N3	$S_{11}(1535)$	1535	150	$1/2^-$	****
N4	$S_{11}(1650)$	1655	150	$1/2^-$	****
N8	$D_{15}(1675)$	1675	150	$5/2^-$	****
N9	$F_{15}(1680)$	1685	130	$5/2^+$	****
N5	$D_{13}(1700)$	1700	150	$3/2^-$	***
N6	$P_{11}(1710)$	1710	100	$1/2^+$	***
N7	$P_{13}(1720)$	1720	270	$3/2^+$	****
P5	$F_{15}(1860)$	1860	270	$5/2^+$	**
P1	$P_{11}(1880)$	1870	235	$1/2^+$	**
P4	$D_{13}(1875)$	1875	220	$3/2^-$	***
P2	$P_{13}(1900)$	1900	500	$3/2^+$	***
P3	$F_{15}(2000)$	2050	198	$5/2^+$	**
M1	$D_{13}(2120)$	2120	330	$3/2^-$	**
L1	$\Lambda(1405)$	1405	50	$1/2^-$	****
L2	$\Lambda(1600)$	1600	150	$1/2^+$	***
L3	$\Lambda(1670)$	1670	35	$1/2^-$	****
L4	$\Lambda(1800)$	1800	300	$1/2^-$	***
L5	$\Lambda(1810)$	1810	150	$1/2^+$	***
L6	$\Lambda(1520)$	1519.54	15.6	$3/2^-$	****
L7	$\Lambda(1690)$	1690	60	$3/2^-$	****
L8	$\Lambda(1890)$	1890	100	$3/2^+$	****
S1	$\Sigma(1660)$	1660	100	$1/2^+$	***
S2	$\Sigma(1750)$	1750	90	$1/2^-$	***
S3	$\Sigma(1670)$	1670	60	$3/2^-$	****
S4	$\Sigma(1940)$	1940	220	$3/2^-$	***

Table 3.1: Meson and baryon resonances which can be included in a description of the $p(\gamma, K^+)\Lambda$ process. For each resonance, the mass, width, spin, parity, and status are shown. Entries are from Particle Data Tables 2014 [88] except for the P2 width which was taken from the Bayesian analysis of the Ghent group [35].

experimental data. Nonetheless, they concluded that the various ways of treating the background part heavily influence the extracted information about the resonances.

This model comprises the same resonances as the Kaon-MAID model, *i.e.* $S_{11}(1650)$, $P_{11}(1710)$, $P_{13}(1720)$, and $D_{13}(1895)$. In one of the considered variants, they introduced also hyperon resonances in the u channel, namely $\Lambda(1800)$ and $\Lambda(1810)$. Moreover, the $P_{13}(1900)$ has been suggested as the alternate one to the $D_{13}(1895)$ found in [74].

3.2 Resonances with Spin 3/2 and 5/2

In the description of the $p(\gamma, K^+)\Lambda$ process, there are a number of baryon resonances which can contribute either to the resonant or non resonant (background) part of the amplitude. Many of them are of spin 3/2, 5/2 or even higher. In this work, we restrict our analysis only to nucleon resonances with spin 3/2 and 5/2, since higher-spin nucleon resonances have mass higher than 2 GeV, where there is no apparent resonant structure in the data, and to hyperon resonances with spin 3/2. Among these states, the one of highest importance is most probably the $D_{13}(1875)$ whose couplings tend to be very large in comparison with other resonances; the role of other high-spin states is rather in their subtle interplay with other terms creating the resonance pattern in cross sections. In the background part of the amplitude, the only high-spin contributions which we consider are the exchanges of spin-3/2 hyperon resonances in the u channel (see Table 3.1).

The Rarita-Schwinger (R-S) description of high-spin fermion fields includes non physical degrees of freedom connected with their lower-spin content. If the R-S field is off its mass shell, the non physical parts may participate in the interaction, which is then called "inconsistent". Almost two decades ago, Pascalutsa proposed a new consistent interaction theory for massive spin-3/2 fields [90], where the interaction is mediated by the spin-3/2 modes only. The consistency of the theory is ensured by the invariance of the spin-3/2 interaction vertices under the local $U(1)$ gauge transformation of the R-S field. This scheme was generalized to arbitrary high spin by the Ghent group [116] and is used in this work.

The R-S propagator of the spin-3/2 field in terms of the spin-projection operators is [91]

$$S_{\mu\nu}(q) = \frac{\not{q} + m_R}{q^2 - m_R^2 + \mathrm{i} m_R \Gamma_R} P^{(3/2)}_{\mu\nu} - \frac{2}{3m_R^2}(\not{q} + m_R) P^{(1/2)}_{22,\mu\nu} + \frac{1}{m_R\sqrt{3}} \left(P^{(1/2)}_{12,\mu\nu} + P^{(1/2)}_{21,\mu\nu} \right), \tag{3.5}$$

where $P^{(3/2)}_{\mu\nu}$ projects on the spin-3/2 states

$$P^{(3/2)}_{\mu\nu} = g_{\mu\nu} - \frac{1}{3}\gamma_\mu\gamma_\nu - \frac{\not{q}q_\nu\gamma_\mu + q_\mu\gamma_\nu\not{q}}{3q^2}, \tag{3.6}$$

and $P^{(1/2)}_{12,\mu\nu}$, $P^{(1/2)}_{21,\mu\nu}$, and $P^{(1/2)}_{22,\mu\nu}$ project on the spin-1/2 sector

$$P^{(1/2)}_{22,\mu\nu} = \frac{q_\mu q_\nu}{q^2}, \quad P^{(1/2)}_{12,\mu\nu} = \frac{q^\rho q_\nu \sigma_{\mu\rho}}{\sqrt{3}q^2}, \quad P^{(1/2)}_{21,\mu\nu} = \frac{q_\mu q^\rho \sigma_{\rho\nu}}{\sqrt{3}q^2}, \tag{3.7}$$

where $\sigma_{\rho\nu} = \frac{\mathrm{i}}{2}[\gamma_\rho, \gamma_\nu]$.

The gauge invariance of the strong, $K(p_K)\,\Lambda\,N^*(q)$, and electromagnetic, $N^*(q)\,p\,\gamma(k)$, couplings [90] generates the transverse interaction vertices

$$V_\mu^S(K\Lambda N^*) = \frac{f}{m_K m_R}\,\epsilon_{\lambda\mu\alpha\beta}\,\gamma_5\,\gamma^\alpha\,q^\lambda\,p_K^\beta\,, \tag{3.8}$$

and

$$V_\nu^{EM}(N^*p\gamma) = \frac{\mathtt{i}\,\gamma_5}{m_R(m_R+m_p)}\,q^\tau\,[\,g_1 F_{\tau\nu} + g_2\,(\,\gamma_\tau\gamma^\sigma F_{\nu\sigma} - \gamma_\nu\gamma^\sigma F_{\tau\sigma})\,]\,, \tag{3.9}$$

where $F_{\mu\nu} = k_\mu\varepsilon_\nu - \varepsilon_\mu k_\nu$, $\epsilon_{0123} = 1$, and

$$V_\mu^S\,q^\mu \;=\; V_\nu^{EM}\,q^\nu \;=\; 0\,. \tag{3.10}$$

Then it is obvious from Eqs. (3.5) and (3.7) that this property removes all non physical contributions of the spin-1/2 sector to the invariant amplitude. Moreover, one sees in Equation (3.6) that the pole term in $P_{\mu\nu}^{(3/2)}$ also vanishes which makes it possible to include into the model the hyperon exchanges with the spin 3/2 in the u channel (see below).

In general, for arbitrary high spin $n+1/2$ ($n = 1, 2, \ldots$), the transversality of the interaction vertices prevents the momentum-dependent terms in the propagator from contributing, allowing us to write the R-S propagator in the consistent theory only by means of the projection operator onto the pure spin-$(n+1/2)$ state [116]:

$$S_{\mu_1\cdots\mu_n,\nu_1\cdots\nu_n}(q) \to \frac{\not{q}+m_R}{q^2-m_R^2+\mathtt{i}m_R\Gamma_R}P^{(n+1/2)}_{\mu_1\cdots\mu_n,\nu_1\cdots\nu_n}(q). \tag{3.11}$$

The gauge invariance of the interaction results also in a relatively high-power momentum dependence in the invariant amplitude, which rises with rising spin of the R-S field as $\sim q^{2n}$ [116]. For the spin-3/2 field it is apparent from Eqs. (3.8) and (3.9) that the momentum dependence is $\sim q^\lambda q^\tau$, see also (A.39) for the s-channel invariant amplitude. In the case of a contribution of spin-5/2 nucleon resonance, the invariant amplitude can be schematically written as

$$\mathbb{M}_{NBs}^{N^*(5/2)} \sim q^4\frac{\not{q}+m_R}{q^2-m_R^2+\mathtt{i}m_R\Gamma_R}\mathcal{P}^{(5/2)}_{\mu\nu,\lambda\rho}(q)\,\mathcal{O}_{5/2}^{\mu\nu,\lambda\rho}, \tag{3.12}$$

where $\mathcal{P}^{(5/2)}_{\mu\nu,\lambda\rho}(q)$ projects onto the spin-5/2 state [116] and $\mathcal{O}_{5/2}^{\mu\nu,\lambda\rho}$ stands for the remaining structure in the strong and electromagnetic vertices, see (A.50).

This strong momentum dependence from derivatives in the gauge-invariant vertices regularizes the amplitude, but it also causes non physical structures in the energy dependence of the cross section, which needs to be cut off especially above the resonance

region. Therefore, the hadron form factors with a higher, spin-dependent energy power in the denominator and with relatively small values of the cutoff parameter in comparison with standard hadron form factors are used in the RPR model [116, 35]. We have, therefore, also carefully investigated this property in our isobar approach considering various forms of the hadron form factor, see Subsection 3.4 below.

Note that after the substitution $\sqrt{s} \to m_R$ the propagator used in the SL model [32] equals that in Equation (3.5). The interaction Lagrangians in the SL model, constructed as the most general form invariant under the so-called point transformation [85], lead in general to an inconsistent description. Moreover, this point-transformation invariance adds three more free parameters, the off-shell parameters, to each spin-3/2 resonance [85, 57, 59, 60]. Using the consistent formalism in our approach we have avoided this additional uncertainty in the model.

3.3 Resonant Contributions

Nucleon Resonances

For a selection of a set of baryon resonances that preferably describe the world $p(\gamma, K^+)\Lambda$ data, one has to perform thousands of fits assuming all acceptable resonance combinations. To our knowledge, such a robust analysis has been performed by Adelseck and Saghai [3], further extended by the Saclay-Lyon group [32] and by the Ghent group [35] which used more sophisticated technique in the data analysis based on a Bayesian inference method. Another data analysis in the multipole approach was performed by Mart and Sulaksono [78] who considered resonances with spin up to 9/2 with 93 free parameters performing the χ^2 minimization fits to CLAS, LEPS and SAPHIR data. The Ghent group made the Bayesian analysis of a huge number of nucleon resonance combinations and selected two sets of resonances with the highest evidence values. We have chosen one of these solutions, RPR-2011A [35], as a starting point in our analysis. The corresponding resonances are N3, N4, N7, N9, P1, P2, P3, and P4 (see Table 3.1 for notation). Furthermore, we have replenished this set with a few other nucleon resonances, such as $D_{15}(1675)$, $D_{13}(1700)$, $P_{11}(1710)$, and $F_{15}(1860)$. As a result, the last two N^*'s are included in our best fits, BS1 and BS2, since they lead to a decrease of χ^2 and improve the description of data. As we limit ourselves to the $K^+\Lambda$ channel only, there is no need to

introduce Δ resonances which cannot decay to $K^+\Lambda$ because of isospin conservation.

The four-star resonance N3 [$S_{11}(1535)$], which is of crucial importance for the description of η-meson photoproduction, lies below the $K^+\Lambda$ threshold, but its coupling to the $K^+\Lambda$ channel is possible because of its large width and predicted strong coupling to the strangeness sector. In the Bayesian analysis with the RPR model, this resonance was found to contribute with a moderate probability [35], while in the isobar model its coupling strength to the $K^+\Lambda$ channel was found to be quite small [73].

In the KM and Ghent isobar models, the N4, N6, and N7 established resonances were chosen along with the missing resonances P4 [$D_{13}(1875)$] and P1 [$P_{11}(1880)$]. In the SL model [32] for the $K^+\Lambda$ electroproduction, only the well established nucleon resonances N1, N7, and N8 were selected. The older RPR model, RPR 2007 [29, 30, 31], selected N4, N6, N7, P2, and P4 nucleon resonances. The resonances N1, N6, and N8 were excluded in the new Bayesian analysis, whereas N4 and N7 and the missing P1, P2, and P4 resonances were confirmed. Note that, due to large decay widths of most resonances, their contributions overlap each other, which results in interference among many states. This makes the analysis of the resonance content of the invariant amplitude arduous and, even though high-quality data are available, this survey still brings uncertain outcomes (*i.e.* there are several possible solutions which describe the data equally well).

In the past, nucleon resonances P3 and P5 were regarded merely as a one state. However, the Particle Data Group [88] decided recently to consider them to be two separate states. Since both of these states have only two-star status, they are not included in the PDG Summary Tables.

Kaon Resonances

In many studies, the vector K^* and pseudovector K_1 meson resonances were found to be important in the data description [32, 119] and are used in all realistic isobar models. We have, therefore, included them in the basic set of resonances. Let us remind that these two states together with the kaon are the lowest poles in the K^+ and K^* Regge trajectories contained in the Regge [47] and RPR [29, 35] models, which also corroborates the importance of these states.

Hyperon Resonances

The exchanges of hyperon resonances in the u-channel contribute to the background and were not included in some isobar models, *e.g.* in the KM model. They can play, however, an important role in the dynamics as shown in the SL [32] and Ghent isobar [57, 59] models. Particularly, they can compensate the non physically big contributions of the Born terms. Moreover, their presence can significantly improve description of data reducing the χ^2 and shift the value of the hadron cutoff parameter to a harder region [77].

Formerly, mainly the spin-1/2 hyperon resonances were included in the models with inconsistent description of the spin-3/2 baryons. To our knowledge, the only attempt to include a spin-3/2 hyperon resonance in the isobar model was done by the Saclay-Lyon group in Ref. [85], the version C of the SL model. The reason for this limitation was that the pole in the $u = q^2$ variable, which appears in the invariant amplitude from the projection operator $\mathcal{P}^{(3/2)}_{\mu\nu}$ of the propagator (3.5), lies in the physical region ($u = 0$) causing a divergence of the amplitude with the inconsistent interaction. In the consistent formalism, the pole term does not contribute owing to the transversality of the interaction vertices, Equation (3.10), and regularity of the amplitude,

$$V^{EM}_{\mu}(N^*p\gamma)\,\frac{\not{q}+m_R}{u-m_R^2+\mathtt{i}m_R\Gamma_R}\,\frac{1}{3u}(\not{q}\,q^{\nu}\gamma^{\mu}+q^{\mu}\gamma^{\nu}\,\not{q})\,V^{S}_{\nu}(K\Lambda N^*)=0, \tag{3.13}$$

leaving only non zero contributions from the momentum independent terms in the projection operator (3.6). It is therefore safe to include the spin-3/2 hyperon resonances with relatively small masses, see Table 3.1, which are expected to be important in describing the background.

Here we have considered only the spin-3/2 Λ and Σ well established four- or three-star resonances as reported in the Particle Data Tables 2014 [88] (Table 3.1): $\Lambda(1520)\,3/2^-$ (L6), $\Lambda(1690)\,3/2^-$ (L7), and $\Lambda(1890)\,3/2^+$ (L8), with the branching ratios to $N\bar{K}$ 45%, 20-30%, and 20-35%, respectively; $\Sigma(1670)\,3/2^-$ (S3) and $\Sigma(1940)\,3/2^-$ (S4) with 7-13% and < 20%, respectively.

3.4 Hadron Form Factors

Apart from reduction of the Born terms the hadron form factor can also mimic the internal structure of hadrons in the strong vertices which is neglected in the hadrodynamical approach. However, there is still an ambiguity in the selection of a form of the hadron form

factor - one can choose among dipole F_d, multidipole F_{md}, Gaussian F_G, or multidipole-Gaussian shape F_{mdG} [116]:

$$F_d(x, m_R, \Lambda_R) = \frac{\Lambda_R^4}{(x - m_R^2)^2 + \Lambda_R^4}, \tag{3.14a}$$

$$F_{md}(x, m_R, \Lambda_R, J_R) = F_d^{J_R+1/2}(x, m_R, \Lambda_R), \tag{3.14b}$$

$$F_G(x, m_R, \Lambda_R) = \exp[-(x - m_R^2)^2/\Lambda_R^4], \tag{3.14c}$$

$$F_{mdG}(x, m_R, \Lambda_R, J_R, \Gamma_R) = F_d^{J_R-1/2}(x, m_R, m_R\tilde{\Gamma}_R)\, F_G(x, m_R, \Lambda_R), \tag{3.14d}$$

where m_R, J_R, Λ_R, and $x \equiv s, t, u$ stands for the mass and spin of the particular resonance, cutoff parameter of the form factor, and Mandelstam variables, respectively. Moreover, it is required to introduce a modified decay width

$$\tilde{\Gamma}_R(J_R) = \frac{\Gamma_R}{\sqrt{2^{1/2J_R} - 1}}, \tag{3.15}$$

which depends on the spin of the resonance and leads to preserving the interpretation of the resonance decay width as the full width in half maximum (FWHM) of the resonance peak [116].

Since the high-power momentum dependence of the amplitude leads to a substantial growth of the resonance contribution to the cross section, it is needed to introduce a hadron form factor to refine this behavior. In fact, the form factor should ensure that the resonant diagram does not contribute far from the mass pole of the exchanged particle. Unfortunately, a cutoff-value dependence is introduced with the form factor into the cross section. In Figure 3.4, we demonstrate the dependence of the contribution of a particular resonance with spin 5/2 in the s-channel using the dipole (3.14a), multidipole (3.14b), Gaussian (3.14c), and multidipole-Gaussian (3.14d) form factors on various values of the cutoff parameters. The use of the dipole form factor leads to enlarging the tail of the resonant peak whereas the Gaussian form factor creates an artificial cutoff-value dependent peak while the actual resonant peak contributes only as its shoulder. Introducing the spin-dependent form factor, multidipole or multidipole-Gaussian, makes the effect moderate even for larger values of the cutoff parameter. Using the latter form factor makes the contribution almost independent of the cutoff value producing the real resonance pattern in the cross section (see Figure 3.4).

The total amplitude constructed with the help of the effective Lagrangians is gauge invariant. The resonant amplitudes and the u-channel Born contribution are gauge in-

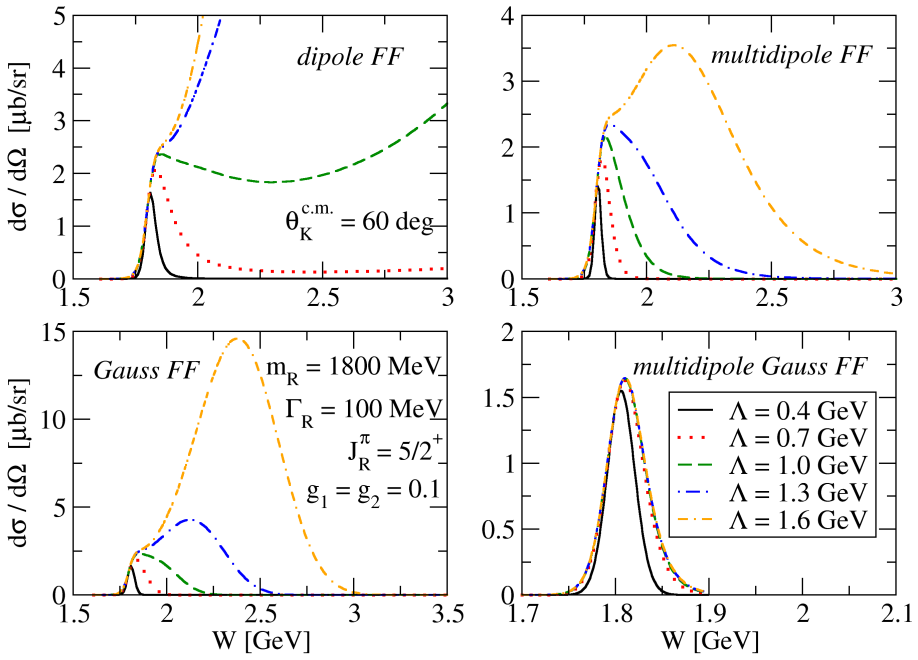

Figure 3.4: Contribution of the spin-5/2 resonance with the mass 1800 and width 100 MeV to the cross section using different form factors. The cutoff-value dependence of the contribution is shown – the larger the cutoff value Λ, the more pronounced the effect.

variant on their own, the gauge non invariant terms occur in the s- and t-channel Born contributions, see Eqs. (A.20) and (A.24) in Appendix A. However, these terms cancel in the sum of these two Born contributions. Unfortunately, while introducing the hadron form factors, these gauge non invariant terms no longer cancel. The remedy is to introduce a contact term which ensures the gauge invariance [57], see Appendix C for more details.

The generally accepted cutoff values lie in the range from approximately 0.7 GeV to 3.0 GeV; the lower the cutoff, the stronger the suppression. The values around the lower limit are considered too soft and the form factors are in this situation regarded as a rather artificial tool to suppress the Born term contribution. As our analysis showed, obtaining a harder cutoff value is much easier than a softer one, which we attribute to the presence of many hyperon resonances in the background.

Values of the cutoff parameters are established when optimizing the model parameters against experimental data. A single common cutoff value Λ_R is assumed for all resonant diagrams whereas for the background terms another value Λ_{bgr} is used.

Chapter 4

An Overview of Regge and Regge-plus-resonance Models

4.1 An Overview of the Regge Model

As was pointed out in the section dealing with the isobar model, a major drawback of such a model is its limited scope in energy. Specifically, a necessary condition for unitarity, the Froissart bound [40], constituting an upper limit on the high-energy behaviour of the cross section is not fulfilled in isobar approaches. A realistic inelastic total cross section is allowed to increase with energy not more than $\ln^2(s/s_0)$, where s_0 is a reference scale conventionally set at 1 GeV. In an isobar model, in contrast, the contribution of background rises as a positive power of s. This rise can be compensated, up to a certain energy, by destructive interferences with other resonant and non resonant contributions. Unfortunately, beyond a few-GeV region, where introducing individual resonances no longer makes sense, unphysical behaviour develops.

In the late fifties, a high-energy framework coined Regge phenomenology [95] was developed as an alternative approach to the isobar model. Regge's starting point was to consider the partial-wave amplitudes as a function of a complex angular momentum

variable. Poles of the amplitude in the complex-momentum frame were suggested to correspond to resonant states which could be classified into several families. The members of such a family, the Regge trajectory, share identical internal quantum numbers, such as strangeness and parity.

At the basis of the Regge theory is the fact that, at energies where individual resonances can no longer be distinguished, the exchange of entire Regge trajectories predominates the reaction dynamics rather than the exchange of individual particles. This high-energy framework applies to the so-called "Regge limit" of extreme forward (in the case of the t-channel exchange) or backward (for the u-channel exchange) scattering angles, corresponding to small $|t|$ or $|u|$, respectively. Since the lightest hyperon, the Λ hyperon, is significantly heavier than a kaon and, therefore, the u-channel poles are located much further from the backward-angle kinematical region than the t-channel poles are from the forward-angle region, the u-channel exchange reggeization, *i.e.* the procedure of requiring the Regge propagator to reduce to the Feynman one at the closest crossed-channel pole, might not lead to good results [29]. What is more, the high-energy data in the backward-angle region are scarce. Therefore, we have chosen to deal with t-channel exchange reggeization only.

Since in the vicinity of the t-channel pole the Regge amplitude is assumed to be identical with the Feynman amplitude for the exchange of the given particle, the Regge theory, in its simplest form, can be formulated by modifying the isobar model. The process of reggeization is quite straightforward and goes as follows: one writes the amplitude for the exchange of the given particle (in the corresponding pole both Feynman and Regge propagators conincide), then interchanges the Feynman propagator with the Regge one,

$$\frac{1}{t - m_X^2} \to \mathcal{P}^X_{Regge}(\alpha_X(t)),$$

and the remnant terms in the amplitude then labels as a Feynman residuum β_X. The amplitude constructed in this way includes effectively exchanges of all particles represented by the given trajectory and reads

$$\mathbb{M}_{Regge}(s,t) = \beta_X(t)\mathcal{P}^X_{Regge}(s, \alpha_X(t)). \tag{4.1}$$

In the case of $K\Lambda$ production, we reggeize contributions of $K^+(494)$ and $K^{*+}(892)$ amplitudes only. For more details on Regge trajectories and propagators see Appendix B.

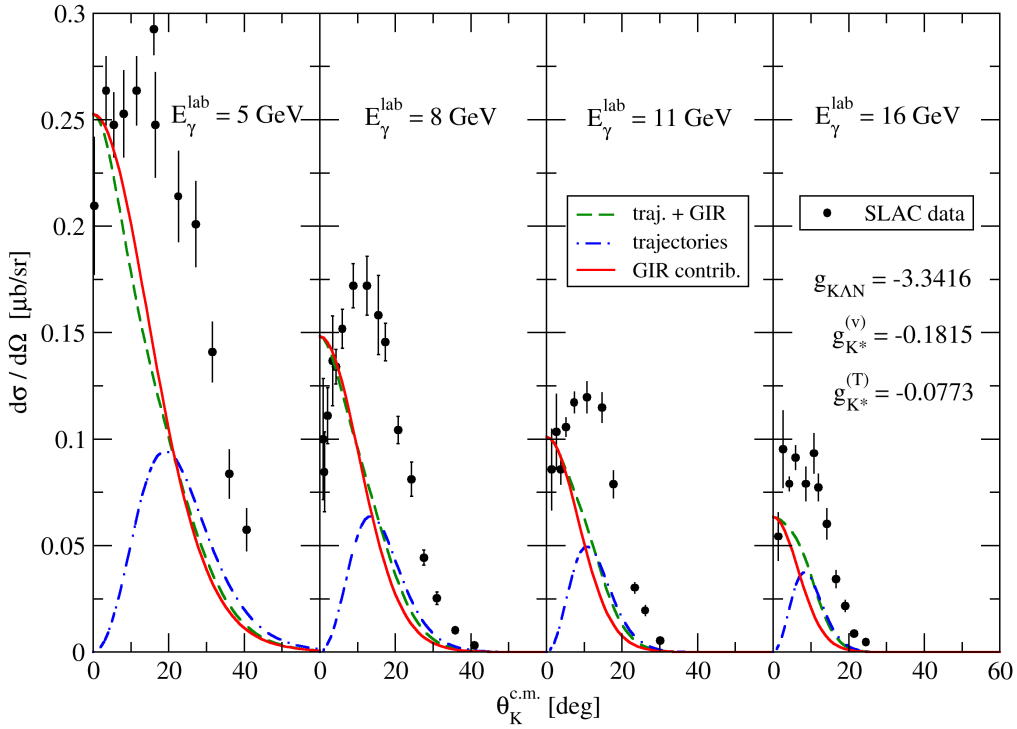

Figure 4.1: The contributions of a Regge part, *i.e.* kaon trajectories and a gauge-invariance fixing term (dashed line), and separately of kaon trajectories (dash-dotted line) and a gauge-invariance fixing term (solid line) to the cross section beyond the resonance region. The predictions were made with one of the best results of the fitting procedure (with $\chi^2/\text{n.d.f.} = 2.56$). The data stem from the SLAC collaboration [16].

In the approach in terms of Feynman diagrams, it is well-known that the t-channel kaon exchange diagram alone is not able to satisfy the gauge invariance. In order to restore gauge invariance, the Regge amplitude for $K\Lambda$ photoproduction should, apart from the $K^+(494)$ and $K^{*+}(892)$ trajectory exchanges, also include a contribution from the electric part of the s-channel Born term (when using pseudoscalar coupling) or from the electric part of the s-channel Born term and a contact term (when using pseudovector coupling) [47]. Since we use the pseudoscalar coupling, it is sufficient to introduce the electric part of the s-channel Born term only. The full amplitude of the Regge model for the $\gamma p \to K^+\Lambda$ process then reads

$$\mathcal{M}_{Regge} = \mathcal{M}_{Regge}^{K^+(494)} + \mathcal{M}_{Regge}^{K^{*+}(892)} + \mathcal{M}_{Feyn}^{p,el} \times \mathcal{P}_{Regge}^{K^+} \times (t - m_{K^+}^2). \qquad (4.2)$$

An anomalous magnetic coupling proportional to $\sigma^{\mu\nu}$ is not included because of the duality hypothesis according to which only all s-channel or all t-channel poles can be included [29]. A combination of both s- and t-channel contributions may lead to double counting of poles. Since in the Regge model we take into account all t-channel poles, the amount of additional poles in the s channel should be reduced to minimum.

Since experimental data in the forward-angle region are scarce, the model predictions are vital for understanding the reaction dynamics in this area. It is not clear whether the cross section shall decrease with kaon center-of-mass angle $\theta_K^{c.m.}$ or rather produce a peak around $\theta_K^{c.m.}$ of 15°. In the Regge model, there are contributions from kaon trajectories and the gauge-fixing term only. As it can be seen in Figure (4.1), the contributions of kaon trajectories produce peak behaviour, whereas the contribution of the gauge-invariance fixing term leads to a decrease in the cross section with kaon angle. The strength of contributions of the gauge-invariance fixing term and the $K^+(494)$ trajectory is governed by the sole coupling constant, $g_{K\Lambda N}$, whereas the K^{*+} trajectory contributes in compliance with its coupling constants $G^{(v,t)}_{K^{*+}}$. Generally, the smaller is the coupling constant $g_{K\Lambda N}$, the more noticeable is the effect of the gauge-invariance fixing term, see Figure (4.3). Apart from the values permitted by the $SU(3)_f$ constraint, we computed the contributions for values of $g_{K\Lambda N}$ beyond the upper limit as well. As it is seen in the Figure (4.3), the contributions of both gauge-invariance fixing term and the $K^+(494)$ trajectory tend to be almost negligible in this case. Moreover, the addition of the $K^+(494)$ trajectory to the gauge-fixing term seems to lead only to a moderate modification of the cross section in the region of central kaon angles, *i.e.* it hardly affects the prediction behaviour in the very forward-angle region, see Figure (4.3). The same holds also for the K^{*+} trajectory which alters the cross-section prediction by the gauge term slightly, even though the trajectory predictions on their own change significantly with the coupling constants $G^{(v,t)}_{K^{*+}}$, see Figure (4.4). What is more, the cross-section predictions are almost independent of the relative sign between the vector $G^{(v)}_{K^{*+}}$ and tensor $G^{(t)}_{K^{*+}}$ coupling of the K^{*+} trajectory. In contrast, the magnitude of the K^{*+} trajectory couplings is important: whereas the value of $g_{K\Lambda N}$ creates a decreasing shape of the cross section, the vector $G^{(v)}_{K^{*+}}$ and tensor $G^{(t)}_{K^{*+}}$ coupling of the K^{*+} trajectory tend to produce a peak in the cross section. Therefore, if the contribution of the K^{*+} trajectory is strong enough, its contribution prevails and the peak develops, see Figure (4.2).

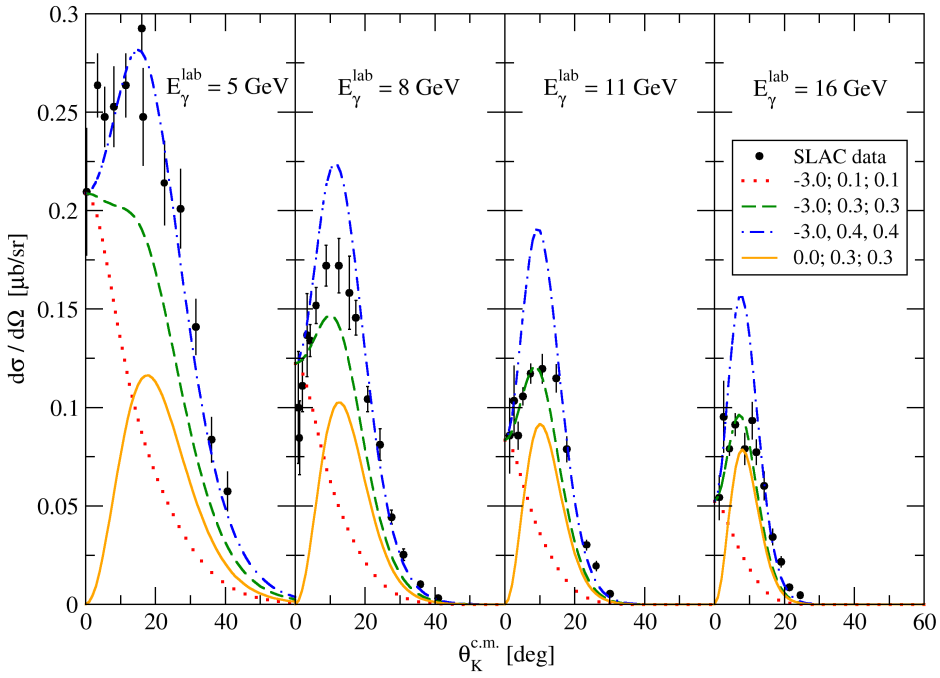

Figure 4.2: The Regge contribution to the cross section is shown for various values of coupling constants. The values in the legend correspond to $g_{K\Lambda N}$, $G^{(v)}_{K^{*+}}$, and $G^{(t)}_{K^{*+}}$ coupling constants, respectively. The dotted, dashed, and dash-dotted lines show the cross-section prediction as a combination of gauge-fixing term, $K^+(494)$, and K^{*+} trajectories, whereas the solid line depicts the contribution of K^{*+} trajectory solely.

At this place, we should note that the SLAC data, shown in Figures 4.1 and 4.2 may be a subject of reanalysis since their comparison with the other data sets, particularly with CLAS data, reveals their wrong normalization. Although both data sets agree in shape, the CLAS cross-section data are systematically lower than the SLAC data approximately by a factor of two [37]. The SLAC data set was, therefore, not used in the fitting procedure of ours and is used merely as an illustration in the considered figures. Nonetheless, we presume that the angular dependence, with a peak at $\theta_K^{c.m.}$ of approximately 15°, will not change in the reanalysis.

It seems that there is only one way to produce a cross section which decreases with kaon angle. This can be accomplished through replenishing the kaon trajectories with the electric part of the Born s-channel term acting as a gauge-fixing mechanism. Moreover, its contribution must be large enough in comparison with the contribution of the K^{*+} trajectory in order to prevent the peak around $\theta_K^{c.m.}$ of 10° from appearing in the cross

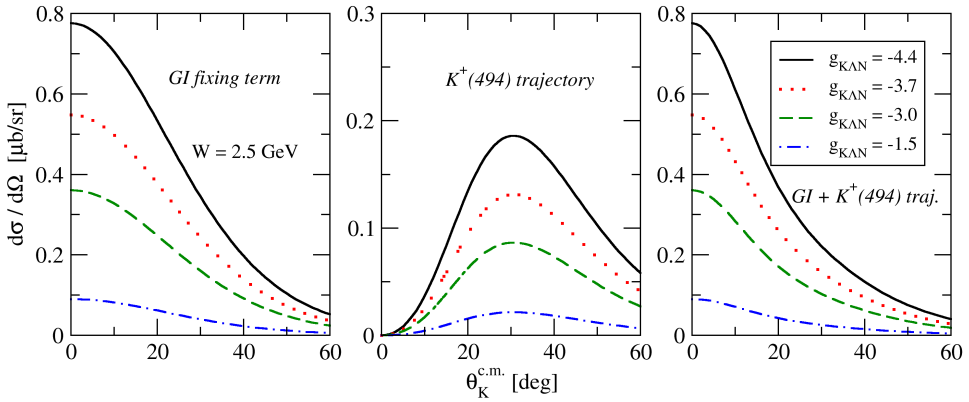

Figure 4.3: Contributions of the gauge-invariance fixing term (left), the $K^+(494)$ trajectory (centre), and combination of both (right) are shown for various values of the coupling constant $g_{K\Lambda N}$. The smaller the coupling constant, the more tangible the effect. For $g_{K\Lambda N} \geq -3.0$, the decrease in the cross section is almost not apparent any more.

section, see Figure (4.2).

The main asset of the Regge model is a reduced number of free parameters to be adjusted to experimental data. There are only three free parameters: $g_{K\Lambda N}$ and $G^{(v,t)}_{K^{*+}}$. However, at energies well beyond the resonance region (*i.e.* for $E^{lab}_{\gamma} > 4\,\text{GeV}$), where these parameters should be fixed by experimental data, there is a limited amount of data accessible: for the $K^+\Lambda$ channel there are merely 72 data, including 56 differential-cross-section data [16], 9 beam-asymmetry data [94], and 7 hyperon-polarization data [118].

4.2 An Overview of the Regge-plus-resonance Model

Although the Regge theory is a high-energy tool by construction, it can reproduce the order of magnitude of the forward-angle pion and kaon photoproduction [29] and kaon electroproduction [48] observables remarkably well even in the resonance region. Nevertheless, it is evident that a pure non resonant description, such as the Regge model, cannot be expected to describe the reaction at energies in the resonance region [29]. The cross section near threshold exhibits structures, such as peaks at certain energies, which might reflect the presence of individual resonances. These are incorporated into the Regge-plus-resonance (RPR) model by extending the reggeized background with a small number of resonant s-channel diagrams. For these diagrams, standard Feynman propagators are assumed where, as in the isobar approach, the resonance finite lifetime

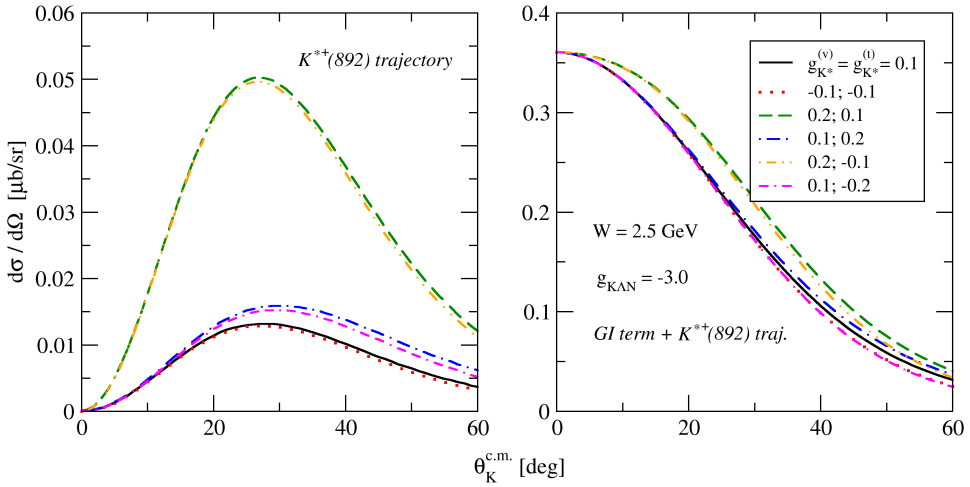

Figure 4.4: Contributions of the $K^{*+}(892)$ trajectory (left) and the combination of the $K^{*+}(892)$ trajectory with a gauge-invariance fixing term (right) are shown for various values of the coupling constants $G^{(v,t)}_{K^{*+}}$ determining the behaviour of the $K^{*+}(892)$ trajectory.

is taken into account through the substitution $s - m_R^2 \to s - m_R^2 + \mathrm{i} m_R \Gamma_R$ in the propagator denominator with the m_R and Γ_R the mass and width of the propagating state, respectively.

This connection between the high- and low-energy region is related to the duality hypothesis which states that the sum of all Regge poles occuring in the t channel through the exchange of Regge trajectory equals the sum of all resonant contributions in the s channel [29]. Thus, in order to avoid double counting, we identify only a small number of dominant resonances and supplement with them the phenomenological background stemming from pure Regge approach. Since the $p(\gamma, K)Y$ processes are largely dominated by background contributions, the few s-channel contributions might be considered rather as subsidiary corrections and, therefore, the double counting is not expected to be a significant issue [29].

The greatest merit of the RPR framework, apart from its wide energy range, consists in its graceful depiction of the non resonant part of the reaction amplitude: only three free parameters are introduced. The isobar models need a significantly larger number of free parameters to describe the background part of the amplitude. Typically, isobar background contribution is comprised of Born terms replenished with $K^*(892)$ and $K_1(1272)$

exchange diagrams and, in many cases, also with hyperon exchanges in the u channel. What is more, the matter of unreasonably large strength of the Born terms does not emerge in the non resonant part of the RPR-model amplitude. As a consequence, no hadron form factors are introduced for the background terms, which makes another difference in the reaction mechanism of the isobar and RPR model. This distinction seems to be of importance particularly for description of the cross section at very small kaon angles [22]. Moreover, we avoid the inclusion of another free parameter, the background cutoff parameter.

In order to retain the RPR approach reasonable, the resonance contributions should vanish in the high-energy region. This is achieved with the help of hadron form factors which should be strong enough not to allow the resonant terms to contribute beyond the resonance region. For this purpose, one usually opts for a multidipole or multidipole-Gaussian shape of the hadron form factor since these two ones fall off with energy much more sharply than, *e.g.* the dipole form factor. Therefore, only the Regge part of the amplitude remains in the high-energy region.

During the fitting procedure, we considered both multidipole and multidipole-Gaussian shapes of the form factor. The use of the former one leads to a smaller χ^2 value than the use of the latter one. Moreover, the cutoff parameter of the multidipole form factor acquires a value of around 1.5 GeV whereas when we assume the multidipole-Gaussian form factor the cutoff parameter is slightly bigger than 2.0 GeV. As it can be seen in the Figure (3.4), the multidipole shape of the form factor is not as strong as the multidipole-Gaussian form factor and lets the non physical behaviour, *e.g.* the second peak in the cross section, develop. In the high-energy region, however, both form factors act satisfactorily as they do not allow the resonances to contribute far beyond the resonance region. Since the multidipole-Gaussian form factor is stronger than the multidipole one by definition, it often obtains a higher value of the cutoff parameter than the multidipole one in order to suppress the contribution of resonant terms equally. In other words, the multidipole form factor needs a lower value of the cutoff parameter to behave similarly to the multidipole-Gaussian form factor with a higher cutoff.

On the contrary, we do not regard a dipole shape of the form factor as a suitable one for the RPR framework since it cannot reliably suppress the nucleon resonances beyond the resonance region. Even though the cutoff parameter of the dipole form factor is

chosen as small as 1 GeV (or even smaller), it still produces non physical behaviour and lets the cross section diverge. Whereas the χ^2/n.d.f. values of models assuming a dipole form factor are comparable with results assuming other form-factor shapes, such models cannot be used for a dependable prediction of the observables.

In the section dealing with the Regge background, it was pointed out that the gauge-fixing term is the one which influences the cross-section prediction at the forward angles most. Little did we say about the resonant contributions which play an important role in this kinematical region as well. Whereas the contributions of sole nucleon resonances are almost zero, there certainly occurs destructive interference between resonant and background terms, which produces cross-section prediction in accordance with experimental data. Probably the most interesting is the contribution of spin-5/2 nucleon resonances, which interferes with background terms in such a way that the spin-1/2 and spin-3/2 nucleon resonances constitute merely a soft amendment to the full-model prediction, see Figure (4.5). While there are non zero contributions of individual amplitude parts at the forward angles, the contributions of background and nucleon resonances separately are almost zero at backward angles. Since, unlike the isobar model, there are no hyperon resonances in the u channel, which would participate in the amplitude and take care of the backward-angle region, the model predictions at backward angles are, in all probability, dominated by interference effects among contributions of resonant terms.

Interestingly, the models coming out of the fitting procedure of ours are able to describe the cross section reliably not only in the forward-angle region but they depict backward angles dependably as well. This is achieved mainly through the inclusion of many nucleon resonances which substitute the hyperon resonances of the isobar model. Since the interference effects among many resonant terms play a substantial role, we are not able to select the sole resonance which contributes most. However, when we omit P1(1870) from the full model, the model fails to reproduce the peak around W of 1.9 GeV, see Figure (4.6), which indicates this resonance to be a dominant one in the backward-angle region. Similar but much less pronounced behaviour can be reached when one omits the N9(1875) resonance. Furthermore, it is apparent that the resonant terms interfere destructively with the background contribution in the near-threshold region in order to suppress the peak around W of approximately 1.65 GeV. Subsequently, the N4(1650) may be of importance as well since its presence leads to a significant drop of the cross-section

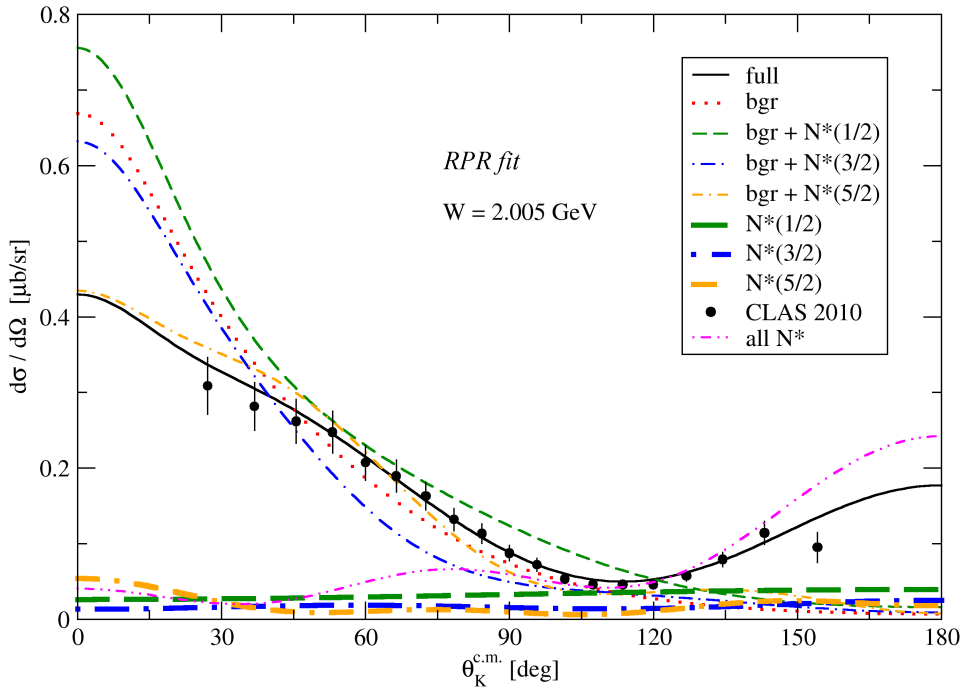

Figure 4.5: Angular dependence of the differential cross section as predicted by the new RPR fit of ours is shown and compared with data stemming from CLAS 2010 [82]. Contribution of sole background, nucleon resonances, and combination of both is shown as well.

prediction, see Figure (4.6).

Variants of the Regge and Regge-plus-resonance Approaches

The first simple Regge model for calculation of high-energy K^+ photoproduction has been constructed by Levy *et al.* [65] using degenerate $K^{*+}(892)$ and $K^{*+}(1420)$ Regge trajectories and the absorption of the low partial waves. However, this approach was criticised in a subsequent analysis by Guidal *et al.* [47]. Whereas the model of Levy *et al.* is not gauge invariant and creates peaks in the differential cross section at large $-t$ that are not observed experimentally, Guidal *et al.* explained that there is no need to introduce absorption or rescattering effects to describe the data and created a model which is gauge invariant.

The Regge-plus-resonance model, capable of describing forward-angle $K^+\Lambda$ photoproduction from the proton, was first published by Corthals *et al.* [29]. While restricting

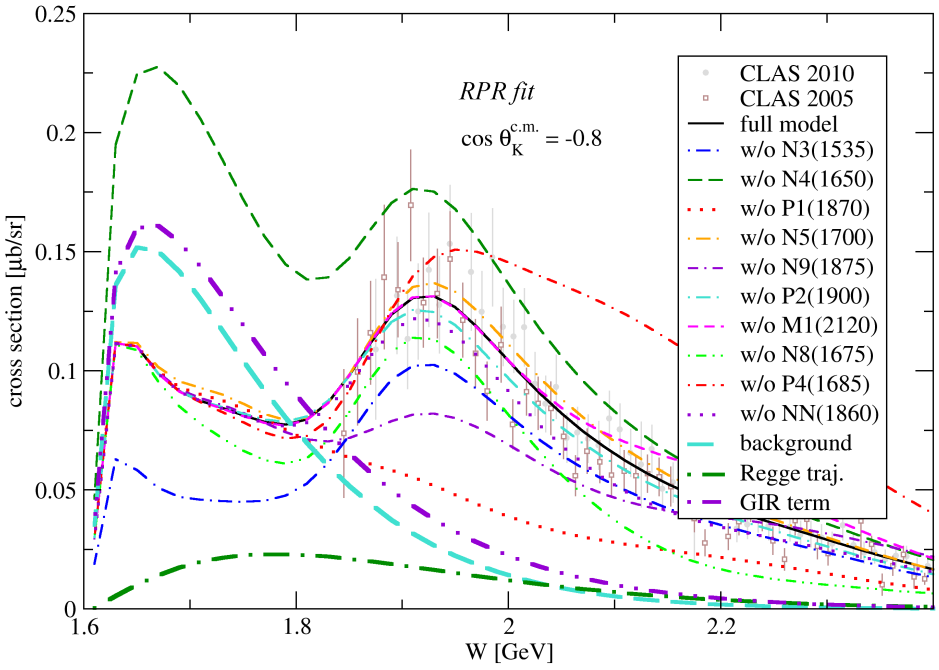

Figure 4.6: The cross-section prediction of the new RPR fit of ours for the very backward angles is shown. Contributions of background, Regge trajectories, and the gauge-invariance restoring term are shown in comparison with the prediction of the full model without a particular resonance.

to nucleon resonances with spin no higher than 3/2, they have exploited the $p(\gamma, K^+)\Lambda$ data for $\cos\theta_K^{c.m.} > 0.35$ to arrive at values of background and resonant couplings [113]. Besides identifying the "core" set of N^*'s contributing to the process, *i.e.* $S_{11}(1650)$, $P_{11}(1710)$, and $P_{13}(1720)$, which can produce good description of the $p(\gamma, K^+)\Lambda$ dynamics in the region under investigation, they showed that the option of rotating K^+ and K^{*+} trajectory phases is not compatible with data in the resonance region [29]. Moreover, they showed that the inclusion of a new resonance to the core set improves the agreement with data significantly and, therefore, they supplemented the core set of N^*'s with the $D_{13}(1900)$ and $P_{13}(1900)$ states, which led to a model coined RPR-2007.

Implementing the consistent formalism for high-spin fermions [115], De Cruz *et al.* [35] performed a robust analysis [55] of 2048 model variants resulting from considering various combinations of 11 N^*'s by computing the Bayesian evidence values against the available $p(\gamma, K^+)\Lambda$ data. Interestingly, all of the best models featuring more than two free parameters contain at least one of the missing resonances. The two best results of the optimizing

procedure were coined RPR-2011A and RPR-2011B which appear to be almost equivalent in $p(\gamma, K^+)\Lambda$ data description and are able to make fair predictions of $p(e, e'K^+)\Lambda$ process [34]. Whereas the former model includes 8 nucleon resonances, namely $S_{11}(1535)$, $S_{11}(1650)$, $F_{15}(1680)$, $P_{13}(1720)$, $P_{11}(1900)$, $P_{13}(1900)$, $D_{13}(1900)$, and $F_{15}(2000)$, the latter one is more economical and contains only 5 N^*'s: $S_{11}(1535)$, $S_{11}(1650)$, $P_{11}(1710)$, $P_{13}(1720)$, $D_{13}(1900)$.

Chapter 5

The Fitting Procedure in Detail

5.1 Adjusting Free Parameters of the Isobar Model

Since the isobar model is an effective model with the coupling constants and cutoff values of hadron form factors undetermined, our goal is to fixate these free parameters to the experimental data during the fitting process.

The free parameters to be adjusted are the coupling constants of the Born terms $g_{K\Lambda N}$ and $g_{K\Sigma N}$, the nucleon, kaon, and hyperon resonances and two cutoff parameters of the hadron form factor. Each spin-1/2 resonance contributes with one parameter whereas higher-spin resonances as well as kaon resonances contribute with two parameters. As well as in the well-known Kaon-MAID model, we assume a single cutoff value Λ_R for all resonant (s-channel) diagrams whereas for background terms another value Λ_{bgr} is used. Altogether, the number of free parameters varies from 25 to 30 depending on the number and spin of considered nucleon and hyperon resonances.

In order to test whether a given hypothetical function describes the given data well, the χ^2 is calculated. The optimum set of free parameters $(c_1, \ldots, c_n)$ for a given set of

data points $(d_1, \ldots, d_N)$ is that with the lowest value of χ^2. The χ^2 is

$$\chi^2 = \sum_{i=1}^{N} \frac{[d_i - p_i(c_1, \ldots, c_n)]^2}{(\sigma_{d_i}^{tot})^2}, \tag{5.1}$$

where N and n are the number of data points and the number of free parameters, respectively, while p_i represents the theoretical prediction of observables (differential cross section, hyperon polarization and beam asymmetry in our case) for the measured data point d_i with the total error given as

$$\sigma_{d_i}^{tot} = \sqrt{(\sigma_{d_i}^{sys})^2 + (\sigma_{d_i}^{stat})^2}, \tag{5.2}$$

where $\sigma_{d_i}^{sys}$ and $\sigma_{d_i}^{stat}$ represent systematic and statistical errors of a given datum, respectively. Whereas systematic errors tend to be strongly correlated within a given data set, the correlation weakens when one uses several independent subsets. Since we assume several data sets (see Subsection D), we have adopted the definition (5.2) similarly to the analysis by Adelseck and Saghai [3]. Some groups, *e.g.* the Ghent group, use even more conservative prescription for the total error [35, 36].

In order to obtain the optimum set of parameters, one is forced to minimize χ^2 in the n dimensional space. In the ideal case, $\chi^2 = \text{n.d.f.}$, where $\text{n.d.f.} = N - n$ is the number of degrees of freedom.

The minimization was performed with the help of the least-squares fitting procedure using the MINUIT code [56]. Since MINUIT uses a non linear transformation for the parameters with limits, which makes worse the accuracy of the resulting parameter when it approaches a boundary value, the limits should be avoided if they are not necessary to prevent the parameters from reaching non physical values. The main coupling constants $g_{K\Lambda N}$ and $g_{K\Sigma N}$ were kept inside the limits of 20% broken SU(3) symmetry

$$-4.4 \leq \frac{g_{K\Lambda N}}{\sqrt{4\pi}} \leq -3.0, \tag{5.3a}$$

$$0.8 \leq \frac{g_{K\Sigma N}}{\sqrt{4\pi}} \leq 1.3. \tag{5.3b}$$

In order not to get too soft or too hard form factors, the cutoff parameters of the hadron form factor were kept inside the limits from 0.7 GeV to 3.0 GeV.

The coupling parameters entering the fitting procedure are always products of the strong and electromagnetic coupling constants. In order to guarantee a correct dimension

of the interaction Lagrangians, the coupling constants have to be normalized appropriately. Since the interaction Lagrangian for the spin-3/2 nucleon resonance contains two derivatives of the R-S field (due to the gauge invariance), the coupling parameters read (see Appendix A)

$$G_1 = \frac{f g_1}{m_R^2 m_K (m_R + m_p)}, \tag{5.4a}$$

$$G_2 = \frac{f g_2}{m_R^2 m_K (m_R + m_p)}. \tag{5.4b}$$

In the case of spin-3/2 hyperon resonances, m_p is replaced with m_Λ. Analogously, the spin-5/2 coupling parameters are normalized as follows (see Appendix A)

$$G_1 = -\frac{f g_1}{16 m_K^4 m_p^4}, \tag{5.5a}$$

$$G_2 = -\frac{f g_2}{32 m_K^4 m_p^5}. \tag{5.5b}$$

The high mass powers in the denominator result in very small values of G_i for $N^*(5/2)$ in comparison with the coupling parameters of lower-spin nucleon resonances.

The hyperon coupling parameters tend to be very large compared with coupling parameters of other resonances. Therefore, we did not take into account results with hyperon coupling parameters boldly bigger than ten.

The overview of experimental data used in the fitting procedure is given in Appendix D.

Results of Fitting the Isobar-Model Parameters

While minimizing the χ^2 it is important to find a global minimum. Since this task occurs in a huge parameter space that has a lot of local minima, the result of the fitting procedure often depends on starting values of the fitted parameters.

Generally, choosing the best solution is not an easy task. The χ^2 value is only a mathematical tool showing the goodness of a fit. However, results with similar χ^2 values can still give rather different predictions of the observables in some kinematic regions. Therefore, not only thorough inspection of the numerical values of the fitted parameters, but also a brief check of the predicted observables is welcome.

We have done several hundreds of fits considering various resonance configurations and different shapes of the hadron form factor. While the set of nucleon resonances chosen in

the RPR-2011A model provided us with a starting point, we have considered many other resonant states during the procedure of fitting.

Since one cannot be sure that the detected minimum is the global one, we have selected several models with similar χ^2. The models differ mainly in the choice of nucleon and hyperon resonances and their coupling constants, cutoff values of the hadron form factor and the shape of the form factor. Particularly, the smallness of hyperon coupling constants plays an important role when deciding if the model should be rejected or not. Since the isobar model is only a tree-level approximation, the couplings larger than one are still justifiable.

During the fitting procedure, we also tried to slightly modify the mass and width of several intermediate particles in the ranges provided by the Particle Data Tables 2014 [88] (or when there were no preferred values). On the one hand, this forced the models to improve their description of the cross section – particularly the reduction of the width of P2 resonance from 500 MeV to a value of about 400 MeV or less led to filling up the second peak in the cross-section data. On the other hand, the modification of the width of P2 resulted in a growth of the χ^2 value and made the description of single-polarization observables worse.

In order to gain insight into the effect of high-spin resonances on the observables, some of the fits were performed with the inconsistent formalism for the spin-3/2 and spin-5/2 resonances used in the SL model. Particularly, the fit of the BS2 model (see below) with the inconsistent formalism led to an enlargement of the χ^2 from 1.64 to 1.91, growth of the cutoff parameter for hadron form factor to almost 3 GeV and decrease of the cross-section prediction in the forward-angle region. In this fit we omitted the spin-3/2 hyperon resonance S4. Generally, the use of the inconsistent high-spin formalism results in larger couplings for spin-5/2 resonances which is due to a different normalization introduced into the coupling parameters (see Equation (5.5)).

The main asset of the presence of high-spin hyperon resonances is the reduction of coupling parameters of spin-1/2 hyperon resonances. With no $Y^*(3/2)$ introduced, the couplings of $Y^*(1/2)$ tend to acquire values at the order of ten or even more. While the $Y^*(3/2)$ are implemented, the couplings of both $Y^*(1/2)$ and $Y^*(3/2)$ are only exceptionally bigger than ten.

In the analysis, we examined the effect of distinct shapes of hadron form factor on the resonance behaviour. As seen from the definition (3.14), the multidipole form factor affects the resonance behaviour more strongly than the dipole one. Therefore, introducing the multidipole form factor generally leads to bigger cutoff parameters for resonances ($\Lambda_{res} \sim 3\,\mathrm{GeV}$) than considering the dipole form factor ($\Lambda_{res} \sim 2\,\mathrm{GeV}$). Unfortunately, we were not able to achieve a single result with $\chi^2 < 2$ using the multidipole-Gaussian form factor. This shape of form factor was introduced by the Ghent group in their Regge-plus-resonance model to strongly suppress the contribution of the nucleon resonances in the high-energy regime. However, it seems that there is no need for introducing such a strong form factor in the isobar model.

The predictions of the models with $\chi^2 < 2$ were tested in the comparison with the experimental data. Particularly, the comparison with hyperon polarization data can reveal a subtle interplay among many resonances. Even though the smallness of χ^2 denotes a good agreement of the model prediction with the data, in the kinematic regions where data are scarce (*e.g.* forward-angle region) the model predictions can still differ.

The best solutions regarding the smallness of the χ^2, values of fitted parameters and correspondence with data were coined BS1 and BS2. Whereas the model coined BS1 was obtained using a multidipole form factor, the BS2 model was gained using a dipole shape of the form factor. Moreover, the mass of the P5 resonance was slightly modified from 1820 MeV in the BS1 model to 1860 MeV in the BS2 model (see Table 5.1 for details).

5.2 Adjusting Free Parameters of the RPR Model

As the Regge-plus-resonance model is an effective model, as well as the isobar model, there are again a number of free parameters to be adjusted to the experimental data. However, since the description of background in the RPR model is very different and much simplier from the one of isobar model, there are much less free parameters in this case.

The set of free parameters consists above all of parameters of nucleon resonances: each spin-1/2 resonance introduces one free parameter whereas every spin-3/2 resonance requires two parameters to be determined. To this set, we add merely three parameters of background, namely $g_{K\Lambda N}$ and $G^{(v,t)}_{K^{*+}}$ which govern the strength of the gauge-fixing-term and $K^+(494)$-trajectory and $K^{*+}(892)$-trajectory contributions, respectively. We

recall that the $g_{K\Lambda N}$ and $G^{(v,t)}_{K^{*+}}$ parameters are the coupling constants at vertices of the first materialization of the corresponding trajectories. Furthermore, we introduce only one free parameter of the hadron form factor: the cutoff parameter for resonant terms. In total, there are from 20 to 25 free parameters depending on the number and spin of considered nucleon resonances. As well as in the isobar-model fit, the $g_{K\Lambda N}$, as the only parameter this time, was not allowed to vary freely but it was kept within the limits of Equation (5.3a).

The use of χ^2 minimization method, definition of total error and normalization for coupling constants of high-spin fields are comprehensively given in Section 5.1 and we will, therefore, skip directly to the outcomes of the fitting procedure.

Results of Fitting the RPR Parameters

Since the study with the RPR model followed the analysis exploiting the isobar approach, where we have identified two sets of N^*'s as the most appropriate ones for data description, we used the nucleonic content of BS models as the starting point in selecting appropriate resonances for data description using the RPR model. However, this starting set led to χ^2/n.d.f. around 3 (N^*'s from BS1 and BS2 let to χ^2/n.d.f. = 3.02 and χ^2/n.d.f. = 2.87, respectively) which still leaves room for improvement. We therefore varied the N^* content and also opted for a couple of N^* states which we have not included in our analysis before; specifically $N^*(2120)$, $N^*(2300)$, and $N^*(2570)$.

In the RPR approach, we need the N^*'s to vanish beyond the resonance region, which can be done with the help of strong hadron form factors, particularly with the multidipole-Gaussian one, Equation (3.14d). Nevertheless, we also examined how other shapes of a form factor, which are rather weaker than the multidipole-Gaussian one by definition, tend to suppress the N^*'s above the resonance region. The only one which can substitute the multidipole-Gaussian form factor and suppress the N^*'s above the resonance region sufficiently is the multidipole form factor. Apparently, the multidipole form factor with a cutoff value Λ around 1.5 GeV behaves similarly to the multidipole-Gaussian form factor with $\Lambda \approx 2.1$ GeV. Provided we use the other shapes of the form factor, *i.e.* dipole or Gaussian shape, the strong-momentum dependence in the amplitude of the high-spin resonance contribution might prevail the cutting behaviour of a form factor and the cross section then could become divergent in the high-energy domain (this holds for a dipole

	BS1	BS2	KM	SL	RPR fit
$g_{K\Lambda N}$	−3.00	−3.00	−3.80	−3.16	−3.47
$g_{K\Sigma^0 N}$	1.11	0.80	1.20	0.91	–
$G_V(K^*)$	−0.18	−0.17	−0.79	−0.05	−0.20
$G_T(K^*)$	0.02	−0.03	−2.63	0.16	−0.08
$G_V(K_1)$	0.28	0.30	3.81	−0.19	–
$G_T(K_1)$	−0.28	−0.23	−2.41	−0.35	–
$G(N1)$	–	–	–	−0.02	–
$G(N3)$	0.10	0.17	–	–	0.09
$G(N4)$	−0.07	−0.05	−0.13	–	−0.07
$G(N5)$	–	–	–	–	0.09
$G(N5)$	–	–	–	–	0.06
$G(N6)$	–	−0.05	−0.26	–	–
$G_1(N7)$	−0.09	−0.07	0.05	−0.04	–
$G_2(N7)$	−0.01	−0.0057	0.61	−0.14	–
$G_1(N8)$	–	–	–	−0.63	−0.001
$G_2(N8)$	–	–	–	−0.05	−0.04
$G_1(P4)$	0.21	0.23	1.10	–	0.05
$G_2(P4)$	0.26	0.26	0.63	–	−0.07
$G_1(P5)$	−0.04	−0.02	–	–	−0.01
$G_2(P5)$	0.04	0.02	–	–	0.01
$G_1(P1)$	–	–	–	–	−0.45
$G_1(P2)$	0.11	0.09	–	–	0.01
$G_2(P2)$	−0.02	−0.01	–	–	0.007
$G_1(P3)$	−0.0003	−0.0018	–	–	–
$G_2(P3)$	−0.0029	−0.0015	–	–	–
$G_1(N9)$	0.05	0.03	–	−0.63	0.03
$G_2(N9)$	−0.05	−0.03	–	−0.05	−0.04
$G_1(M1)$	–	–	–	–	0.06
$G_2(M1)$	–	–	–	–	0.05
$G(L1)$	–	9.67	–	−0.42	–
$G(L3)$	–	–	–	1.75	–
$G(L4)$	−8.39	−11.55	–	–	–
$G(L5)$	–	–	–	−1.96	–
$G_1(L6)$	0.86	–	–	–	–
$G_2(L6)$	−0.09	–	–	–	–
$G_1(L8)$	−2.33	–	–	–	–
$G_2(L8)$	0.0033	–	–	–	–
$G(S1)$	−11.58	−8.09	–	−7.33	–
$G(S2)$	15.77	–	–	–	–
$G_1(S4)$	−8.32	−0.86	–	–	–
$G_2(S4)$	0.81	0.18	–	–	–
Λ_{bgr}	1.88	1.94	0.64	–	–
Λ_{res}	2.74	2.15	1.04	–	1.53
χ^2/n.d.f.	1.64	1.64	–	–	2.32

Table 5.1: Coupling constants, cutoff values, and χ^2 values of the final BS1 and BS2 models and the RPR fit are compared with parameters of the well-known Kaon-MAID and Saclay-Lyon models.

form factor with a cutoff parameter even as small as 0.9 GeV). This again indicates the necessity of introducing a strong form factor so that the observables remain well-behaved beyond the resonance region. According to the value of χ^2, results of the new analysis of ours slightly prefer the choice of the multidipole form factor with a low cutoff parameter to the option for the multidipole-Gaussian form factor with the cutoff parameter slightly higher than 2 GeV.

The best solution which we found is the one with the smallest value of χ^2 and in accordance with experimental data. In this best fit, which we refer to simply as the RPR fit throughout this work, the resonant content overlaps only partly with that in either BS models or in the RPR-2011A model (*e.g.* only six out of ten nucleon resonances are the same in both cases), the multidipole shape of the form factor is employed and the χ^2/n.d.f. acquires a value of 2.32, see Table 5.1 for details.

In the past, before we derived the formulae for high-spin nucleon resonances in the consistent formalism, we had performed a fit exploiting the inconsistent formalism for high-spin N^*'s. At that time, we used the set of five N^*'s which were selected in the version RPR-2011B [35, 36] of the Ghent RPR model as a starting point in the fitting procedure and subsequently varied the N^*'s included in the model. We ended up, however, with the same nucleon resonances which we originally had and the only difference between results of our analysis and the analysis of the Ghent group is thus the values of coupling constants. We coined the resulting models RPR-1 and RPR-2 [21, 22] and it is important to note that they differ in the set of data we used in the fit. Both of the models were fitted to the cross-section data of CLAS and LEPS collaborations; the RPR-1 model to data of the whole angular range while the RPR-2 model only to the data in the forward hemisphere (*i.e.* $\theta_K^{c.m.} < 90°$). The major difference between these two models lies in the description of the non resonant part of the amplitude since magnitudes and signs of coupling constants of K^+ and K^{*+} trajectories vary in both models, which might be important for predictions of the cross section at very small kaon angles and higher energies [22]. The RPR-2 model, having positive relative sign between the vector and tensor coupling constants of the K^{*+} trajectory, predicts a steep angular dependence of the cross section beyond the resonance region. As the subsequent analysis of ours showed, the magnitude of $g_{K\Lambda N}$ coupling constant might be crucial at small kaon angles as well: it governs the strength of the gauge-fixing-term contribution which produces (in

combination with kaon trajectories) either a peak around $\theta_K^{c.m.} = 20^\circ$ in the cross section (for higher values of $g_{K\Lambda N}$) or a decreasing cross section with kaon angle (for lower values of $g_{K\Lambda N}$). Note that in the RPR-1 model the $g_{K\Lambda N}$ was allowed to vary freely, which led to its value of -1.45 being slightly outside of the limits usually imposed on $g_{K\Lambda N}$.

Chapter 6

A Study of the $p(\gamma, K^+)\Lambda$ Process

In this section, we present the new isobar models BS1 and BS2 and the new Regge-plus-resonance fit for photoproduction of $K^+\Lambda$ and compare their predictions for the cross section, hyperon polarization, beam asymmetry, and target asymmetry with the data and results of the older models Saclay-Lyon and Kaon-MAID and the RPR-2011A model. Note that the numerical results of the Saclay-Lyon and Kaon-MAID models have been obtained by using our code with the parameters presented in Table 5.1; the results of the RPR-2011A model originate from the web page [106] where all the RPR models of the Ghent group are available for calculations.

The nucleon-resonance content of the BS1 and BS2 models almost does not differ, see Table 5.1. In comparison with the BS1 model, the BS2 model contains only one more resonance, the $P_{11}(1710)$, with a small coupling constant. The coupling constants of the other nucleon resonances have the same sign and their values are very similar. This set of N^*'s significantly overlaps with that suggested by the Ghent group in their RPR-2011A model [36]. The only difference, except for the $P_{11}(1710)$, is that the two-star resonance $P_{11}(1880)$ with spin 1/2 in the RPR-2011A was replaced with the almost equal mass two-star spin-5/2 resonance $F_{15}(1860)$ in our models.

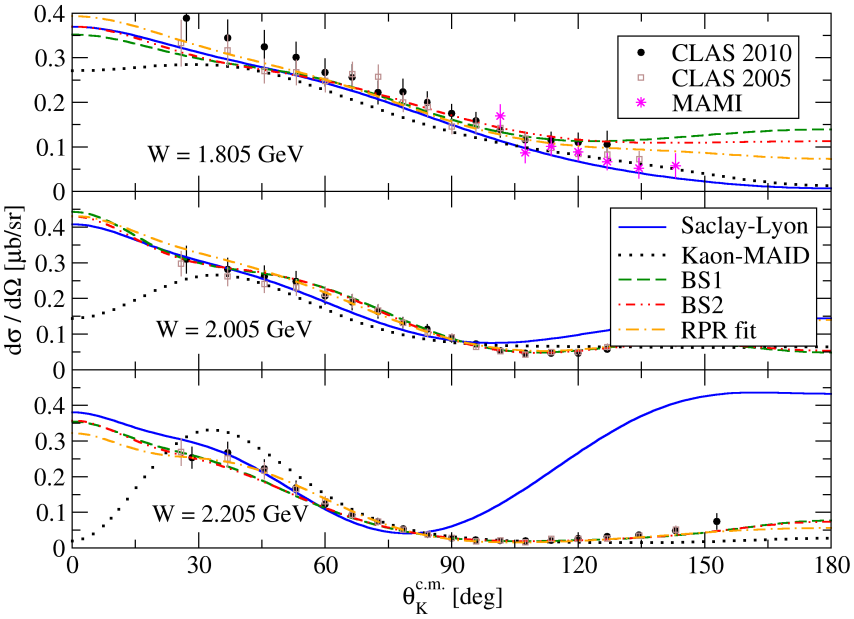

Figure 6.1: Angular dependence of the cross section is shown for three values of the c.m. energy. In the forward-angle region, the Saclay-Lyon (solid curve), BS1 (dashed curve), and BS2 (dash-double dotted curve) models and the new RPR fit predict decreasing dependence of the cross section. In contrast, the Kaon-MAID model (dotted curve) predicts a bump around $\theta_K^{c.m.} = 30°$. The data are from the CLAS 2005 [17], CLAS 2010 [82], and MAMI [61] collaborations.

Although the set of nucleon resonances, which were revealed as important for data description in the fitting procedure leading to the creation of BS models, constituted a starting point in the fitting of RPR parameters, the content of considered nucleon resonances markedly differ in isobar and RPR approaches. Only six out of ten N^* states included in the RPR fit are included in both BS models as well; these are $S_{11}(1535)$, $S_{11}(1650)$, $D_{13}(1875)$, $P_{13}(1900)$, $D_{15}(1675)$, $F_{15}(1680)$, and $F_{15}(1860)$ (see Table 5.1). Interestingly, the coupling constants of $S_{11}(1535)$, $S_{11}(1650)$, and $F_{15}(1680)$ acquire almost the same values in all models. Furthermore, the inclusion of $D_{13}(2120)$, which was suggested as one of the three most dominant N^* states in the elementary $K^+\Lambda$ photoproduction [101], has led to a moderate decrease of the χ^2 value and was, therefore, included in the final set of nucleon resonances in the RPR fit.

More differences between BS1 and BS2 models are observed in the description of the background. The values of the main coupling constants, $g_{K\Lambda N}$ and $g_{K\Sigma N}$, and those for K^* and K_1 exchanges are very similar and the signs are identical except for the

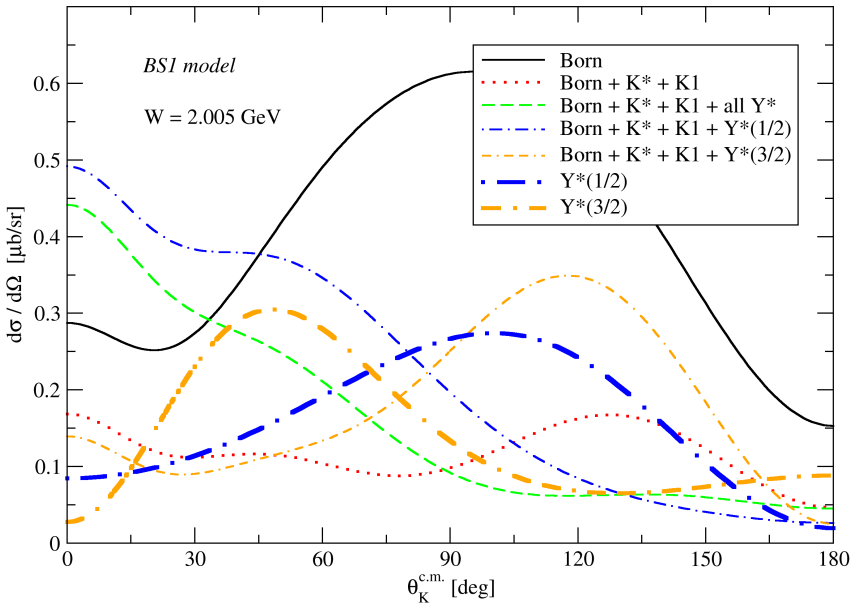

Figure 6.2: Angular dependence of differential cross section for various background contributions to the total amplitude. The figure collects calculations with sole Born terms and their combinations with either kaon or hyperon resonances.

tensor coupling of K^* which has the opposite sign. In both models the value of $g_{K\Lambda N}$ is at the upper limit allowed in fitting (5.3a), which suggests a considerable violation of SU(3) symmetry. A similar result was reached by David *et al.* [32], the value of $g_{K\Lambda N}$ in the Saclay-Lyon model is of -3.16, whereas older analyses, *e.g.* [2, 3], found the $g_{K\Lambda N}$ near the lower limit of -4.4. Note that the differences in these coupling constants, particularly $g_{K\Sigma N}$ and $G^{(t)}_{K^{*+}}$, might have an impact on the model predictions in the $n(\gamma, K^0)\Lambda$ process [21]. This channel may be therefore exploited to distinguish the BS models.

Needless to say, there is an immense difference in description of background in isobar and RPR models as the RPR approach assumes exchanges of a whole family of resonant states instead of exchanges of individual resonances. The $g_{K\Lambda N}$, which is the only parameter not allowed to vary freely in the RPR fitting procedure, is near the upper limit which is in accordance with results obtained with isobar models. We recall the discussion in Section 4.1 connecting the $g_{K\Lambda N}$ value with the description at small kaon angles which shows the paramount importance of fine-tuning this coupling constant. The vector and tensor couplings of the K^{*+} are both negative and the vector coupling is more than two

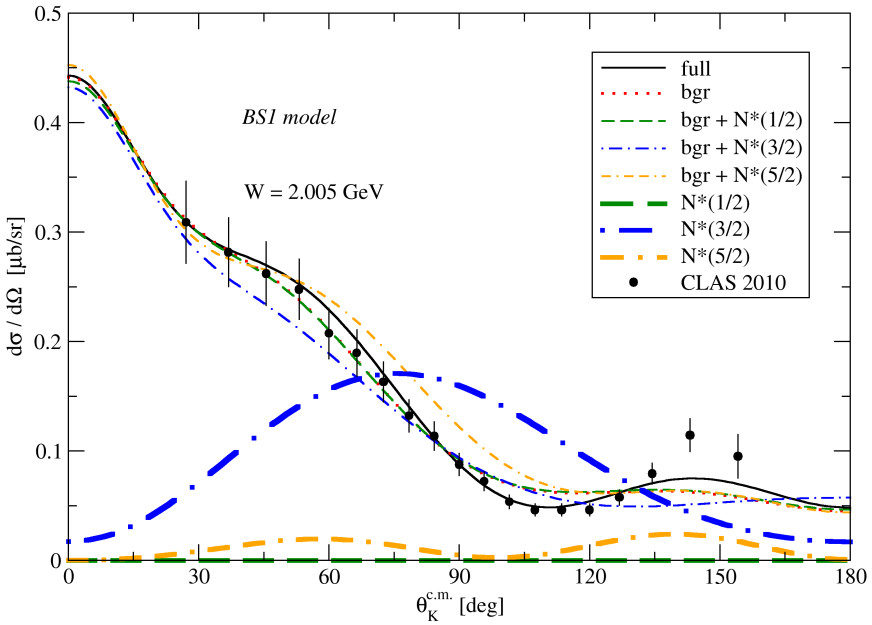

Figure 6.3: Angular dependence of differential cross section as predicted by various parts of the amplitude with an emphasis placed on the resonant part is shown.

times bigger than the tensor one (see Table 5.1). The K^{*+} trajectory, therefore, creates a peak in the cross section around 30°. The behaviour of Regge background depends on relative signs and magnitudes of $g_{K\Lambda N}$ and $G^{(v,t)}_{K^{*+}}$ but for the value of $g_{K\Lambda N}$ kept inside the limit of the broken SU(3)$_f$ it generally produces a cross section which decreases with kaon angle.

Significant differences between BS1 and BS2 models are found in the included sets of hyperon resonances and their couplings. The BS2 contains only one spin-3/2 hyperon resonance S4 and three spin-1/2 resonances L1, L4, and S1, whereas BS1 includes three spin-3/2 resonances L6, L8, and S4 and only one spin-1/2 resonance L4, see Table 3.1 for notation. The general feature of the presented models and other solutions found during the fitting procedure is that the coupling strengths of the hyperon exchanges tend to be relatively large in comparison with the typical values obtained for the couplings of the nucleon resonances [103]. This experience is similar to that gained in the analyses by the Saclay-Lyon [32] and Ghent [59] groups on a role of the hyperon resonances in $p(\gamma, K^+)\Lambda$. Note that in version C of the Saclay-Lyon model [85] the only $\Lambda(1890)\,3/2^+$ (L8) resonance was included in the inconsistent formalism; they concluded, however, that this resonance

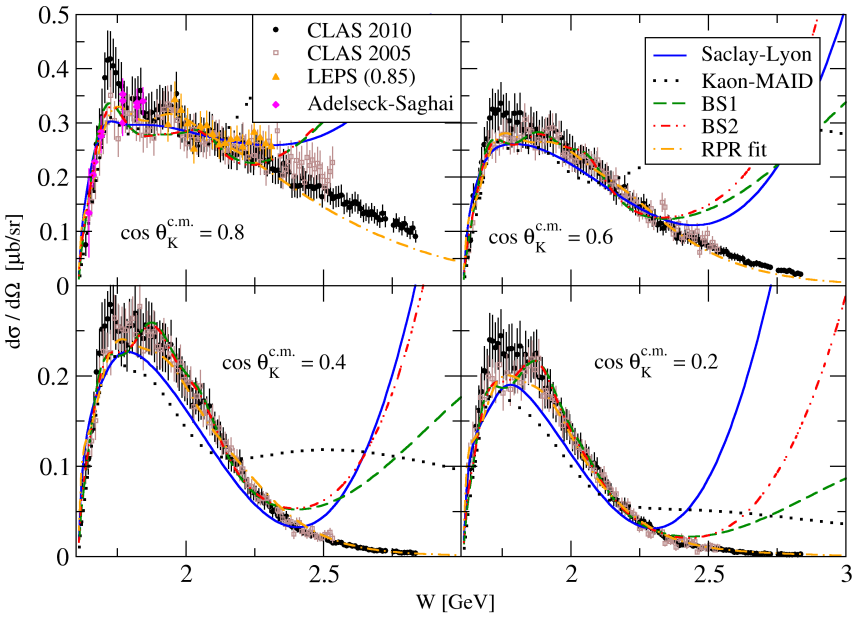

Figure 6.4: Differential cross section in dependence on the c.m. energy W is shown for various kaon angles in the forward hemisphere of kaon angle $\theta_K^{c.m.}$. Notation of the curves is the same as in the Figure 6.1. The data are from CLAS 2005 [17], CLAS 2010 [82], LEPS [108] and from the publication of Adelseck and Saghai [3]. The LEPS data are for $\cos\theta_K^{c.m.} = 0.85$ as indicated in the figure.

is not required by the data set available at that time, *i.e.* before 1998. Reasonable values of the hyperon couplings, $-20 \leq G(Y^*) \leq 20$, were therefore used in our analysis as a criterion for a model selection. These observations suggest that, whereas the current new experimental data are able to fix relatively well the set of nucleon resonances producing genuine resonance patterns in the observables, they still cannot determine uniquely the non resonant part of the amplitude (background). Therefore, one still cannot select a set of hyperon resonances contributing to the process without ambiguity.

Let us note that, in view of the achieved quality of data description, the total number of resonances included in BS1 and BS2, 16 and 15, respectively, is quite moderate in comparison with the older models KM and SL and the recent models by Mart [78, 72] and Maxwell [81]. In contrast, there are only 8 resonances included in the RPR fit of ours. This, however, comes as no surprise since the number of hyperon resonances in the isobar model is substituted for two kaon trajectories in the RPR model.

Angular dependence of the calculated cross sections in comparison with the CLAS data is shown in Figure 6.1 for three energies. The RPR fit, BS1 and BS2 models give very similar predictions which differ from predictions of the other models mainly in the forward- and backward-angle regions. In the region of small kaon angle, $\theta_K^{c.m.} < 40°$, the new models predict descending angular dependence like the SL model, contrary to the KM which predicts a very suppressed cross sections for energies $W \geq 2$ GeV. In the backward-angle region, all of the models agree with the KM describing the data very well. The subtle difference between the BS1 and BS2 model in the description of backward angles (apparent for $W = 1.805\,\text{GeV}$) can be assigned to the sign change of the tensor coupling of K^*. One may conclude that the RPR fit and BS1 and BS2 models describe the cross sections in the full angular and considered energy regions very well, being consistent with experimental data and with each other. Note that the consistency of the cross sections in the very small kaon-angle region with the results of the SL model (Figure 6.1) and the fact that these cross sections are dominated by the spin-flip part of the amplitude could predetermine the new models for successful predictions of the cross sections in the production of the hypernuclei, like the Saclay-Lyon model [23, 54, 27, 112].

The model dynamics in the small-angle area is driven mainly by the background contributions in which the spin-1/2 hyperon resonances, surprisingly, play a very important role (Figure 6.2). In spite of their large contribution at backward angles, they give the largest contribution in the forward-angle region when combined with the Born terms. On the other hand, the spin-3/2 hyperon resonances combined with the Born terms contribute predominantly in the backward-angle region. The role of kaon resonances is to suppress the Born-term contributions in the central-angle region.

The spin-3/2 and spin-5/2 nucleon resonances contributing mainly in the central-angle region are also important in the forward-angle region (Figure 6.3). They contribute in combination with the background terms. Moreover, they give rather diverse results: the spin-5/2 resonances raise the cross section making the peak around $\theta_K^{c.m.} = 45°$ whereas the spin-3/2 resonances lead to a decrease of the cross section for kaon angles around 60°.

In Figures 6.4 and 6.5 we show resonance effects in the energy-dependent differential cross section for four kaon angles in the forward and backward hemisphere, respectively, as they are revealed by the data and the models. First, let us note that the resonance pattern revealed by the CLAS data around $W = 1.7$ GeV for the forward angles is sharper in

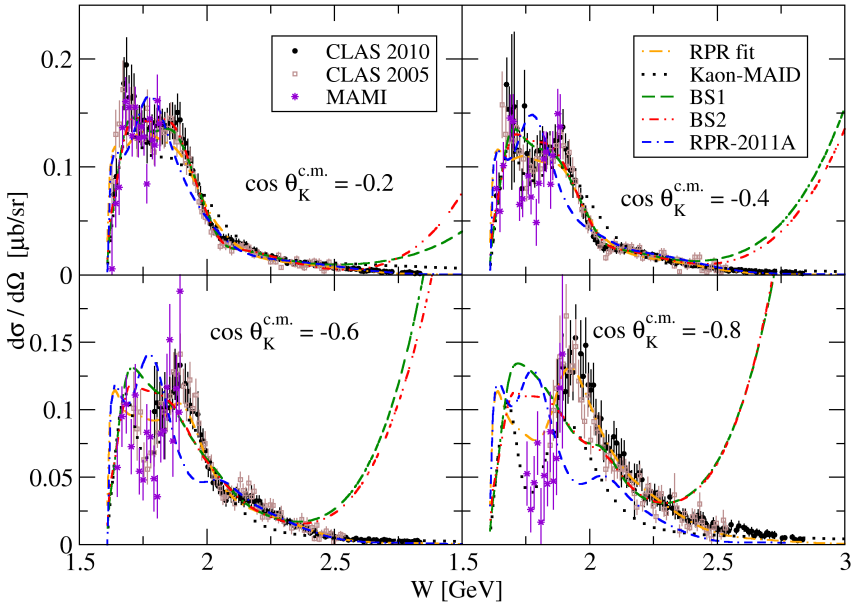

Figure 6.5: Differential cross section in dependence on the c.m. energy W is shown for various kaon angles in the backward hemisphere of kaon angle $\theta_K^{c.m.}$. Notation of the curves and the data is the same as in Figures 6.1 and 6.4, respectively. The amount of MAMI data was reduced approximately by a factor of five in order to make the figure more transparent. Instead of the prediction of Saclay-Lyon model, which does not work well at backward kaon angles (see Figure 4 in Ref. [103]), we compare predictions of the new RPR fit (dash-dotted curve) and RPR-2011A model [106] (double dash-dotted curve) with the rest of isobar models considered in this work.

the CLAS data set from 2010 than in the older one from 2005. The new models predict conservative cross sections lying in between these data sets preferring rather the older data. The $P_{11}(1710)$ in BS2 is not strong enough to make the peak around 1.7 GeV sharper. The older CLAS data set is also favoured by the hybrid RPR-2011A and RPR-2011B models [35, 36] and the RPR fit which we show in Figure 6.4. Moreover, the RPR fit is apparently the only model capable of describing the peak around 1.9 GeV in the forward-angle region. Both new isobar models BS1 and BS2 predict a peak around 1.9 GeV in the central- and backward-angle regions but not at very small kaon angles. In the forward-angle region some strength is also apparent around $W = 2$ GeV modelled by the higher-mass resonances $P_{13}(1900)$, $F_{15}(2000)$, and $D_{13}(1875)$. The strong growth of the cross section in the threshold region is described by the BS1 and BS2 models satisfactorily, better than by the Saclay-Lyon model. The RPR fit agrees well with

the cross-section data from threshold up to energies of several GeV where the nucleon resonances vanish and the kaon trajectories prevail. However, the RPR fit is not able to describe the resonance pattern in the cross-section data at larger kaon angles.

In the region of backward angles, where the experimental data are not plentiful, particularly for large kaon angles and W very close to the threshold, there are two broad peaks apparent in the cross section. Although the Kaon-MAID model seems to be the most reliable isobar model in this kinematical region capturing both peaks of the cross section partially, none of the presented isobar models can, however, capture this behaviour reliably. Since the Saclay-Lyon prediction lies below the data from the threshold up to approximately 2 GeV and then rapidly diverges (see Figure 4 in Ref. [103]) we do not show it in Figure 6.5 and rather compare our new RPR fit with RPR-2011A model and other models (the predictions of RPR-2011A were computed using the web interface StrangeCalc available at [106]). Whereas the BS models tend to produce nearly a plateau near the threshold, the Regge-based models create several peaks in the cross section. The magnitude of the RPR-2011A-model prediction agrees well with the data for kaon angles at $\cos\theta_K^{c.m.}$ of -0.2 and -0.4 but this model entirely fails to reproduce the peak in the cross section slightly below 2 GeV at very backward angles. It seems that the only model capable of describing this peak is the new RPR fit of ours, which works sufficiently well also at central kaon angles. This pleasing behaviour is achieved in all probability by the inclusion of a number of nucleon resonant states which may substitute the hyperon resonances used for a background description in the isobar model. We regard the $P_{11}(1880)$ and $D_{13}(1875)$ resonances as the most important ones for the model to describe that peak as the model without these resonances fails to reproduce the data in this region. However, we cannot claim this with certainty since there are many interference terms among a number of different resonant states which enter the game and shadow the contributions of sole resonances. The peak next to the threshold of the process can be assigned to the contribution of background - this contribution rises from the threshold, reaches its peak at approximately 1.65 GeV and then falls steadily.

The new isobar models, eligible for the resonance region, describe data well up to energy $W \approx 2.4$ GeV. Above this energy their cross-section predictions systematically rise, overshooting the data, which is more apparent at forward angles in Figure 6.4 and which is a well-known feature of isobar models. In the new models, the contributions of

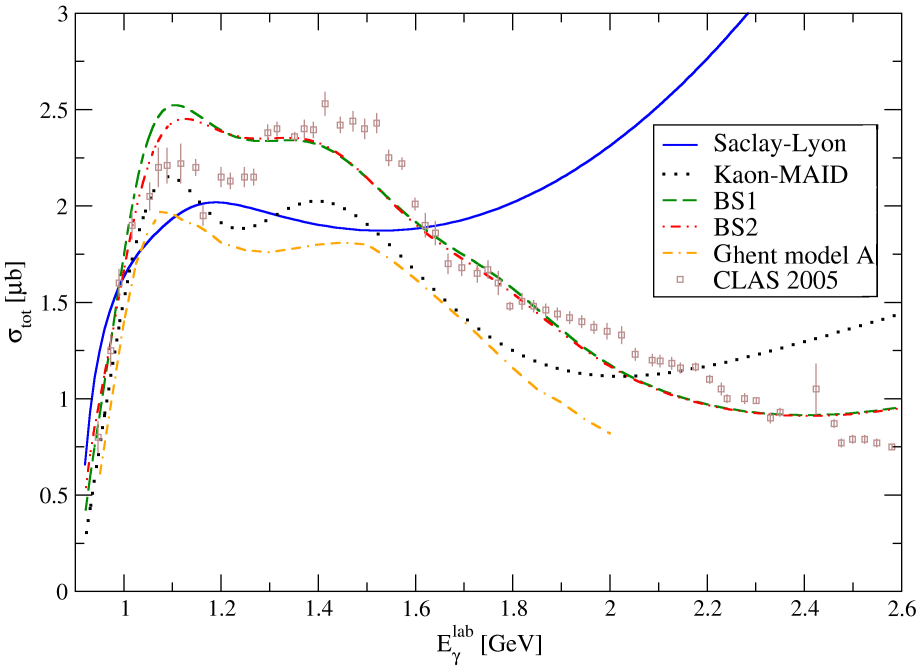

Figure 6.6: Model predictions of the $p(\gamma, K^+)\Lambda$ total cross section. For comparison, the Ghent isobar model (model A) was added as read from Figure 7 in Ref. [57]. Notation of the rest of the curves is the same as in the Figure 6.1. Data stem from Figure 20 in Ref. [17].

the nucleon resonances in the s channel are regularized by the strong-enough hadron form factors as shown in Figure 3.4. The high-energy divergence is therefore created mainly by the background part of the amplitude. This divergent behaviour, however, differs for various models: in the Kaon-MAID model, predictions start diverging at forward angles above 2.2 GeV (the maximum energy for which the model was constructed) but predictions of the Saclay-Lyon model strongly overshoot the data at backward angles above 2 GeV. This divergent behaviour of the isobar models is also well seen in the energy dependence of the total cross section as shown in Figure 6.6. Whereas the KM model begins to diverge at $E_\gamma^{lab} = 2.2\,\text{GeV}$, *i.e.*, beyond its scope, the SL model produces a divergent behaviour above $E_\gamma^{lab} = 1.6\,\text{GeV}$. Note, however, that the KM, SL, and Ghent models were fitted to the old SAPHIR data and, therefore, slightly underestimate the current CLAS data (see Figure 20 in Ref. [17]).

In the extreme forward-angle region, the discrepancies between different model predictions are substantial, especially for $E_\gamma^{lab} > 1.5$ GeV, see Figure 6.7. The BS1, BS2, and

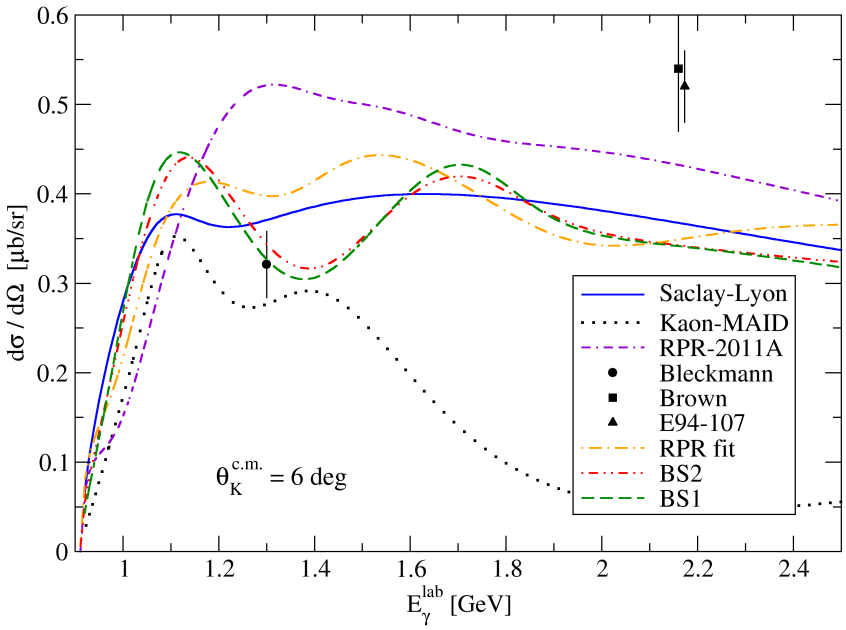

Figure 6.7: Predictions of the differential cross section for photoproduction at $\theta_K^{c.m.} = 6°$ is shown for several models. The only available photoproduction data point in this region is from Bleckmann *et al* [13]. The data points of Brown [19] and E94-107 [71] are for electroproduction with a very small value of the virtual-photon mass $|k^2|$. Notation of the curves is the same as in the Figure 6.1.

Saclay-Lyon models predict similar magnitudes of the cross section in the whole energy range shown, but the Kaon-MAID model reveals a strong reduction of the results for higher energies due to suppression of the proton exchange by the hadron form factors. Recall that the BS1 and BS2 models also contain the form factors and that the strength they predict at small angles is made by another, more complex mechanism – interference effects of the hyperon resonances with the Born terms and of higher-spin nucleon resonances with the background – discussed above. The energy dependence of the SL result is quite flat being dominated by the non resonant proton exchange, which is not suppressed in SL, while the BS1 and BS2 models predict two broad peaks at $E_\gamma^{lab} = 1.1\,\text{GeV}$ ($W = 1.7$ GeV) and $E_\gamma^{lab} = 1.7\,\text{GeV}$ ($W = 2$ GeV). A double-peak structure is visible in the RPR-fit prediction as well. This is created by destructive interference of N^*'s and the background since the Regge trajectories on their own would produce a smooth cross-section prediction with a very broad peak around E_γ^{lab} of 1.5 GeV overshooting the datum of Bleckmann *et al.* [13] by a factor of two but being in concert with the electroproduction

data shown at $E_\gamma^{lab} = 2.2\,\mathrm{GeV}$. The RPR-2011A of the Ghent group gives rather a non resonant character of the cross section for this angle.

It is well-known that for kaon angles smaller than $\theta_K^{c.m.} = 25°$ there are almost no available experimental data. As a consequence, the models cannot be reliably tested in this region, which increases uncertainties in calculations of the hypernucleus production spectra [23, 20]. In Figure 6.7, the only datum for photoproduction is that by Bleckmann *et al.* [13] at $E_\gamma = 1.3$ GeV, which is consistent with all model predictions shown. The other two data points are from the measurements of electroproduction with almost real photons, *e.g.* $-k^2 = 0.07$ $(\mathrm{GeV/c})^2$ for the JLab experiment E94-107 [71], which prefer predictions of the SL, BS1, and BS2 models. Note that the electroproduction cross section consists of more parts (see the electroproduction cross-section formula (2.13)) which can, in fact, contribute. Particularly, the longitudinal amplitudes may have a strong contribution to the cross section. An estimation can be made to determine the cross section for the unpolarized photon beam σ_T [71]. The E94-107 datum is then shifted considerably downwards to roughly $\sigma_T = 0.38\,\mu\mathrm{b/sr}$, being consistent with predictions of almost all models shown in Figure 6.7.

The spin observables are very important in fine-tuning the interference among many different contributions. Plenty of new high-quality data for hyperon polarization and several tens for beam asymmetry and target polarization are now available. These data were also used in fitting the BS1 and BS2 models. In Figures 6.8, 6.9, 6.10, 6.11, and 6.12 we compare results of the models with the LEPS, CLAS, and GRAAL data.

In the case of hyperon polarization, the Born terms on their own yield zero contribution but their interference with other terms appears to be important, especially the interference with the nucleon resonances. The models were fitted to the hyperon polarization data from the threshold up to W of 2.225 GeV. In this energy range and mainly in the central-angle region, the data are captured by the BS1 and BS2 models well. On the other hand, the Saclay-Lyon and Kaon-MAID models do not even fit the shape of the data (except for $\theta_K^{c.m.}$ around 90° where the structures in data are not so prominent). Note, however, that these old models were not fitted to the hyperon polarization or beam-asymmetry data as these data were not available at that time. The CLAS 2010 hyperon-polarization data set for adjusting the RPR free parameters was used in its entirety, *i.e.* from W of 1.625 GeV up to 2.835 GeV. The RPR fit can nicely capture the shape of data although

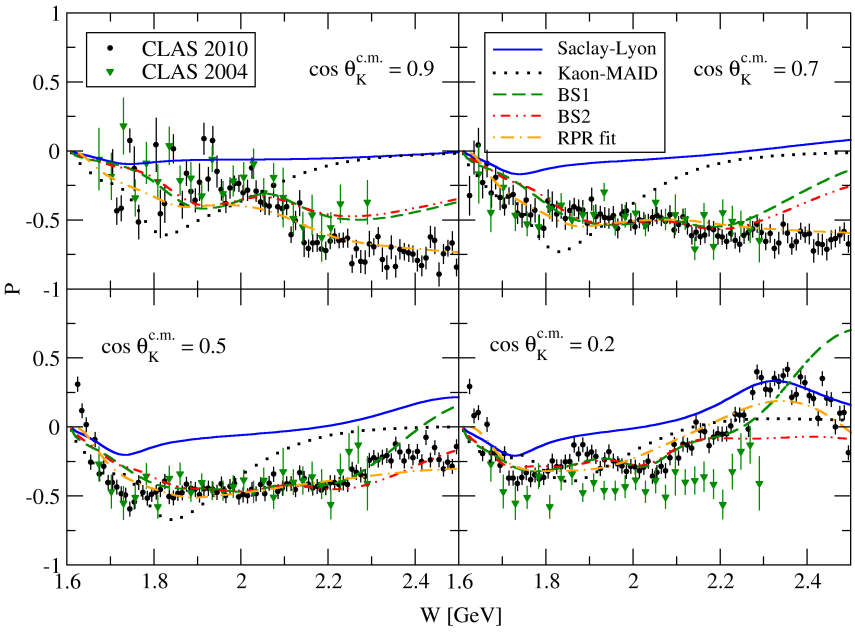

Figure 6.8: Results for energy dependent hyperon polarization P are shown for several forward kaon angles $\theta_K^{c.m.}$. Notation of the curves is the same as in the Figure 6.1. The CLAS 2010 and CLAS 2004 data originate from Refs. [82] and [83], respectively.

in the backward hemisphere of $\theta_K^{c.m.}$ (see Figure 6.9) it cannot reproduce the peak in the data such as the BS models do. Note that the CLAS 2004 data [83] were not used in the fitting procedure of either isobar model or RPR model and serve, therefore, merely for illustration and comparison.

For photon laboratory energy higher than 1.9 GeV, the BS1, BS2 and Kaon-MAID models describe the beam-asymmetry data satisfactorily, whereas the Saclay-Lyon model tends to underpredict the data in the whole energy range. The RPR fit is able to predict the beam asymmetry very similarly to the BS models and, in addition, works slightly better at lower energies. Needless to say, the shape of the predicted curve is governed by the interference among many terms involved in the amplitude, *e.g.* the Regge background in the RPR fit describes the data well only up to $\theta_K^{c.m.}$ of 30°, for $\theta_K^{c.m.} > 30°$ it largely overshoots the data. In the BS models, the background on its own is, similarly to the background in the RPR fit, able to describe the data for $\theta_K^{c.m.} < 30°$, for larger angles it predicts the beam asymmetry which decreases steadily with kaon angle. It is, therefore, the addition of N^* states that leads to a dependable, though not perfect, prediction of the

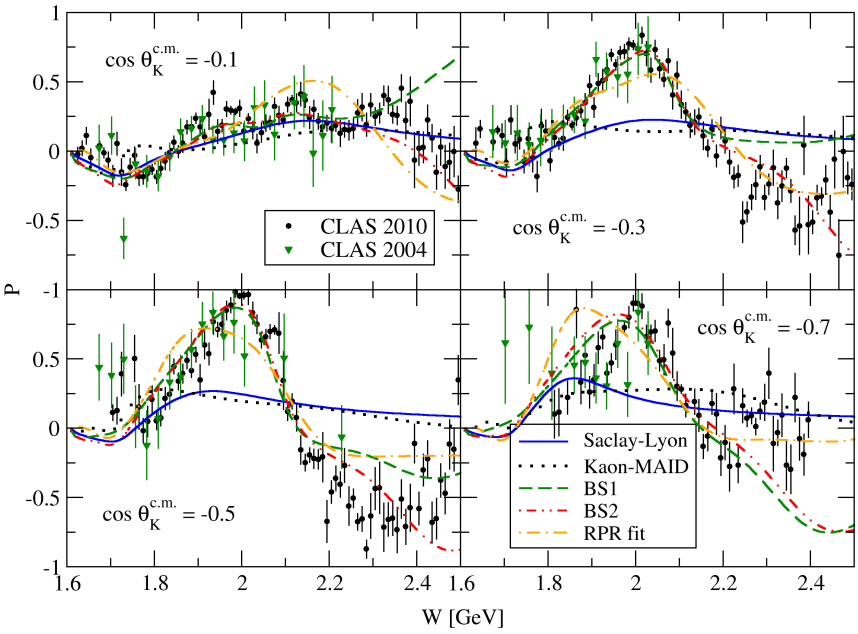

Figure 6.9: Same as Figure 6.8 but for kaon angles $\theta_K^{c.m.}$ in the backward hemisphere. Notation of the curves is the same as in the Figure 6.1. The CLAS 2010 and CLAS 2004 data stem from Refs. [82] and [83], respectively.

beam asymmetry. Note that the data at lower energies, Figure 6.11, have larger relative errors and therefore they cannot restrict the model parameters as much as the data for energies larger that 1.9 GeV.

Whereas the free parameters of BS models and the new RPR model were adjusted to cross-section, hyperon-polarization and beam-asymmetry data, the GRAAL data on target polarization were not used. Thus, Figure 6.12 collects merely predictions of these models. Needless to say, the older isobar models were not fitted to these data as well, since at that time, there were no GRAAL target-polarization data. However, the Kaon-MAID model captures the shape of data quite well in the kinematic region shown. The Saclay-Lyon model tends to overpredict the data at forward angles and at backward angles its predictions sharply decrease, which is not suggested by data. The new BS models work well primarily at higher energies and in the hemisphere of forward angles where they capture the behaviour of data very well. Near the threshold, the BS models do not give a reasonable description of data, since their predictions are positive whereas the data are negative (see particularly the BS1-model prediction in Figure 6.12). Similarly, BS-model

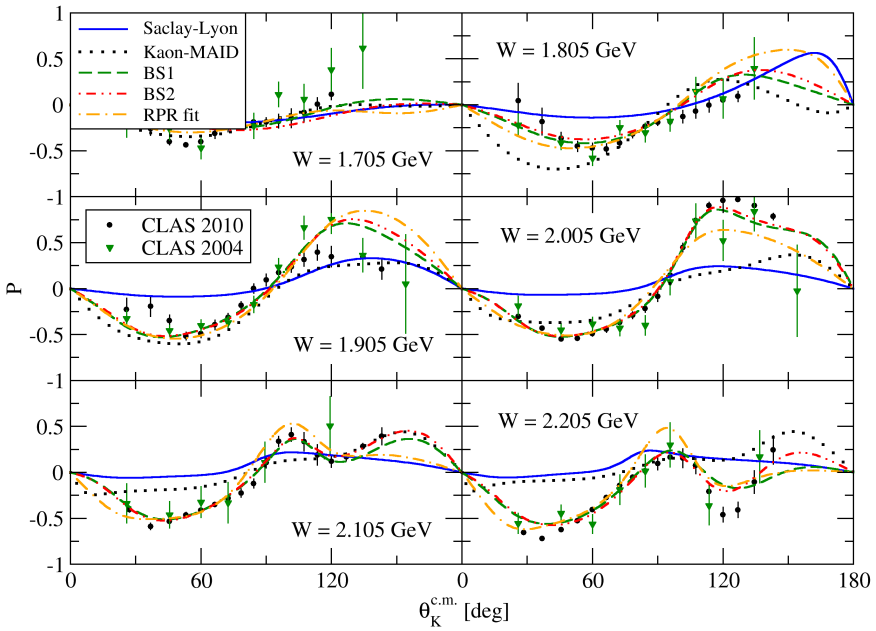

Figure 6.10: Results for the angular dependence of hyperon polarization P are shown for several c.m. energies W. Notation of the curves is the same as in the Figure 6.1. The CLAS 2010 and CLAS 2004 data are from Refs. [82] and [83], respectively.

predictions at higher energies and at backward angles are negative while data are positive. The RPR fit is able to capture only roughly the shape of data and its predictions in some kinematic regions suffer from the similar imperfection as the predictions of BS models.

The exchanges of the nucleon resonances in the s channel constitute the resonant structure in the cross section. The effect of a particular resonance strongly depends on the magnitude and sign of its coupling constants, but this effect is hard to estimate in the kaon photoproduction due to an overlap of many resonances and occurrence of the complicated background. In Figure 6.13 we show effects of the nucleon resonances in the BS1 model on the forward-angle differential cross section. The contributions of a particular resonance on its own, in its combination with the background, and a prediction of the full model without the resonance are shown. Comparing the latter with the full result, one can infer an importance of the particular resonance in this kinematic region.

In the BS1 model, the contribution of the subthreshold N3 resonance is small, as can be concluded from the relatively small value of its coupling parameter, Table 5.1. However, N3 significantly lowers, by 20 – 30%, the background contribution, which is important in

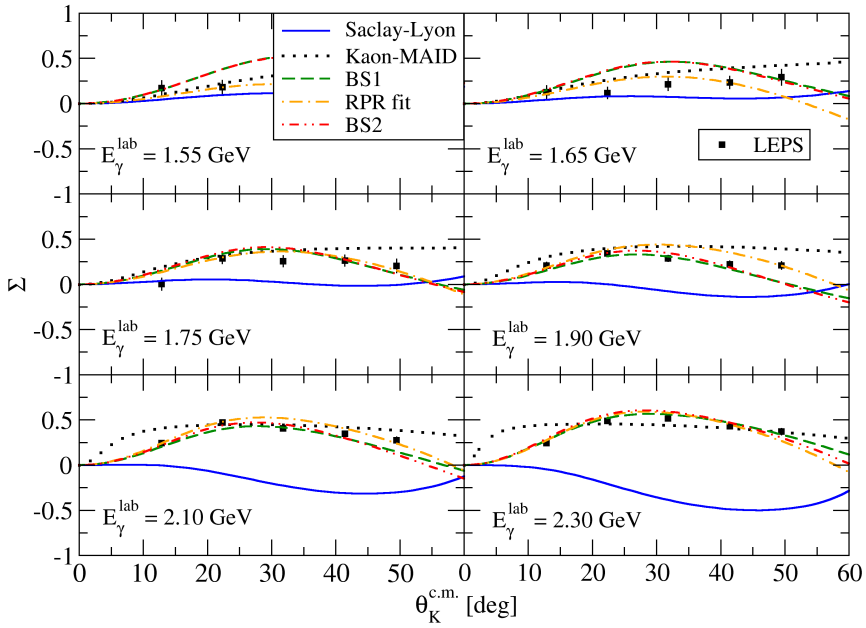

Figure 6.11: Results for the angular dependence of beam asymmetry Σ are shown for several photon lab energies. Notation of the curves is the same as in the Figure 6.1. The LEPS data are from Ref. [108] and the errors are statistical only.

the threshold region where it balances the contribution of N4. Omitting this resonance therefore leads to a growth of the cross section in the threshold region. Similarly, a strong effect is apparent for the N4, N7, and P2 resonances, where the latter two resonances affect the cross section rather at larger energies. On the other hand, the influence of the resonances P3, P5, and N9 on the forward-angle cross section is very small. Their influence is apparent only for energies above 2 GeV. The contributions of the spin-5/2 resonances N9 and P5 start to rise sharply around 2.2 GeV, which instigates the introduction of strong hadron form factors, *e.g.* the multidipole or multidipole-Gaussian [36]. This effect is not seen for the P3 resonance because it is shifted to higher energies due to its larger mass. Since the BS2 model contains, except for the N6, the same nucleon resonances with very similar values of the coupling parameters, it behaves in a manner similar to the BS1 model.

In Figures 6.14 and 6.15, the predictions of double-polarization observables C_x, C_z, O_x, and O_z are shown for various kaon angles. Whereas the C_z is large and positive over the kinematic regions shown in Figure 6.14, the C_x data lie below zero. As both

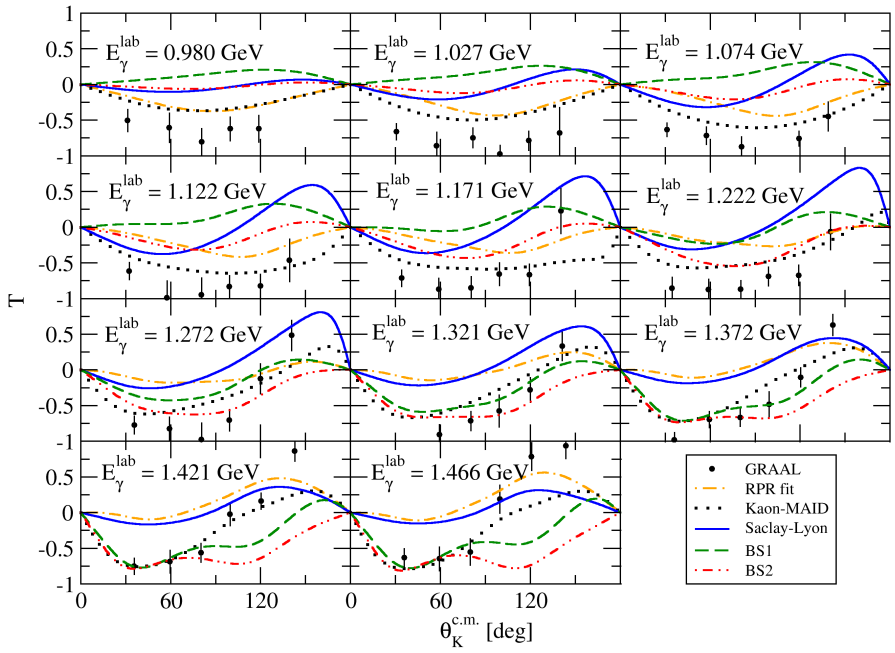

Figure 6.12: Angular dependence of the target asymmetry T is shown for several photon lab energies. Notation of the curves is the same as in the Figure 6.1. The GRAAL data are from Ref. [67] and the errors are the quadratic sums of statistical and systematic uncertainties.

observables show similar fluctuations but C_x is typically smaller than C_z, it approximately holds that $C_z \approx C_x + 1$ [100]. Our new models as well as the well-known Kaon-MAID and Saclay-Lyon models were not fitted to these data sets. Therefore, the figures show the predictive power of considered models. The Saclay-Lyon model fails to reproduce the C_z data for larger kaon angles (whereas the data are positive, the model predictions have the opposite sign). The correspondence between other model predictions and the C_x and C_z data sets is considerably better: the Kaon-MAID predictions are of the same sign as the data and the BS models capture even the shape of the data. In the case of O_x and O_z the concord between model predictions and data is apparently worse since the data are shifted slightly upwards in all regions in comparison with the predictions of models, except for O_x at E_γ^{lab} of 0.980 GeV where the predictions of models have the right magnitude. The only other exception is the Saclay-Lyon prediction of O_x at higher energies where its magnitude is comparable with data. The BS models tend to reproduce the shape of the O_x and O_z data partly in all regions whilst the Kaon-MAID model

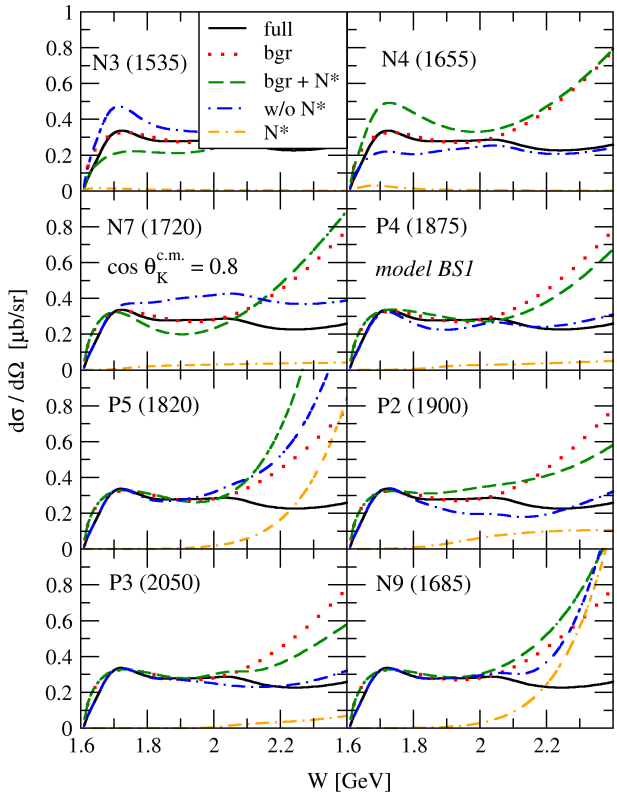

Figure 6.13: Analysis of the resonant part of the BS1 model. Contributions of background (dotted curve), included nucleon resonances (double dash-dotted curve), and their combination with background (dashed curve) to the differential cross section are compared with the full BS1 model (solid curve) and the BS2 model when omitting a particular nucleon resonance (dash-dotted curve).

fails to describe the O_z data at E_γ^{lab} of 0.980 GeV and 1.222 GeV where its prediction is negative whereas data are positive.

Our findings on the nucleon resonances agree quite well with the results of the Bayesian analysis which used the Regge-plus-resonance model [36]. In this analysis, the N3, N4, and N7 resonances have acquired large relative probabilities, 13, 34, and 99, respectively, that they contribute to the kaon photoproduction process. Importance of these resonances was confirmed in our analysis. However, the resonances N9 and P3 were also shown to contribute significantly; their relative probabilities are 16 and 18, respectively, in the RPR-based analysis contrary to our findings which we attribute to the smaller energy window of our analysis (P3 and N9 contribute more at higher energies as shown in Figure 6.13). In the Bayesian analysis, it was shown that the N5, N6, and N8 resonances are not required

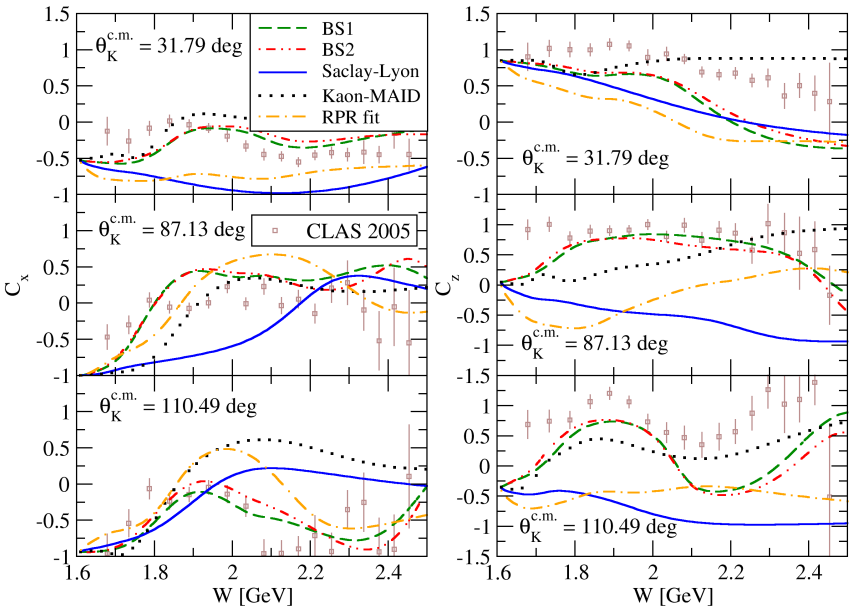

Figure 6.14: Double-polarization observables C_x and C_z are shown for various kaon angles. Since none of the models were fitted to the C_x or C_z data, the figure collects merely predictions of the models. Notation of the curves is the same as in the Figure 6.1 and the data stem from the CLAS 2005 analysis [18].

to describe the $\gamma p \to K^+\Lambda$ data which is also consistent with our conclusions, except for N6 in the BS2 model with the very small coupling parameter $G(N6) = -0.05$. The two-star spin-1/2 resonance $P_{11}(1880)$ (P1) was excluded in our analysis whereas it was included into the set of probable resonances in the Bayesian analysis with the relative probability 11. The spin-5/2 state with near mass, $N^*(1860)$ (P5), was assumed in both new models instead. Note that adding P1 into the models does not improve the χ^2 too much but it raises the number of considered resonances which we tried to keep as small as possible (according to the principle of the Occam's razor).

Whereas for description of resonance region, we have isobar and Regge-plus-resonance model at hand, the only applicable model for the study of the high-energy region is the RPR model. In this approach, all nucleon resonances, which create the resonance pattern observed in the resonance region, are supposed to vanish and one is therefore left with the background part of the amplitude only. This consists of K^+ and K^{*+} trajectories supplemented with another term ensuring the gauge-invariance restoration and it is governed by merely three parameters. A comprehensive description of the Regge background

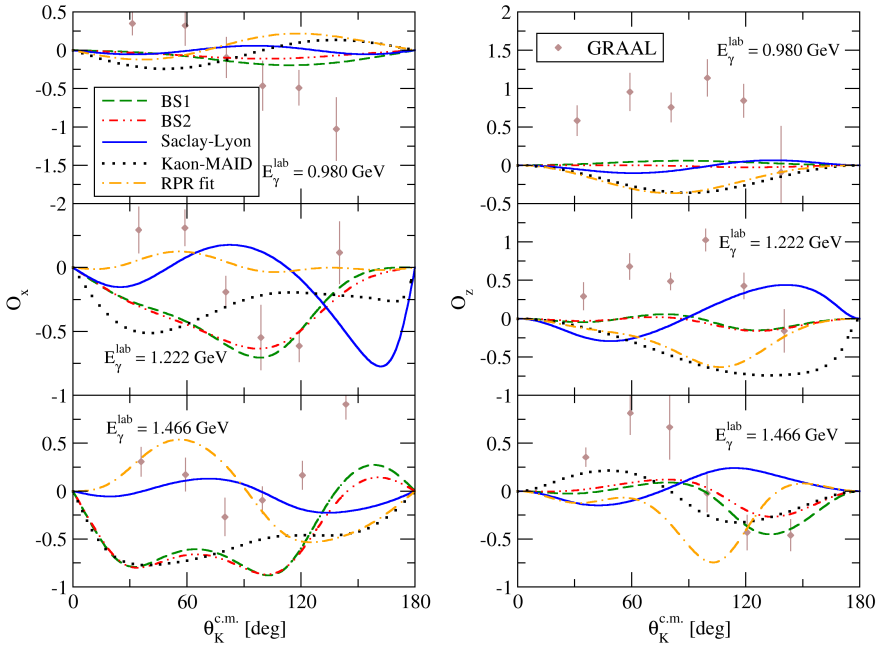

Figure 6.15: Double-polarization observables O_x and O_z are shown for various kaon angles. Since none of the models were fitted to the these data, the figure collects merely predictions of the models. Notation of the curves is the same as in the Figure 6.1 and the data stem form the GRAAL analysis [67]. The errors are quadratic sums of statistical and systematic uncertainties.

together with the term restoring the gauge invariance is given in the Section 4.1 and here we will therefore focus on the resonant part of the fit with Regge-plus-resonance model.

As it can be read off Figures 6.16 and 6.17, the nucleon resonances really act only in the resonance region and their contributions vanish beyond W of approximately 2.5 GeV. In the Figure 6.16, a subtle interplay among various nucleon resonances and the background part of the amplitude is shown. The background part, consisting of kaon trajectories solely, can capture the magnitude of the cross section but, for obvious reasons, it cannot predict the resonance pattern. It is the set of N^*'s, that creates the resonance pattern with two broad peaks by interfering destructively with the kaon trajectories. Probably the most perceptible contribution stem from $P_{11}(1880)$, which interfere destructively with the background terms and, what is particularly interesting, its combination with background creates a double peak structure in the cross section. On the other hand, omitting the higher-spin nucleon resonances almost does not change the cross-section prediction of the full model. Since the contributions of N^* can hardly be distinguished from one another in

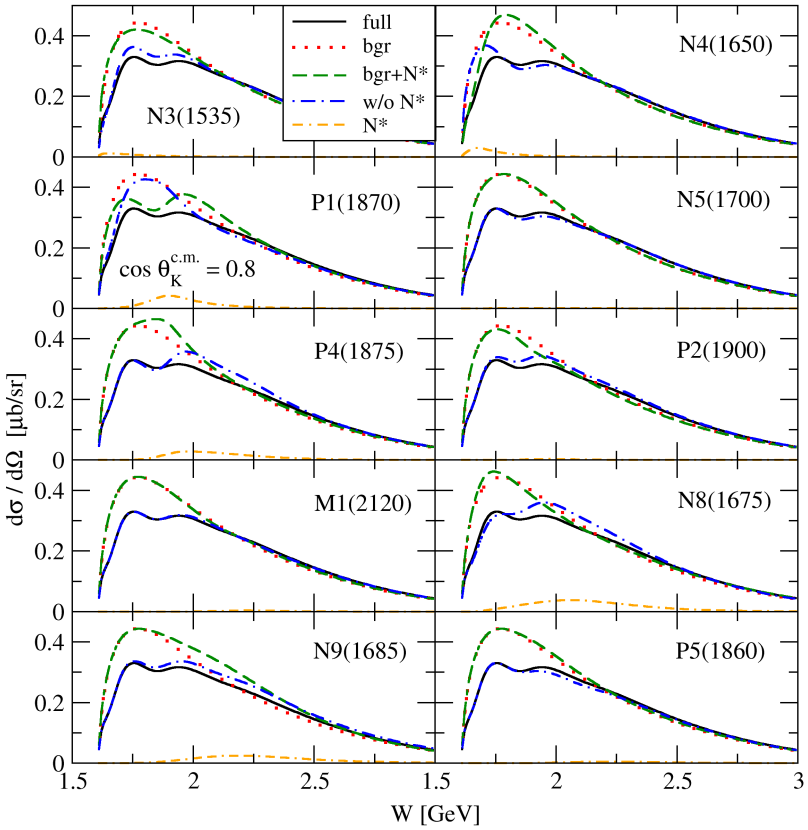

Figure 6.16: Analysis of resonant part of the new RPR fit in the forward-angle region. The figure collects predictions of the cross section from various parts of the amplitude and shows also the interference between background and N^*'s and the effect of N^*'s on their own. Notation is the same as in the Figure 6.13.

Figure 6.16, the Figure 6.17 shows them grouped according to their spin and with a better resolution. The spin-1/2 nucleon resonances $S_{11}(1535)$ and $S_{11}(1650)$ are responsible for the peak in the threshold region, whereas the rest of N^*'s create the peak around 2 GeV. Interestingly, the majority of the N^* contributions are shifted from the position of their poles towards higher energies. This is true also for spin-5/2 nucleon resonances $D_{15}(1675)$ and $F_{15}(1680)$, which, according to the value of their masses, should contribute rather to the threshold peak (see Figure 6.17).

What is more, the Figure 6.17 illustrates very nicely the overall situation in the search for dominant resonances in the $K^+\Lambda$ production. As there are many N^* states which can contribute to the $p(\gamma, K^+)\Lambda$ process and which in many cases overlap each other,

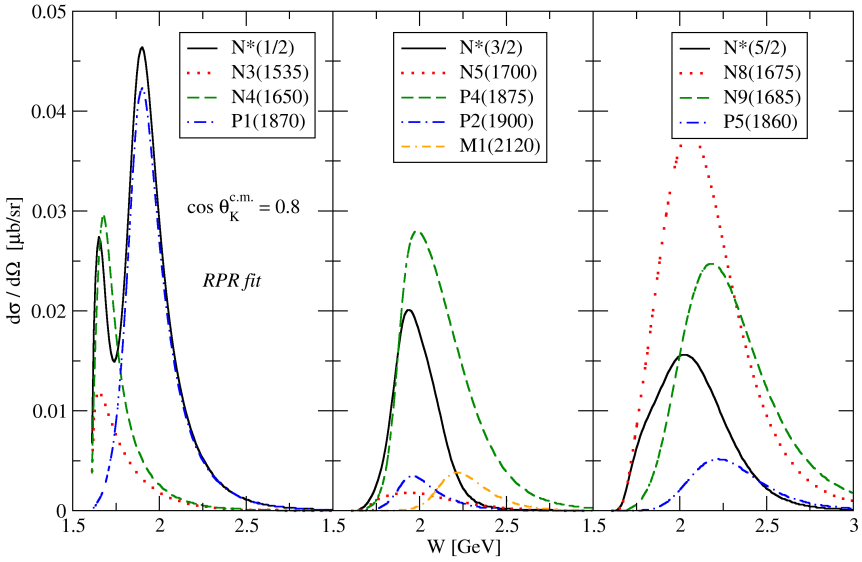

Figure 6.17: Analysis of resonant part of the new RPR fit for $\cos\theta_K^{c.m.} = 0.8$. The nucleon resonances shown are put into groups according to their spin.

the interference among their contributions is developed. The interference can either be constructive (*e.g.* the second peak in the contribution of $N^*(1/2)$) or destructive (*e.g.* the total contribution of spin-5/2 nucleon resonances in the RPR fit), depending on the values and signs of coupling constants of the nucleon resonances involved. A sharp reader may notice that the coupling parameter of $S_{11}(1535)$ is, in its absolute value, larger than the coupling of $S_{11}(1650)$ and the contribution of $S_{11}(1535)$ should be, therefore, more significant than the contribution of the $S_{11}(1650)$ resonance in the threshold area (see Figure 6.17). However, the $S_{11}(1535)$ resonance lies below the threshold and therefore contributes to the $p(\gamma, K^+)\Lambda$ cross section only partly. All this makes from the determination of dominant resonant states in the $p(\gamma, K^+)\Lambda$ reaction a tantalizing task.

Chapter 7

Conclusion and Outlook

The purpose of this work was to provide a deep overview of the kaon photoproduction, since this reaction can provide a novel view on the nucleon excitation spectrum which has become a cornerstone of modern hadron physics, and to report on latest achievements that were done in this field of physics. In this concluding section, we summarize the progress recently made and provide outlook for a future work.

7.1 The Isobar Approach

In this work, we have presented two new isobar models BS1 and BS2 for the description of the $p(\gamma, K^+)\Lambda$ process in the energy range from the threshold to $W = 2.4$ GeV. The models provide satisfactory description of experimental data in the whole energy region and for all kaon angles. Their predictions for the cross sections at small kaon angles, being consistent with the results of the Saclay-Lyon model, suggest that the models can give reasonable values of the cross sections for the hypernucleus production. Construction of a new isobar model utilizing new precise data which could be used as an input in the hypernucleus calculations was one of the aims of this work.

In the construction of the single-channel models based on an effective Lagrangian we have utilized the consistent formalism by Pascalutsa for description of baryon fields with

higher spin (3/2 and 5/2 in our case). This formalism ensures that only the physical degrees of freedom contribute in the baryon exchanges. Moreover, it provides regular amplitudes which are especially important for the u-channel exchanges allowing the inclusion of hyperon resonances with spin 3/2. These resonances were found to play an important role in description of the background part of the amplitude. They have not been considered in the older isobar models with the inconsistent formalism, except for the version C of the Saclay-Lyon model [85].

The set of selected nucleon resonances with spins 1/2, 3/2, and 5/2 contributing most to the process agrees well with that selected in the Bayesian analysis with the Regge-plus-resonance model by the Ghent group. We mostly confirm their result on the structure of the resonant part of the amplitude. The differences for the resonance part, *e.g.* different forms of the hadron form factor, stem from the fact that we limit our analysis only to the resonance region. As for the missing resonances, we confirm the importance of the $P_{13}(1900)$ and $D_{13}(1875)$ states for a reasonable data description. We have found, however, that the spin-5/2 state $N^*(1860)$, recently included in the PDG Tables, is preferable to the spin-1/2 state $P_{11}(1880)$ included in the Bayesian analysis.

Special attention was paid to the analysis of the background part of the amplitude, which is important for a correct description of the forward-angle cross sections. In the background, which is a complicated effect of many various contributions in the isobar approach, the hyperon-resonance exchanges with spin 1/2 and 3/2 together with the Born terms appeared to be important components in the forward- and backward-angle regions, respectively. However, the current extensive data set still does not allow one to select the most significant hyperon resonances in the u channel unambigously.

In the analysis, several forms of the hadron form factors were considered; we have chosen the dipole and multidipole forms as the most suitable for the data description exploiting the isobar model. The obtained values of the cutoff parameters, around 2 GeV, suggest rather hard form factors.

The free parameters of the models were adjusted by fitting the cross section, hyperon polarization, and the beam asymmetry to new high-quality data from CLAS and LEPS and to older data. The overall number of resonances in the models, 15 and 16, is quite moderate in view of complexity of the kaon photoproduction in comparison with π or η photoproductions.

7.2 The Regge-plus-resonance Approach

Besides the two new isobar models BS1 and BS2 of ours, we have presented also a new Regge-plus-resonance fit to the data for the $p(\gamma, K^+)\Lambda$ process, which is able to give a reliable description of data from the threshold of the process up to energy of several GeV. Prior to the fitting procedure, we had introduced the consistent formalism, proposed in Ref. [90], for exchanges of spin-3/2 and spin-5/2 nucleon resonances as these resonances apparently play an important role in the resonant part of the amplitude.

Our primary motivation for the work with the hybrid RPR model was its particularly simple description of background where the Regge kaon trajectories demanding only three parameters to adjust are introduced. As can be seen from the figures presented in this work, this prescription is not only elegant, but very powerful since it can capture the magnitude of the cross section. In order to describe the resonance pattern revealed by experimental data, we have introduced several resonant states of the nucleon. As the initial set, we took the N^*'s revealed in the work of De Cruz *et al.* [36] as the states with the highest probability of contributing to the $p(\gamma, K^+)\Lambda$ process and varied them throughout the procedure. In comparison with the isobar-model fitting procedure, there were less parameters to optimize (thanks to the simple description of background) and we had more experimental data at hand (in fact, we used the same data sets as in the fitting procedure of free parameters of isobar model, but this time we were not restricted to the resonance region only).

In the analysis, we have paid close attention to the choice of hadron form factor, exploiting its dipole, multidipole, Gaussian and multidipole-Gaussian shape. We have revealed the multidipole shape of the hadron form factor as the most appropriate one since its inclusion leads to a lower value of χ^2 than the inclusion of other form-factor types and its cutoff parameter acquires a reasonable value of approximately 1.5 GeV. On the other hand, the multidipole-Gaussian form factor seems to be overly strong by definition and its cutoff parameter then has a value of 3.0 GeV.

The RPR-fit predictions of observables are in concert with experimental data in the kinematic regions shown. The behaviour of cross-section predictions at backward angles where the RPR fit is able to nicely reproduce the peak revealed by data is particularly interesting.

7.3 Outlook

The work on the elementary amplitude will continue since it might be very fruitful for the further work on hypernucleus production: we would like to investigate the excitation spectra of light hypernuclei such as ${}^{3}_{\Lambda}$H, ${}^{3}_{\Lambda}$He, ${}^{4}_{\Lambda}$H, and ${}^{7}_{\Lambda}$He. The study of excitation spectra of light hypernuclei can provide additional knowledge of hypernucleus structure and shed more light on the long-standing issue of the charge-symmetry breaking term of the Λ-N interaction.

We would like to extend the model in order to describe photoproduction not only with a Λ hyperon in the final state but also with Σ hyperons in the final state. On the one hand, an implementation of Δ resonances will be needed in this case; on the other hand, a study of further reaction channels will help better understand the underlying dynamics. Moreover, we want to deal with the production on deuterium targets. An extension towards kaon electroproduction, which requires introduction of electromagnetic form factors and consideration of the longitudinal component of the amplitude, will be accomplished as well.

Another possibility how to improve the model is to account for the unitarity by making the widths of the nucleon resonances energy-dependent functions as it was done, *e.g.* in the Kaon-MAID model.

Bibliography

[1] R. Erbe *et al.* (ABBHHM collaboration), *"Multipion and Strange-Particle Photoproduction of Protons at Energies up to 5.8 GeV,"* Phys. Rev. **188**, 2060 (1969)

[2] R. A. Adelseck, C. Bennhold, and L. E. Wright, *"Kaon photoproduction operator for use in nuclear physics,"* Phys. Rev. C **32**, 1681 (1985)

[3] R. A. Adelseck, B. Saghai, *"Kaon photoproduction: Data consistency, coupling constants, and polarization observables,"* Phys. Rev. C **42** (1990) 108

[4] P. Achenbach *et al.*, *"Strange hadronic physics in electroproduction experiments at the Mainz Microtron,"* Nucl. Phys. A **881** (2012) 187-198

[5] K. Althoff, M. Gies, H. Herr, E. Hilger, V. Kadansky *et al.*, *"Photoproduction of $K^+\Lambda$ on Polarized Protons,"* Nucl.Phys. B **137** (1978) 269275

[6] S. Anefalos Pereira *et al.*, *"Differential cross section of $\gamma n \to K^+\Sigma^-$ on bound neutrons with incident photons from 1.1 to 3.6 GeV,"* Phys. Lett. B **688** (2010) 289

[7] P. Ambrozewicz *et al.*, *"Separated structure functions for the exclusive electroproduction of $K^+\Lambda$ and $K^+\Sigma^0$ final states,"* Phys. Rev. C **75**, 045203 (2007)

[8] A. V. Anisovich*et al.*, *"Baryon resonances and polarization transfer in hyperon photoproduction,"* Eur. Phys. J. A **34**, 243 (2007)

[9] I. S. Barker, A. Donnachie, J. K. Storrow, *"Complete experiments in pseudoscalar photoproduction,"* Nucl. Phys. B **95** (1975) 347

[10] C. B. Bebek *et al.*, *"Electroproduction of K^+ Mesons in the Forward Direction,"* Phys. Rev. Lett. **32**, 21 (1974)

[11] C. B. Bebek *et al.*, *"Electroproduction of K^+ Mesons Along the Virtual-Photon Direction,"* Phys. Rev. D **15**, 594 (1977)

[12] M. Benmerrouche, R. M. Davidson, and N. C. Mukhopadhyay, *"Problems of describing spin-3/2 baryon resonances in the effective Lagrangian theory,"* Phys. Rev. **C 39**, 2339 (1989)

[13] A. Bleckmann *et al.*, Z. Phys. **239**, 1 (1970)

[14] B. Borasoy, P. C. Bruns, U.-G. Meissner, and R. Nissler, *"A gauge-invariant chiral unitary framework for kaon photo- and electroproduction on the proton,"* Eur. Phys. J. A **34**, 161 (2007)

[15] E. Botta, T. Bressani, and G. Garbarino, *"Strangeness nuclear physics: a critical review on selected topics,"* Eur. Phys. J. A (2012) **48**: 41

[16] A. Boyarski *et al.* (SLAC collaboration), *"Photoproduction of $K^+\Lambda$ and $K^+\Sigma^0$ from hydrogen from 5 GeV to 16 GeV,"* Phys. Rev. Lett. **22** (1969) 11311133

[17] R. Bradford *et al.* (CLAS collaboration), *"Differential cross sections for $\gamma + p \to K^+ + Y$ for Λ and Σ^0 hyperons,"* Phys.Rev. **C73** (2006) 035202

[18] R. Bradford *et al.* (CLAS collaboration), *"First measurement of beam-recoil observables C_x and C_z in hyperon photoproduction,"* Phys. Rev. C **75** (2007) 035205

[19] C. N. Brown *et al.*, *"Coincidence Measurements of Single K^+ Electroproduction,"* Phys. Rev. Lett **28**, 1086 (1972)

[20] P. Bydžovský, T. Mart, *"Analysis of the consistency of kaon photoproduction data with Λ in the final state,"* Phys. Rev. C **76**, 065202 (2007)

[21] P. Bydžovský, D. Skoupil, *"Present status of isobar models for elementary kaon photoproduction,"* Genshikaku Kenkyu 57 (S3), 86 (2013), arXiv:1211.2684[nucl-th]

[22] P. Bydžovský, D. Skoupil, *"Theory of the electromagnetic production of hyperons,"* Nucl. Phys. A **914**, (2013) 14-22

[23] P. Bydžovský, M. Sotona, T. Motoba, K. Itonaga, K. Ogawa, and O. Hashimoto, *"Electromagnetic Production of Medium-Mass Λ-Hypernuclei,"* Nucl. Phys. A **881** (2012) 199217

[24] S. Capstick and W. Roberts, *"Quark Models of Baryon Masses and Decays,"* Prog. Part. Nucl. Phys. **45**, S241 (2000)

[25] D. S. Carman *et al.*, *"First Measurement of Transferred Polarization in the Exclusive* $\vec{e}p \to eK^+\vec{\Lambda}$ *Reaction,"* Phys. Rev. Lett. **90**,131804 (2003)

[26] W.-T. Chiang, F. Tabakin, T.-S. Lee, and B. Saghai, *"Coupled-channel study of* $\gamma + p \to K + \Lambda$*,"* Phys. Lett. B **517**, 101-108 (2001)

[27] F. Cusanno *et al.* (Jefferson Lab Hall A Collaboration), *"High-Resolution Spectroscopy of* ${}^{16}_{\Lambda}N$ *by Electroproduction,"* Phys. Rev. Lett. **103**, 202501 (2009)

[28] P. D. B. Collins, *"An Introduction to Regge Theory and High Energy Physics,"* Cambridge Monographs on Mathematical Physics, Cambridge University Press, 1977,

[29] T. Corthals, J. Ryckebusch, and T. Van Cauteren, *"Forward-angle* $K^+\Lambda$ *photoproduction in a Regge-plus-resonance approach,"* Phys. Rev. **C 73** (2006) 045207

[30] T. Corthals, T. Van Cauteren, J. Ryckebusch, and D. G. Ireland, *"Regge-plus-resonance treatment of the* $p(\gamma, K^+)\Sigma^0$ *and* $p(\gamma, K^0)\Sigma^+$ *reactions at forward kaon angles,"* Phys. Rev. C **75**, 045204 (2007)

[31] T. Corthals, T. Van Cauteren, P. Vancraeyveld, J. Ryckebusch, and D. G. Ireland, *"Electroproduction of kaons from the proton in a Regge-plus-resonance approach,"* Phys. Lett. B **656**, 186 (2007)

[32] J. C. David, C. Fayard, G. H. Lamot, and B. Saghai, *"Electromagnetic production of associated strangeness,"* Phys. Rev. C **53**, 2613 (1996)

[33] R. M. Davidson, R. Workman, *"Form factors and photoproduction amplitude,"* Phys. Rev. C **63**, 025210 (2001)

[34] L. De Cruz, *"Bayesian model selection for electromagnetic kaon production in the Regge-plus-resonance framework,"* PhD thesis, Ghent University, 2011 http://inwpent5.ugent.be/papers/phdlesley.pdf

[35] L. De Cruz, T. Vrancx, P. Vancraeyveld, and J. Ryckebusch, *"Bayesian Inference of the Resonance Content of $p(\gamma, K^+)\Lambda$,"* Phys. Rev. Lett. **108**, 182002 (2012)

[36] L. De Cruz, J. Ryckebusch, T. Vrancx, and P. Vancraeyveld, *"Bayesian analysis of kaon photoproduction with the Regge-plus-resonance model,"* Phys. Rev. C **86**, 015212 (2012)

[37] B. Dey, C. Meyer, *"Normalization discrepancies in photoproduction reactions,"* arXiv:1106.0479 [hep-ph]

[38] P. L. Donoho and R. L. Walker, *"Photoproduction of K^+ Mesons on Hydrogen,"* Phys. Rev. **107**, 1198 (1957)

[39] T. Feuster, U. Mosel, *"Photon- and meson-induced reactions on the nucleon,"* Phys. Rev. C **59** (1999) 460

[40] M. Froissart, *"Asymptotic behavior and subtractions in the Mandelstam representation,"* Phys.Rev. **123** (1961) 10531057

[41] T. Fujii *et al.*, *"Photoproduction of K^+ Mesons and Polarization of Λ^0 Hyperons in the 1-GeV Range,"* Phys. Rev. D **2**, 439 (1970)

[42] A. Gal, E. V. Hungerford, D. J. Millener, *"Strangenss in Nuclear Physics,"* arXiv:1605.00557 [nucl-th]

[43] F. Garibaldi *et al.*, *"High resolution hypernuclear spectroscopy at Jefferson Lab Hall A,"* Nucl. Phys. A **914** (2013) 34-40

[44] K. H. Glander, J. Barth, W. Braun, J. Hannappel, N. Jopen *et al.*, *"Measurement of $\gamma p \to K^+\Lambda$ and $\gamma p \to K^+\Sigma^0$ at photon energies up to 2.6 GeV,"* Eur. Phys. J. A **19** (2004) 251273, arXiv:nucl-ex/0308025

[45] S. Goers *et al.*, *"Measurement of $\gamma p \to K^0\Sigma^+$ at photon energies up to 1.55 GeV,"* Phys. Lett. B **464**, 331 (1999)

[46] M. Guidal, J. M. Laget, and M. Vanderhaegen, *"Pseudoscalar meson photoproduction at high energies: from the Regge regime to the hard scattering regime,"* Physics Letters B **400** (1997) 6-11

[47] M. Guidal, J. M. Laget, and M. Vanderhaegen, *"Pion and kaon photoproduction at high energies: forward and intermediate angles,"* Nucl. Phys. A **627**, 645 (1997)

[48] M. Guidal, J. M. Laget, and M. Vanderhaegen, *"Exclusive electromagnetic production of strangeness on the nucleon: Regge analysis of recent data,"* Phys. Rev. C **68**, 058201(R) (2003)

[49] H. Haberzettl, C. Bennhold, T. Mart and T. Feuster, *"Gauge-invariant tree-level photoproduction amplitudes with form factors,"* Phys. Rev. C **58**, R40(R) (1998)

[50] J. He, *"The* $\Sigma(1385)$ *photoproduction from proton within a Regge-plus-resonance approach,"* arXiv:1311.0571 [nucl-th]

[51] K. Hicks *et al.* (LEPS collaboration), *"Measurement of the* $\vec{\gamma}p \to K^+\Lambda$ *reaction at backward angles,"* Phys. Rev. C **76** (2007) 042201

[52] S. S. Hsiao, D. H. Lu, and S. N. Yang, *"Pseudovector versus pseudoscalar coupling in kaon photoproduction reexamined,"* Phys. Rev. C **61**, 068201 (2000)

[53] B. Han, M. Cheoun, K. Kim, and I. T. Cheon, *"An isobaric model for kaon photoproduction,"* Nucl. Phys. A **691**, 713 (2001)

[54] M. Iodice *et al.* (Jefferson Lab Hall A Collaboration), *"High Resolution Spectroscopy of* ${}^{12}_{\Lambda}B$ *by Electroproduction,"* Phys. Rev. Lett. **99**, 052501 (2007)

[55] D. G. Ireland, S. Janssen, and J. Ryckebusch, *"A genetic algorithm analysis of* N^* *resonances in* $p(\gamma, K^+)\Lambda$ *reactions,"* Nucl. Phys. A **740** (2004) 147-167

[56] F. James and M. Roos, MINUIT, CERN Report No. D506, 1981

[57] S. Janssen, J. Ryckebusch, D. Debruyne, and T. Van Cauteren, *"Kaon photoproduction: Background contributions, form-factors and missing resonances,"* Phys. Rev. C **65**, 015201 (2001)

[58] S. Janssen, J. Ryckebusch, D. Debruyne, and T. Van Cauteren, *"*Σ *photoproduction in the resonance region,"* Phys. Rev. C **66**, 035202 (2002)

[59] S. Janssen, J. Ryckebusch, W. Van Nespen, D. Debruyne, and T. Van Cauteren, *"The role of hyperon resonances in $p(\gamma, K^+)\Lambda$ processes,"* Eur. Phys. J. A **11**, 105 (2001)

[60] S. Janssen, D. G. Ireland, J. Ryckebusch, *"Extraction of N^* information from the limited $p(\gamma, K^+)\Lambda$ data set,"* Phys. Lett. B **562**, 51 (2003)

[61] T. C. Jude *et al.*, *"$K^+\Lambda$ and $K^+\Sigma^0$ photoproduction with fine center-of-mass energy resolution,"* Phys. Lett. B **735** (2014) 112-118

[62] B. Julia-Diaz, B. Saghai, T.-S. H. Lee, and F. Tabakin, *"Dynamical coupled-channels approach to hadronic and electromagnetic kaon-hyperon production on the proton,"* Phys. Rev. C **73**, 055204 (2006)

[63] T. K. Kuo, *"Low-Energy Photoproduction of Λ^0 and K^+ from Protons,"* Phys. Rev. **129**, 2264 (1963)

[64] R. Lawall *et al.*, *"Measurement of the reaction $\gamma p \to K^0\Sigma^+$ at photon energies up to 2.6 GeV,"* Eur. Phys. J. A **24**, 275 (2005)

[65] N. Levy, W. Majerotto, and B. J. Read, *"Kaon Photoproduction,"* Nucl. Phys. **55** (1973) 493

[66] A. Lleres, O. Bartalini, V. Bellini, J. P. Bocquet, P. Calvat *et al.* (GRAAL collaboration), *"Polarization observable measurements for $\gamma p \to K^+\Lambda$ and $\gamma p \to K^+\Sigma^0$ for energies up to 1.5 GeV,"* Eur.Phys.J. **A31** (2007) 7993

[67] A. Lleres *et al.* (GRAAL collaboration), *"Measurement of beam-recoil observables O_x, O_z and target asymmetry for the reaction $\gamma p \to K^+\Lambda$,"* Eur.Phys.J. **A39** (2009) 149161

[68] N. Kaiser, T. Waas, W. Weise, *"SU(3) chiral dynamics with coupled channels eta and kaon photoproduction,"* Nucl. Phys. A **612** (1997) 297

[69] H. Kohri *et al.*, *"Differential cross section and photon-beam asymmetry for the $\vec{\gamma}n \to K^+\Sigma^-$ reaction at $E_\gamma = 1.5 - 2.4$ GeV,"* Phys. Rev. Lett. **97** (2006) 082003

[70] G. Knöchlein, D. Drechsler, and L. Tiator, *"Photo- and Electroproduction of Eta Mesons,"* Z. Phys. A **352** (1995) 327

[71] P. Markowitz and A. Acha, *"Low Q^2 Kaon Electroproduction,"* Int. J. Mod. Phys. E **19**, 2383 (2010)

[72] T. Mart, *"Electromagnetic production of kaons near threshold,"* Phys. Rev. C **82**, 025209 (2010)

[73] T. Mart, *"Coupling strength of the $N^*(1535)S_{11}$ to the $K^+\Lambda$ channel,"* Phys. Rev. C **87**, 042201(R) (2013)

[74] T. Mart and C. Bennhold, *"Evidence for a missing nucleon resonance in kaon photoproduction,"* Phys. Rev. C **61**, 012201(R) (1999);

[75] T. Mart, C. Bennhold, H. Haberzettl, and L. Tiator, *"Kaon-MAID," Online* `http://portal.kph.uni-mainz.de/MAID//kaon/kaonmaid.html`

[76] T. Mart, C. Bennhold, C. E. Hyde-Wright, *"Constraints on Coupling Constants Through Charged Σ Photoproduction,"* Phys. Rev. C **51**, R1074 (1995)

[77] T. Mart, N. Nurhadiansyah, *"Are Hyperon Resonances Required in the Elementary $K^+\Lambda$ Photoproduction?"* Few-Body Syst 54: 1729-1739

[78] T. Mart, A. Sulaksono, *"Kaon photoproduction in a multipole approach,"* Phys. Rev. C **74**, 055203 (2006)

[79] O. V. Maxwell, *"New fit to the reaction $\gamma p \to K^+\Sigma^0$,"* Phys. Rev. C **92**, 044614 (2015)

[80] O. V. Maxwell, *"Model dependence in the photoproduction of kaons from protons and deuterons,"* Phys. Rev. C **70**, 044612 (2004)

[81] O. V. Maxwell, *"Model and form factor dependence in the reaction $ep \to e'K^+\Lambda$,"* Phys. Rev. C **76**, 014621 (2007)

[82] M. E. McCracken *et al.* (CLAS collaboration), *"Differential cross section and recoil polarization measurements for the $\gamma + p \to K + \Lambda$ reaction using CLAS at Jefferson Lab,"* Phys. Rev. C **81** (2010) 025201

[83] J. W. McNabb *et al. "Hyperon photoproduction in the nucleon resonance region,"* Phys.Rev. C **69** (2004) 042201

[84] T. Miyoshi *et al.*, *"High Resolution Spectroscopy of the ${}^{12}_{\Lambda}B$ Hypernucleus Produced by the $(e,e'K^+)$ Reaction,"* Phys. Rev. Lett. **90**, 232502 (2003)

[85] T. Mizutani, C. Fayard, G.-H. Lamot, and B. Saghai, *"Off-shell effects in the electromagnetic production of strangeness,"* Phys. Rev. C **58**, 75 (1998)

[86] R. M. Mohring *et al.*, *"Separation of the longitudinal and transverse cross sections in the ${}^1H(e,e'K^+)\Lambda$ and ${}^1H(e,e'K^+)\Sigma^0$ reactions,"* Phys. Rev. C **67**, 055205 (2003)

[87] K. Ohta, *"Electromagnetic Interactions of Extended Nucleons"* Phys. Rev. C **40**, 1335 (1989)

[88] K. A. Olive *et al.*, *"Review of Particle Physics,"* Chin. Phys. C **38**, 090001 (2014)

[89] V. Pascalutsa, *"On the interaction of spin-3/2 particles,"* arXiv:hep-ph/9412321

[90] V. Pascalutsa, *"Quantization of an interacting spin-3/2 field and the Δ isobar,"* Phys. Rev. **D 58**, 096002

[91] V. Pascalutsa and R. Timmermans, *"Field theory of nucleon to higher-spin baryon transitions,"* Phys. Rev. C **60**, 042201(R)

[92] C. Paterson, *"Polarization observables in strangeness photoproduction with CLAS at Jefferson Lab,"* PhD Thesis, University of Glasgow, 2008 `http://nuclear.gla.ac.uk/npe-theses/Paterson_thesis.pdf`

[93] A. de la Puente, O. V. Maxwell, and B. A. Raue, *"New fit to the reaction $\gamma p \to K^+\Lambda$,"* Phys. Rev. C **80**, 065205 (2009)

[94] D. J. Quinn *et al.*, *"A study of charged pseudoscalar meson photoproduction from hydrogen and deuterium with 16 GeV linearly polarized photons,"* Phys. Rev. D **20** (1979) 1553

[95] T. Regge, *"Introduction to Complex Orbital Momenta,"* Nuovo Cimento **14**, 951 (1959)

[96] A. M. Sandorfi *et al.*, *"Calculations of Polarization Observables in Pseudoscalar Meson Photo-production Reactions,"* arXiv:0912.3505v3

[97] A. Sarantsev *et al.*, *"Decays of baryon resonances into* ΛK^+, $\Sigma^0 K^+$ *and* $\Sigma^+ K^0$ *,"* Eur. Phys. J. **A25**, 441-453 (2005)

[98] J. Schaffner-Bielich, *"Strangeness in Compact Stars,"* Nucl. Phys. A **835**, 279 (2010)

[99] V. Shklyar, H. Lenske, and U. Mosel, *"Coupled-channel analysis of* $K\Lambda$ *production in the nucleon resonance region,"* Phys. Rev. C **72** 015210 (2005)

[100] R. A. Schumacher, *"Polarization of Hyperons in Elementary Photoproduction,"*, arXiv:nucl-ex/0611035

[101] R. A. Schumacher, M. M. Sargsian, *"Scaling and resonances in elementary* $K^+\Lambda$ *photoproduction,"* Phys. Rev. C **83**, 025207 (2011)

[102] A. Silverman, R. R. Wilson, and W. M. Woodward, *"Photoproduction of* K *Mesons in Hydrogen,"* Phys. Rev. **108**, 501 (1957)

[103] D. Skoupil, P. Bydžovský, *"Photoproduction of* $K\Lambda$ *on the Proton,"* Phys. Rev. C **93**, 025204 (2016)

[104] M. Sotona, S. Frullani, *"Electroproduction of Strangeness and Spectroscopy of Light Hypernuclei,"* Prog. Theor. Phys. Suppl. **117**, 151 (1994)

[105] S. Steininger and U.-G. Meissner, *"Threshold kaon photo- and electroproduction in SU(3) baryon chiral perturbation theory,"* Phys. Lett. B **391**, 446 (1997)

[106] StrangeCalc - A Web Interface for Computing with Ghent models [cited on 27$^{\text{th}}$ May, 2016], `http://rprmodel.ugent.be/calc/`

[107] J. J. de Swart, *"The Octet Model and its Clebsch-Gordan Coefficients,"* Rev. Mod. Phys. **35**, 916 (1963)

[108] M. Sumihama *et al.* (LEPS Collaboration), *"The* $\gamma + p \to K + \Lambda$ *and* $\gamma + p \to K + \Sigma^0$ *reactions at forward angles with photon energies from* 1.5 *to* 2.4 *GeV,"* Phys. Rev. C **73** (2006) 035214

[109] H. Thom, *"Phenomenological Analysis of* $K^+\Lambda$ *Photoproduction,"* Phys. Rev **151**, 1322 (1966)

[110] M. Q. Tran *et al.*, *"Measurement of $\gamma p \to K^+\Lambda$ and $\gamma p \to K^+\Sigma^0$ at photon energies up to 2 GeV,"* Phys. Lett. B **445**, 20 (1998)

[111] K. Tsukada *et al.*, *"Photoproduction of neutral kaons on a liquid deuterium target in the threshold region,"* Phys. Rev. C **78**, 014001 (2008) *ibid.* **83** (2011) 039904(E)

[112] G. M. Urcioli *et al.* (Jefferson Lab Hall A Collaboration), *"Spectroscopy of ${}^{9}_{\Lambda}Li$ by electroproduction,"* Phys. Rev. C **91**, 034308 (2015)

[113] P. Vancraeyveld, *"Regge-plus-resonance approach to strangeness production from the deuteron,"* PhD Thesis, Ghent University, 2011, `http://inwpent5.ugent.be/papers/phdpietervan.pdf`

[114] P. Vancraeyveld, L. De Cruz, J. Ryckebusch, T. Van Cauteren, *"Regge-plus-resonance predictions for kaon photoproduction from the neutron,"* Phys. Lett. B **681** (2009) 428-433

[115] T. Vrancx, L. De Cruz, J. Ryckebusch, and P. Vancraeyveld, *"Consistent interactions for high-spin baryons,"* arXiv:1108.0780

[116] T. Vrancx, L. De Cruz, J. Ryckebusch, and P. Vancraeyveld, *"Consistent interactions for high-spin fermion fields,"* Phys. Rev. **C 84** (2011) 045201

[117] T. Vrancx, J. Ryckebusch, and J. Nys, *"$K^+\Lambda$ electroproduction above the resonance region,"* arXiv:1404.4156v [nucl-th]

[118] G. Vogel *et al.*, *"Recoil polarization in $K^+\Lambda$ photoproduction at 5 GeV,"* Phys. Lett. B **40** (1972) 513516

[119] R. A. Williams, C.-R. Ji, and S. R. Cotanch, *"Hyperon electroproduction in a crossing and duality constrained model,"* Phys. Rev. C **46**, 1617 (1992)

[120] R. Workman, *"Comment on Kaon photoproduction: Data consistency, coupling constants, and polarization observables,"* Phys. Rev. C **44**, 552 (1991)

[121] R. Zegers *et al.* (LEPS collaboration), *"Beam polarization asymmetries for the $p(\gamma, K^+)\Lambda$ and $p(\gamma, K^+)\Sigma^0$ reactions at $E_\gamma = 1.5 - 2.4\,GeV$,"* Phys. Rev. Lett. **91** (2003) 092001

[122] Zhenping Li, *"Kaon photoproduction off nucleons in the chiral quark model,"* Phys. Rev. C **52**, 1648 (1995)

[123] Zhenping Li, Hongxing Ye, and Minghui Lu, *"Unified approach to pseudoscalar meson photoproductions off nucleons in the quark model,"* Phys. Rev. C **56**, 1099 (1997)

Appendix A

Contributions to the Invariant Amplitude

We consider the process

$$\gamma_V(k) + p(p) \to K^+(p_K) + \Lambda(p_\Lambda) \tag{A.1}$$

with corresponding four-momenta given in the parentheses. The four-momentum of the intermediate particle is denoted by $q = p + k = p_K + p_\Lambda$. In the next sections, we summarize the invariant amplitudes with no hadron form factors. These are introduced in the manner shown in Appendix C. The electromagnetic form factors are explicitly included in the Born contributions only. For the rest of the contributions, they are introduced merely by multiplying the coupling parameter with appropriate electromagnetic form factor.

Before we start writing out the formulae of various contributions to the amplitude, let us introduce the convention which we use in our work. The metric tensor has the usual form of

$$g^{\mu\nu} = \mathrm{diag}\,(1, -1, -1, -1).$$

The Pauli matrices are given by

$$\sigma_1 = \begin{pmatrix} 0 & 1 \\ 1 & 0 \end{pmatrix}, \quad \sigma_2 = \begin{pmatrix} 0 & -\mathtt{i} \\ \mathtt{i} & 0 \end{pmatrix}, \quad \sigma_3 = \begin{pmatrix} 1 & 0 \\ 0 & -1 \end{pmatrix}, \tag{A.2}$$

and fulfil following relations

$$\sigma^i \sigma^j = \mathtt{i}\varepsilon_{ijk}\sigma^k, \quad [\sigma^i, \sigma^j] = 2\mathtt{i}\varepsilon_{ijk}\sigma^k, \quad \{\sigma^i, \sigma^j\} = 2\delta_{ij}. \tag{A.3}$$

The Dirac matrices are defined as 4×4 matrices that fulfill the anticommutation relations

$$\{\gamma^\mu, \gamma^\nu\} = \gamma^\mu\gamma^\nu + \gamma^\nu\gamma^\mu = 2g^{\mu\nu}.$$

In the four-dimensional Minkowski space, there exist several representations of Dirac matrices and we choose the standard form which in terms of Pauli matrices reads

$$\gamma^0 = \begin{pmatrix} \hat{1} & 0 \\ 0 & -\hat{1} \end{pmatrix}, \quad \gamma^j = \begin{pmatrix} 0 & \sigma^j \\ -\sigma^j & 0 \end{pmatrix}, \tag{A.4}$$

where $j = 1, 2, 3$ and $\hat{1}$ denotes a 2×2 unit matrix. With the help of γ^μ's we can define a product

$$\gamma_5 = \mathtt{i}\gamma_0\gamma_1\gamma_2\gamma_3, \tag{A.5}$$

which obeys the commutation relation

$$\{\gamma_\mu, \gamma_5\} = 0, \tag{A.6}$$

and has the property of $\gamma_5^\dagger = \gamma_5$. A tensor $\sigma^{\mu\nu}$ is defined as

$$\sigma^{\mu\nu} = \frac{\mathtt{i}}{2}[\gamma^\mu, \gamma^\nu]. \tag{A.7}$$

We also use the well-known Feynman slash notation, *i.e.* $\not{a} = a_\mu\gamma^\mu$, where a is a four-vector. The $\epsilon_{\mu\nu\alpha\beta}$ denotes the totally antisymmetric Levi-Civita symbol, where $\epsilon_{0123} = 1$, and the electromagnetic tensor reads

$$F_{\mu\nu} = \partial_\mu A_\mu - \partial_\nu A_\mu,$$

where ∂_μ and A_μ are the four gradient and four-vector potential, respectively.

For casting the invariant amplitudes to the compact form of Equation (2.7), especially in the case of contributions stemming from $N^*(3/2)$ and $N^*(5/2)$ exchanges, it is convenient to employ a relation

$$-\mathtt{i}\varepsilon^{\mu\nu\alpha\beta}\gamma_5\gamma_\beta = \gamma^\mu\gamma^\nu\gamma^\alpha - g^{\mu\nu}\gamma^\alpha - g^{\nu\alpha}\gamma^\mu + g^{\mu\alpha}\gamma^\nu. \tag{A.8}$$

The positive- and negative-energy four-component spinors $u(p)$ and $v(p)$ of an on-shell particle with four-momentum p^μ and mass m are the solutions of the Dirac equation

$$(\not{p} - m)\, u(p) = 0, \tag{A.9a}$$

$$(\not{p} + m)\, v(p) = 0. \tag{A.9b}$$

For reader's convenience, we write out also the forms of propagators for exchanges of various resonances. Spin-0, spin-1 and spin-1/2 propagators are given in the standard way, which can be found in every proper textbook of quantum field theory, and read

$$P_0 = \frac{1}{q^2 - m^2 + \mathtt{i}m\Gamma}, \tag{A.10a}$$

$$P_1^{\mu\nu} = \frac{1}{q^2 - m^2 + \mathtt{i}m\Gamma}\left(-g^{\mu\nu} + \frac{q^\mu q^\nu}{m^2}\right), \tag{A.10b}$$

$$P_{1/2} = \frac{\not{q} + m}{q^2 - m^2 + \mathtt{i}m\Gamma}, \tag{A.10c}$$

where q, m, and Γ are four-momentum, mass and width of the considered resonance, respectively. In order to account for a finite lifetime of the resonance, we introduce the width Γ of the resonance in the denominator of the propagator.

The Rarita-Schwinger propagator for particles with spin 3/2 can be written down in terms of spin-projection operators $P_{\mu\nu}^{(J)}$, *i.e.*

$$S_{\mu\nu}(q) = \frac{\not{q} + m}{q^2 - m^2 + \mathtt{i}m\Gamma} P_{\mu\nu}^{(3/2)} - \frac{2}{3m^2}(\not{q} + m) P_{22,\mu\nu}^{(1/2)} + \frac{1}{m\sqrt{3}}\left(P_{12,\mu\nu}^{(1/2)} + P_{21,\mu\nu}^{(1/2)}\right), \tag{A.11}$$

where the operator

$$P_{\mu\nu}^{(3/2)} = g_{\mu\nu} - \frac{1}{3}\gamma_\mu\gamma_\nu - \frac{\not{q}q_\nu\gamma_\mu + q_\mu\gamma_\nu\,\not{q}}{3q^2} \tag{A.12}$$

projects only spin-3/2 states and complies with a relation $\gamma^\mu P_{\mu\nu}^{(3/2)} = P_{\mu\nu}^{(3/2)}\gamma^\nu = q^\mu P_{\mu\nu}^{(3/2)} = q^\nu P_{\mu\nu}^{(3/2)} = 0$. The terms

$$P_{22,\mu\nu}^{(1/2)} = \frac{q_\mu q_\nu}{q^2}, \qquad P_{12,\mu\nu}^{(1/2)} = \frac{q^\rho p_\nu \sigma_{\mu\rho}}{\sqrt{3}q^2}, \qquad P_{21,\mu\nu}^{(1/2)} = \frac{q_\mu q^\rho \sigma_{\rho\nu}}{\sqrt{3}q^2} \tag{A.13}$$

are projection operators projecting spin-1/2 states [12].

Propagator of spin-5/2 particles in terms of projection operators reads [116]

$$\begin{aligned}P_{\mu\nu,\lambda\rho}(q) = \Bigg[& \frac{\not{q}+m}{q^2+m^2}\mathcal{P}^{(5/2)} - \frac{4}{5m^2}(\not{q}+m)\mathcal{P}^{(3/2)}_{11} + \frac{1}{m\sqrt{5}}\left(\mathcal{P}^{(3/2)}_{12}+\mathcal{P}^{(3/2)}_{21}\right) \\ & + \frac{2}{5m^4}(\not{q}+m)(q^2-m^2)\mathcal{P}^{(1/2)}_{11} - \frac{1}{5m^2}(\not{q}+m)\mathcal{P}^{(1/2)}_{33} \\ & + \frac{\sqrt{3}}{5m^2}(\not{q}+m)\left(\mathcal{P}^{(1/2)}_{12}+\mathcal{P}^{(1/2)}_{21}\right) - \frac{\sqrt{6}}{5m^3}(q^2-m^2)\left(\mathcal{P}^{(1/2)}_{13}+\mathcal{P}^{(1/2)}_{31}\right) \\ & - \frac{\sqrt{2}}{5m}\left(\mathcal{P}^{(1/2)}_{32}+\mathcal{P}^{(1/2)}_{23}\right)\Bigg]_{\mu\nu,\lambda\rho}(q).\end{aligned} \tag{A.14}$$

The projection operators have the form

$$\begin{aligned}\mathcal{P}^{(5/2)}_{\mu\nu;\lambda\rho}(q) = & \frac{1}{2}(\mathcal{P}_{\mu\lambda}\mathcal{P}_{\nu\rho}+\mathcal{P}_{\mu\rho}\mathcal{P}_{\nu\lambda}) - \frac{1}{5}\mathcal{P}_{\mu\nu}\mathcal{P}_{\lambda\rho} \\ & - \frac{1}{10}(\mathcal{P}_\mu\ \mathcal{P}_\lambda\mathcal{P}_{\nu\rho}+\ \mathcal{P}_\mu\ \mathcal{P}_\rho\mathcal{P}_{\nu\lambda}+\ \mathcal{P}_\nu\ \mathcal{P}_\lambda\mathcal{P}_{\mu\rho}+\ \mathcal{P}_\nu\ \mathcal{P}_\rho\mathcal{P}_{\mu\lambda}),\end{aligned} \tag{A.15a}$$

$$\mathcal{P}^{(3/2)}_{11,\mu\nu;\lambda\rho}(q) = \frac{1}{2}(\mathcal{P}_{\mu\lambda}\mathcal{Q}_{\nu\rho}+\mathcal{P}_{\nu\lambda}\mathcal{Q}_{\mu\rho}+\mathcal{P}_{\mu\rho}\mathcal{Q}_{\nu\lambda}+\mathcal{P}_{\nu\rho}\mathcal{Q}_{\mu\lambda}) - \frac{1}{6q^2}\mathcal{R}_{\mu\nu}\mathcal{R}_{\lambda\rho}, \tag{A.15b}$$

$$\mathcal{P}^{(3/2)}_{22,\mu\nu;\lambda\rho}(q) = \frac{1}{10}(\mathcal{P}_\mu\ \mathcal{P}_\lambda\mathcal{P}_{\nu\rho}+\ \mathcal{P}_\mu\ \mathcal{P}_\rho\mathcal{P}_{\nu\lambda}+\ \mathcal{P}_\nu\ \mathcal{P}_\lambda\mathcal{P}_{\mu\rho}+\ \mathcal{P}_\nu\ \mathcal{P}_\rho\mathcal{P}_{\mu\lambda}) - \frac{2}{15}\mathcal{P}_{\mu\nu}\mathcal{P}_{\lambda\rho}, \tag{A.15c}$$

$$\begin{aligned}\mathcal{P}^{(3/2)}_{21,\mu\nu;\lambda\rho}(q) = & \frac{1}{2\sqrt{5}q^2}\left[q_\lambda(\mathcal{P}_\mu\mathcal{P}_{\nu\rho}+\ \mathcal{P}_\nu\mathcal{P}_{\mu\rho})+q_\rho(\mathcal{P}_\mu\mathcal{P}_{\nu\lambda}+\ \mathcal{P}_\nu\mathcal{P}_{\mu\lambda})\right]\not{q} \\ & - \frac{1}{3\sqrt{5}q^2}\mathcal{P}_{\mu\nu}\mathcal{R}_{\lambda\rho}\not{q} = -\mathcal{P}^{(3/2)}_{12,\lambda\rho;\mu\nu}(q)\end{aligned} \tag{A.15d}$$

$$\mathcal{P}^{(1/2)}_{11,\mu\nu;\lambda\rho}(q) = \mathcal{Q}_{\mu\nu}\mathcal{Q}_{\lambda\rho}, \quad \mathcal{P}^{(1/2)}_{22,\mu\nu;\lambda\rho}(q) = \frac{1}{3}\mathcal{P}_{\mu\nu}\mathcal{P}_{\lambda\rho}, \quad \mathcal{P}^{(1/2)}_{33,\mu\nu;\lambda\rho}(q) = \frac{1}{6q^2}\mathcal{R}_{\mu\nu}\mathcal{R}_{\lambda\rho}, \tag{A.15e}$$

$$\mathcal{P}^{(1/2)}_{21,\mu\nu;\lambda\rho}(q) = \frac{1}{\sqrt{3}}\mathcal{P}_{\mu\nu}\mathcal{Q}_{\lambda\rho} = \mathcal{P}^{(1/2)}_{12,\lambda\rho;\mu\nu}(q), \tag{A.15f}$$

$$\mathcal{P}^{(1/2)}_{31,\mu\nu;\lambda\rho}(q) = \frac{1}{q^2\sqrt{6}}\mathcal{R}_{\mu\nu}\mathcal{Q}_{\lambda\rho}\not{q} = -\mathcal{P}^{(1/2)}_{13,\lambda\rho;\mu\nu}(q), \tag{A.15g}$$

$$\mathcal{P}^{(1/2)}_{23,\mu\nu;\lambda\rho}(q) = -\frac{1}{3\sqrt{2}q^2}\mathcal{P}_{\mu\nu}\mathcal{R}_{\lambda\rho}\not{q} = -\mathcal{P}^{(1/2)}_{32,\lambda\rho;\mu\nu}(q), \tag{A.15h}$$

with

$$\mathcal{P}_{\mu\nu}(q) = g_{\mu\nu} - \frac{1}{q^2}q_\mu q_\nu, \quad \mathcal{Q}_{\mu\nu}(q) = \frac{1}{q^2}q_\mu q_\nu, \tag{A.16a}$$

$$\mathcal{R}_{\mu\nu}(q) = q_\mu\ \mathcal{P}_\nu+\ \mathcal{P}_\mu q_\nu = \gamma_\mu q_\nu + \gamma_\nu q_\mu - \frac{2}{q^2}\not{q}q_\mu q_\nu. \tag{A.16b}$$

A.1 Born s Channel

The electromagnetic γpp vertex function reads

$$V_\mu^{EM} = F_1(k^2)\gamma_\mu + \frac{1-F_1(k^2)}{k^2}k_\mu \gamma\cdot k + \mathtt{i}\frac{F_2(k^2)}{2m_p}\sigma_{\mu\nu}k^\nu, \tag{A.17}$$

where $F_1(k^2)$ and $F_2(k^2)$ are the standard electromagnetic proton Dirac form factors, $F_1(0)=1$ and $F_2(0)=\kappa_p$, where κ_p is the anomalous proton magnetic moment. In the strong $K\Lambda p$ vertex, the pseudoscalar coupling is used

$$V_S = \mathtt{i}g_{K\Lambda p}\gamma_5. \tag{A.18}$$

The invariant amplitude reads

$$\mathbb{M}_{Bs} = \bar{u}(p_\Lambda)V_S\frac{\not{p}+\not{k}+m_p}{s-m_p^2}V_\mu^{EM}\varepsilon^\mu u(p), \tag{A.19}$$

and can be cast into the form (2.7)

$$\begin{aligned}\mathbb{M}_{Bs} = \bar{u}(p_\Lambda)\gamma_5\Big[&\mathcal{A}_1\mathcal{M}_1 + \mathcal{A}_2\mathcal{M}_2 + \mathcal{A}_4\mathcal{M}_4\\ &+ \mathcal{A}_6\mathcal{M}_6 + g_{K\Lambda p}\frac{k\cdot\varepsilon}{k^2}\Big]u(p),\end{aligned} \tag{A.20}$$

where the last term in the brackets is the gauge-invariance breaking term. One then gets for the scalar amplitudes

$$\mathcal{A}_1 = \frac{g_{K\Lambda p}}{s-m_p^2}\left(F_1+F_2\right), \tag{A.21a}$$

$$\mathcal{A}_2 = 2\frac{g_{K\Lambda p}}{s-m_p^2}F_1 \tag{A.21b}$$

$$\mathcal{A}_4 = \frac{g_{K\Lambda p}}{s-m_p^2}\frac{F_2}{m_p} = -2\mathcal{A}_6. \tag{A.21c}$$

A.2 Born t Channel

The electromagnetic vertex factor for pseudoscalar mesons K^+ reads

$$V_\mu^{EM} = F(k^2)(2p_K-k)_\mu + \frac{1-F(k^2)}{k^2}(2p_K-k)\cdot q\, q_\mu, \tag{A.22}$$

where $F(0)=1$. The strong interaction vertex factor is the same as in (A.18). The invariant amplitude has the form

$$\mathbb{M}_{Bt} = \bar{u}(p_\Lambda)V_S\frac{1}{t-m_K^2}V_\mu^{EM}\varepsilon^\mu u(p), \tag{A.23}$$

which can again be cast to the compact form

$$\mathbb{M}_{Bt} = \bar{u}(p_\Lambda)\gamma_5 \left[\mathcal{A}_2\mathcal{M}_2 + \mathcal{A}_3\mathcal{M}_3 - g_{K\Lambda p}\frac{k\cdot\varepsilon}{k^2}\right] u(p), \tag{A.24}$$

where the last term in the brackets is the same gauge-invariance breaking term as in the Born s-channel contribution, Equation (A.20), but with the opposite sign. Therefore, these two terms cancel in the total amplitude of the process and the gauge invariance remains preserved. There are only two non zero scalar amplitudes

$$\mathcal{A}_2 = -\mathcal{A}_3 = 2\frac{g_{K\Lambda p}}{t-m_K^2}F. \tag{A.25}$$

A.3 Born u Channel

The electromagnetic $\gamma\Lambda\Lambda$ vertex factor has the form

$$V_\mu^{EM} = F_1(k^2)\left[\gamma_\mu - \frac{k_\mu \gamma\cdot k}{k^2}\right] + \mathtt{i}\frac{F_2(k^2)}{2m_\Lambda}\sigma_{\mu\nu}k^\nu, \tag{A.26}$$

where $F_1(0) = 0$ and $F_2(0) = \kappa_\Lambda$. The strong interaction vertex factor is the same as in (A.18). The Born u-channel amplitude reads

$$\mathbb{M}_{Bu} = \bar{u}(p_\Lambda)V_\mu^{EM}\frac{\not{p}_\Lambda - \not{k} + m_\Lambda}{u-m_\Lambda^2}V_S\,\varepsilon^\mu u(p) \tag{A.27}$$

and the scalar amplitudes $\mathcal{A}_j$ are

$$\mathcal{A}_1 = \frac{g_{K\Lambda p}}{u-m_\Lambda^2}(F_1+F_2), \tag{A.28a}$$

$$\mathcal{A}_3 = 2\frac{g_{K\Lambda p}}{u-m_\Lambda^2}F_1, \tag{A.28b}$$

$$\mathcal{A}_5 = \frac{g_{K\Lambda p}}{u-m_\Lambda^2}\frac{F_2}{m_\Lambda} = 2\mathcal{A}_6. \tag{A.28c}$$

A.4 Non-Born s Channel: $N^*(1/2^\pm)$ Exchange

The amplitude for this contribution has the form

$$\mathbb{M}_{NBs}^{N^*(1/2)} = \mathtt{i}\bar{u}(p_\Lambda)g_{K\Lambda R}\gamma_5\Gamma\frac{\not{p}+\not{k}+m_R}{s-m_R^2+\mathtt{i}m_R\Gamma_R}\times\frac{\mu_{pR}}{m_p+m_R}\sigma^{\mu\nu}k_\nu\Gamma\varepsilon_\mu u(p). \tag{A.29}$$

In the case of nucleon resonances we have to distinguish resonances with the positive and negative parity P. This can be done by using Γ in the form

$$\Gamma = \begin{cases} 1, & P=+1 \\ \gamma_5, & P=-1 \end{cases} \tag{A.30}$$

The scalar amplitudes are

$$\mathcal{A}_1 = \frac{g_{K\Lambda R}}{s - m_R^2 + \mathtt{i} m_R \Gamma_R} \frac{m_R \pm m_p}{m_R + m_p} \mu_{pR}, \tag{A.31a}$$

$$\mathcal{A}_4 = \pm \frac{g_{K\Lambda R}}{s - m_R^2 + \mathtt{i} m_R \Gamma_R} \frac{2\mu_{pR}}{m_p + m_R}, \tag{A.31b}$$

$$\mathcal{A}_6 = -\frac{1}{2}\mathcal{A}_4, \tag{A.31c}$$

where the upper (lower) sign corresponds with the case of positive (negative) parity of the nucleon resonance.

A.5 Non-Born s Channel: $N^*(3/2^{\pm})$ Exchange

Free, *i.e.* on-shell, Rarita-Schwinger field for a particle with spin 3/2 fulfills the Dirac equation

$$(\mathtt{i}\, \partial\!\!\!/ - m)\psi^\mu = 0 \tag{A.32}$$

and conditions $\gamma_\mu \psi^\mu = \partial_\mu \psi^\mu = 0$.

Interaction Lagrangians for strong and electromagnetic vertices for spin-3/2 particle are adopted from Ref. [90]. The appropriate form of $\mathcal{L}_{int}$ for the strong vertex is

$$\mathcal{L}_S = \frac{f}{m_R m_K} \epsilon^{\mu\nu\alpha\beta} \bar{\psi}_\Lambda \gamma_5 \gamma_\alpha (\partial_\mu \psi_\nu)(\partial_\beta \phi_K^*) \Gamma, \tag{A.33}$$

where ψ_Λ, ψ_ν, and ϕ_K are wave functions of the hyperon, spin-3/2 resonance and kaon, respectively. We introduce the Γ as defined in (A.30) to distinguish the positive-parity resonance from the resonance with negative parity. In order to achieve a correct dimension of $\mathcal{L}_{int}$, we divided the coupling constant f by masses of the kaon m_K and the considered resonance m_R. The interaction Lagrangian for an electromagnetic vertex reads

$$\begin{aligned} \mathcal{L}_{EM} &= \frac{g_{\gamma pR}}{m_R(m_R + m_p)} \Gamma [\bar{\psi}_p \Theta_{\alpha\beta,\mu\nu} G^{\alpha\beta} F^{\mu\nu}]^\dagger \\ &= \frac{g_{\gamma pR}}{m_R(m_R + m_p)} \Gamma [2(1 + 2a_1)(\partial^\alpha \bar{\psi}^\beta)\psi_p F_{\alpha\beta} \\ &\quad - a_1(\partial^\alpha \bar{\psi}^\beta)\gamma_\beta \gamma^\sigma \psi_p F_{\alpha\sigma} + a_1(\partial^\alpha \bar{\psi}^\beta)\gamma_\alpha \gamma^\sigma \psi_p F_{\beta\sigma}], \end{aligned} \tag{A.34}$$

where $\Theta_{\alpha\beta,\mu\nu} = g_{\alpha\mu} g_{\beta\nu} + a_1 g_{\alpha\mu} \gamma_\beta \gamma_\nu$ and $G^{\alpha\beta} = \partial^\alpha \psi^\beta - \partial^\beta \psi^\alpha$. Again, a normalization was introduced to the electromagnetic interaction Lagrangian so that its dimension is correct.

The first term in the lowest line of (A.34) cancels the projection operators of spin-1/2 which are present in the Rarita-Schwinger propagator, but vanishes when contracted with a propagator of spin-3/2 particle (A.12),

$$P^{(3/2)}_{\nu\beta}\gamma^{\beta}[q\cdot k\ \not{\varepsilon} - q\cdot\varepsilon\ \not{k}] = 0, \tag{A.35}$$

and therefore does not contribute to the propagation of spin-3/2 mode either. In the Rarita-Schwinger propagator of spin-3/2 particles, only operators projecting on the spin-3/2 sector are left, which physically means that solely spin-3/2 particles do propagate.

In the subsequent formulae, we use a shorthand notation for electromagnetic coupling constants,

$$g_1 \equiv 2(1+2a_1)g_{\gamma pR}, \quad g_2 \equiv a_1 g_{\gamma pR}. \tag{A.36}$$

The corresponding vertex factors then read

$$V^{S}_{\nu} = \frac{f}{m_R m_K}\Gamma\,\epsilon_{\mu\nu\lambda\rho}\gamma_5\gamma^{\lambda}q^{\mu}p^{\rho}_{K}, \tag{A.37a}$$

$$\begin{aligned} V^{EM}_{\beta} = {} & \frac{\mathtt{i}g_1}{m_R(m_R+m_p)}\Gamma q^{\alpha}(k_{\alpha}\varepsilon_{\beta} - k_{\beta}\varepsilon_{\alpha}) \\ & + \frac{\mathtt{i}g_2}{m_R(m_R+m_p)}\Gamma\left\{\not{q}(k_{\beta}\not{\varepsilon} - \not{k}\varepsilon_{\beta}) - \gamma_{\beta}[q\cdot k\ \not{\varepsilon} - q\cdot\varepsilon\ \not{k}]\right\}. \end{aligned} \tag{A.37b}$$

Both of them vanish when contracted with the four-momentum of the exchanged particle

$$V^{S}_{\mu}q^{\mu} = V^{EM}_{\nu}q^{\nu} = 0, \tag{A.38}$$

which consequently leads to the cancellation of all spin-1/2 projection operators (A.13) and the third term in the operator projecting on spin-3/2 modes (A.12). As in the denominator of that term there is a squared four-momentum of the exchanged particle, which can be zero in the u-channel, its cancellation enables the use of this formalism for exchanges of spin-3/2 hyperon resonances as well.

The amplitude of the spin-3/2 contribution reads

$$\begin{aligned} \mathbb{M}^{N^*(3/2)}_{NBs} = {} & \bar{u}(p_\Lambda)\,\Gamma\,\frac{\mathtt{i}f}{m_R m_K}\,\epsilon_{\mu\nu\lambda\rho}\,\gamma_5\,\gamma^{\lambda}q^{\mu}p^{\rho}_{K}\times\frac{\not{q}+m_R}{s-m_R^2+\mathtt{i}m_R\Gamma_R}\left(g^{\nu\beta}-\frac{1}{3}\gamma^{\nu}\gamma^{\beta}\right) \\ & \times\frac{1}{m_R(m_R+m_p)}\left(g_1 q^{\alpha}F_{\alpha\beta} + g_2\,\not{q}F_{\beta\alpha}\,\gamma^{\alpha} - g_2\gamma_{\beta}\,q^{\alpha}\,F_{\alpha\tau}\,\gamma^{\tau}\right)\Gamma\,\gamma_5\,u(p), \end{aligned} \tag{A.39}$$

where g_1 and g_2 are the electromagnetic coupling constants and f is the strong coupling constant. Casting the amplitude to the compact form (2.7), the individual scalar

amplitudes $\mathcal{A}_j$ read

$$\begin{aligned}\mathcal{A}'_1 = & -\frac{G_1}{3}(q\cdot p_\Lambda \pm m_R m_\Lambda)\, q\cdot k + \frac{G_2}{3}(2s\, q\cdot p_\Lambda - 3s\, k\cdot p_\Lambda \\ & + 2s\, m_p m_\Lambda \mp m_R m_\Lambda\, q\cdot k \pm 2s\, m_R m_\Lambda \pm 2 m_p m_R q\cdot p_\Lambda + 2 q\cdot p_\Lambda\, q\cdot k),\end{aligned} \tag{A.40a}$$

$$\begin{aligned}\mathcal{A}'_2 = & G_1\left[s\, k\cdot p_\Lambda \mp m_R m_p\, k\cdot p_\Lambda - \frac{1}{3} q\cdot p_\Lambda\, k^2 \mp \frac{1}{3} m_R m_\Lambda k^2\right] \\ & + G_2\left[-2s\, k\cdot p_\Lambda \mp \frac{1}{3} m_\Lambda m_R k^2 + \frac{2}{3} k^2\, q\cdot p_\Lambda\right],\end{aligned} \tag{A.40b}$$

$$\mathcal{A}'_3 = G_1(\pm m_R m_p - s) q\cdot k + G_2(2 q\cdot k - k^2)s, \tag{A.40c}$$

$$\begin{aligned}\mathcal{A}'_4 = & G_1\left[-\frac{1}{3} s\, m_\Lambda + \frac{1}{3}(m_p \mp m_R)\, q\cdot p_\Lambda \pm \frac{1}{3} m_\Lambda m_p m_R \pm m_R\, k\cdot p_\Lambda\right] \\ & - G_2\left[-s\, m_\Lambda \mp \frac{1}{3} m_\Lambda m_p m_R + \frac{2}{3} m_p\, q\cdot p_\Lambda\right],\end{aligned} \tag{A.40d}$$

$$\mathcal{A}'_5 = \mp G_1 m_R\, q\cdot k + G_2(\pm m_R + m_p)s, \tag{A.40e}$$

$$\begin{aligned}\mathcal{A}'_6 = & G_1\left[\mp \frac{1}{3} m_\Lambda m_p m_R \mp m_R\, k\cdot p_\Lambda + \frac{1}{3} m_\Lambda s - \frac{1}{3} q\cdot p_\Lambda\,(m_p \mp m_R)\right] \\ & + G_2\left[-\frac{1}{3} m_\Lambda s \mp \frac{1}{3} m_\Lambda m_p m_R + \frac{2}{3} q\cdot p_\Lambda\,(m_p \pm m_R)\right],\end{aligned} \tag{A.40f}$$

where the coupling parameters G_1 and G_2 are given in Equation (5.4) and the upper (lower) sign corresponds with the case of positive (negative) parity of the nucleon resonance.

Each amplitude $\mathcal{A}'_i$, $i = 1, \ldots, 6$, has to be multiplied by the propagator denominator

$$\mathcal{A}_i = \frac{1}{s - m_R^2 + \mathrm{i} m_R \Gamma_R}\mathcal{A}'_i. \tag{A.41}$$

A.6 Non-Born s Channel: $N^*(5/2^\pm)$ Exchange

In general, a wave function of spin-$(n + 1/2)$ particle has a form

$$\Psi_{\mu_1\ldots\mu_n} = \gamma^{\nu_1}\ldots\gamma^{\nu_n} G_{\mu_1\ldots\mu_n\nu_1\ldots\nu_n}. \tag{A.42}$$

For a particle with spin 5/2 we then have

$$\Psi_{\mu\nu} = \gamma^\alpha\gamma^\beta G_{\mu\nu,\alpha\beta}, \tag{A.43}$$

where $G_{\mu\nu,\alpha\beta}$ is a gauge-invariant field for the spin-5/2 theory and reads [116]

$$\begin{aligned}G_{\mu\nu,\alpha\beta} = & -\partial_\mu\partial_\nu\psi_{\alpha\beta} - \partial_\alpha\partial_\beta\psi_{\mu\nu} \\ & + \frac{1}{2}(\partial_\mu\partial_\alpha\psi_{\nu\beta} + \partial_\mu\partial_\beta\psi_{\nu\alpha} + \partial_\nu\partial_\alpha\psi_{\mu\beta} + \partial_\nu\partial_\beta\psi_{\mu\alpha}).\end{aligned} \tag{A.44}$$

With the help of the relation $G_{\mu\nu,\alpha\beta} = G_{\mu\nu,\beta\alpha}$ and the formulation of $G_{\mu\nu,\alpha\beta}$, the wave function (A.43) can be recast to

$$\begin{aligned}\Psi_{\mu\nu} &= \gamma^\alpha\gamma^\beta G_{\mu\nu,\alpha\beta} = \frac{1}{2}(\gamma^\alpha\gamma^\beta + \gamma^\beta\gamma^\alpha)G_{\mu\nu,\alpha\beta} = g^{\alpha\beta}G_{\mu\nu,\alpha\beta} \\ &= g^{\alpha\beta}\Big(- \partial_\mu\partial_\nu g_{\alpha\lambda}g_{\beta\rho} - \partial_\alpha\partial_\beta g_{\mu\lambda}g_{\nu\rho} + \frac{1}{2}\partial_\mu\partial_\alpha g_{\nu\lambda}g_{\beta\rho} \\ &\quad + \frac{1}{2}\partial_\mu\partial_\beta g_{\nu\lambda}g_{\alpha\rho} + \frac{1}{2}\partial_\nu\partial_\alpha g_{\mu\lambda}g_{\beta\rho} + \frac{1}{2}\partial_\nu\partial_\beta g_{\mu\lambda}g_{\alpha\rho}\Big)\psi^{\lambda\rho}.\end{aligned} \tag{A.45}$$

For the exchange of $N^*(5/2)$, we use the consistent formalism [116] and the interaction Lagrangian of the strong vertex then reads

$$\mathcal{L}_S = \frac{f}{m_K^4}\bar{\psi}_\Lambda\Gamma\Psi_{\mu\nu}\partial^\mu\partial^\nu\phi_K^*. \tag{A.46}$$

Inserting the spin-5/2 wave function of the form (A.45), the strong vertex factor is

$$V^S_{\lambda\rho} = -\frac{f}{m_K^4}\Gamma[(p_K\cdot q)^2 g_{\lambda\rho} + q^2 p_{K\lambda}p_{K\rho} - 2q\cdot p_k\, q_\rho p_{K\lambda}]. \tag{A.47}$$

The interaction Lagrangian of the electromagnetic interaction is given as

$$\mathcal{L}_{EM} = -\frac{g_1}{(2m_p)^4}\bar{\Psi}_{\alpha\beta}\gamma_\nu\partial^\alpha\psi_p F^{\nu\beta}\Gamma - \frac{\mathtt{i}g_2}{(2m_p)^5}\bar{\Psi}_{\alpha\beta}\partial_\nu\partial^\alpha\psi_p F^{\nu\beta}\Gamma \tag{A.48}$$

and the electromagnetic vertex factor can be easily derived as

$$\begin{aligned}V^{EM}_{\sigma\tau} &= [q\cdot p\, q_\beta g_{\sigma\tau} + q^2 g_{\beta\tau}p_\sigma - q\cdot p\, q_\tau g_{\beta\sigma} - q_\beta q_\tau p_\sigma] \\ &\quad\times\left[\frac{g_1}{(2m_p)^4}(\not{k}g^{\alpha\beta} - k^\beta\gamma^\alpha) + \frac{g_2}{(2m_p)^5}\Big(k\cdot p\, g^{\alpha\beta} - k^\beta p^\alpha\Big)\right]\Gamma.\end{aligned} \tag{A.49}$$

Provided we lay both vertex factors around the full propagator of the spin-5/2 particle, non physical lower-spin components vanish. Thus, only spin-5/2 particle really propagates.

The amplitude for the $N^*(5/2^\pm)$ exchange reads

$$\begin{aligned}\mathbb{M}^{N^*(5/2)}_{NBS} &= -\frac{f}{m_K^4}\bar{u}(p_\Lambda)\gamma_5\Gamma\, q^2 p_K^\mu p_K^\nu \frac{\not{q} + m_R}{s - m_R^2 + \mathtt{i}m_R\Gamma_R} \\ &\quad\times\mathcal{P}_{\mu\nu,\lambda\rho}(q)\, q^2\, p^\lambda\left[\frac{g_1}{(2m_p)^4}\,\gamma_\alpha\, F^{\alpha\rho} + \frac{g_2}{(2m_p)^5}p_\alpha\, F^{\alpha\rho}\right]\Gamma\, u(p).\end{aligned} \tag{A.50}$$

Casting the amplitude to the compact form (2.7), the scalar amplitudes then read

$$\begin{aligned}\mathcal{A}_1' = G_1\Big\{ &\mp Q_{p_\Lambda p}Q_{kp_\Lambda} \pm \frac{1}{5}Q_{p_\Lambda p_\Lambda}Q_{kp} - \frac{1}{5}Q_{kp_\Lambda}(B\, q\cdot p + Cm_p) \\ &+ \frac{1}{5}Q_{p_\Lambda p}[2Cm_p + (2s - q\cdot k)B]\Big\} - \frac{G_2}{5}Q_{p_\Lambda p}Ck\cdot p,\end{aligned} \tag{A.51a}$$

$$\begin{aligned}
\mathcal{A}_2' = G_1\Big\{ &\pm Q_{p_\Lambda p}(k^2 q\cdot p_\Lambda - 2sk\cdot p_\Lambda) \mp \frac{1}{5}Q_{p_\Lambda p_\Lambda}k^2(q\cdot p + s) \\
&- \frac{1}{5}[\mp 2q\cdot p_\Lambda\, k\cdot p_\Lambda\, q\cdot k s \pm k^2(q\cdot p_\Lambda)^2(q\cdot k + s) + 2sm_R m_\Lambda k\cdot p_\Lambda q\cdot k \\
&- m_R m_\Lambda k^2 q\cdot p_\Lambda(q\cdot k + s) + Cm_p k^2 q\cdot p_\Lambda] - \frac{1}{5}Q_{p_\Lambda p}k^2 B\Big\} \\
&+ G_2\Big\{(m_R \pm m_p)Q_{p_\Lambda p}D - \frac{1}{5}(m_R \pm m_p)k^2 q\cdot p Q_{p_\Lambda p_\Lambda} \\
&+ \frac{1}{5}(sk\cdot p_\Lambda - k^2 q\cdot p_\Lambda)(Bm_p q\cdot k - Ck\cdot p) - \frac{1}{5}Q_{p_\Lambda p}Bm_p k^2\Big\},
\end{aligned} \tag{A.51b}$$

$$\begin{aligned}
\mathcal{A}_3' = G_1\Big\{ &\pm sQ_{p_\Lambda p}(2k\cdot p + k^2) - \frac{1}{5}s[(2k\cdot p\, q\cdot k - k^2 q\cdot p)B - m_p k^2 C]\Big\} \\
&+ G_2\Big\{s(m_R \pm m_p)k\cdot p\, Q_{p_\Lambda p} - \frac{1}{5}sk\cdot p(Bm_p q\cdot k - Ck\cdot p)\Big\},
\end{aligned} \tag{A.51c}$$

$$\begin{aligned}
\mathcal{A}_4' = G_1\Big\{ &\frac{1}{5}(m_R \mp m_p)q\cdot k Q_{p_\Lambda p_\Lambda} - AQ_{p_\Lambda p} \\
&+ \frac{1}{5}\{q\cdot p_\Lambda[Bm_p q\cdot k + C(2k^2 + k\cdot p) + 2s\, m_R k\cdot p_\Lambda] \pm 2k\cdot p_\Lambda s^2 m_\Lambda\} \\
&- \frac{1}{5}Q_{p_\Lambda p}[m_\Lambda(m_R m_p \mp 3s) + (3m_R \mp m_p)q\cdot p_\Lambda]\Big\} \\
&+ G_2\Big\{ \pm \frac{1}{5}k^2 q\cdot p Q_{p_\Lambda p_\Lambda} \mp DQ_{p_\Lambda p} + \frac{1}{5}DE - \frac{1}{5}Q_{p_\Lambda p}[m_R m_\Lambda(k^2 \mp s) \\
&+ q\cdot p_\Lambda(m_R m_p \mp k^2) \pm s(q\cdot p_\Lambda - m_\Lambda m_p)]\Big\},
\end{aligned} \tag{A.51d}$$

$$\begin{aligned}
\mathcal{A}_5' = G_1\Big\{ &s(\pm m_p - m_R)Q_{p_\Lambda p} - \frac{1}{5}s(Bm_p q\cdot k - Ck\cdot p)\Big\} \\
&+ G_2\Big\{ \pm sk\cdot p\, Q_{p_\Lambda p} + \frac{1}{5}Esk\cdot p\Big\},
\end{aligned} \tag{A.51e}$$

$$\begin{aligned}
\mathcal{A}_6' = G_1\Big\{ &AQ_{p_\Lambda p} - \frac{1}{5}q\cdot p(\pm m_p - m_R)Q_{p_\Lambda p_\Lambda} - \frac{1}{5}q\cdot p_\Lambda(Bm_p q\cdot k - Ck\cdot p) \\
&- \frac{1}{5}Q_{p_\Lambda p}[m_\Lambda(\pm s - m_R m_p) + A]\Big\} - G_2\Big\{ \pm q\cdot p_\Lambda\, k\cdot p\, Q_{p_\Lambda p} \\
&\pm \frac{1}{5}q\cdot p\, k\cdot p\, Q_{p_\Lambda p_\Lambda} + \frac{1}{5}q\cdot p_\Lambda\, k\cdot p E + \frac{1}{5}Q_{p_\Lambda p}B\, k\cdot p\Big\},
\end{aligned} \tag{A.51f}$$

where the coupling parameters G_1 and G_2 are given as in Equation (5.5) and

$$A = q\cdot p_\Lambda(\pm m_p - m_R), \tag{A.52a}$$

$$B = \pm q\cdot p_\Lambda - m_\Lambda m_R, \tag{A.52b}$$

$$C = \pm sm_\Lambda - m_R\, q\cdot p_\Lambda, \tag{A.52c}$$

$$D = k^2\, q\cdot p_\Lambda - s\, k\cdot p_\Lambda, \tag{A.52d}$$

$$E = m_p\, C - q\cdot p\, B, \tag{A.52e}$$

where the upper (lower) sign corresponds with the case of positive (negative) parity of the nucleon resonance.

The terms $Q_{p_\Lambda p}$, Q_{kp_Λ}, $Q_{p_\Lambda p_\Lambda}$ and Q_{kp} include four-momenta products given by the general prescription

$$Q_{XY} = s\, X\cdot Y - X\cdot q\, Y\cdot q, \tag{A.53}$$

the notation of four-momenta X and Y is given in Equation (A.1).

Each amplitude $\mathcal{A}'_i$, $i = 1,\ldots,6$, has to be multiplied by the propagator denominator as in Equation (A.41).

A.7 Non-Born t Channel: $K_1(1270)$ and $K^*(892)$ Exchanges

The amplitude for the pseudovector meson $K_1(1270)$ ($J^\pi = 1^+$) exchange reads

$$\begin{aligned}\mathbb{M}^{K_1}_{NBt} = \bar u(p_\Lambda)\frac{g}{m}&[g_{\alpha\mu}\, k\cdot(p-p_\Lambda) - k_\alpha(p-p_\Lambda)_\mu]\\ &\times\frac{\left(-g^{\alpha\lambda} + (p-p_\Lambda)^\alpha(p-p_\Lambda)^\lambda/m^2_{K_1}\right)}{t - m^2_{K_1} + \mathtt{i}m_{K_1}\Gamma_{K_1}}\\ &\times\left[f_V\gamma_\lambda\gamma_5 + \frac{f_T}{m_\Lambda + m_p}(\not p_\Lambda - \not p)\gamma_\lambda\gamma_5\right]\varepsilon^\mu u(p).\end{aligned} \tag{A.54}$$

And the scalar amplitudes $\mathcal{A}_j$ are given as

$$\mathcal{A}_2 = \frac{-2G_T}{(m_\Lambda + m_p)(t - m^2_{K_1} + \mathtt{i}m_{K_1}\Gamma_{K_1})}\, p_\Lambda\cdot k, \tag{A.55a}$$

$$\mathcal{A}_3 = \frac{2G_T}{(m_\Lambda + m_p)(t - m^2_{K_1} + \mathtt{i}m_{K_1}\Gamma_{K_1})}\, p\cdot k, \tag{A.55b}$$

$$\mathcal{A}_4 = \frac{G_V + G_T(m_\Lambda - m_p)(m_\Lambda + m_p)}{t - m^2_{K_1} + \mathtt{i}m_{K_1}\Gamma_{K_1}}, \tag{A.55c}$$

$$\mathcal{A}_5 = -\mathcal{A}_4. \tag{A.55d}$$

with $G_{V,T} = g f_{V,T}/m$. The mass scale m is arbitrarily chosen as 1 GeV.

The vector meson $K^*(892)$ ($J^\pi = 1^-$) exchange amplitude is

$$\begin{aligned}\mathbb{M}^{K^*}_{NBt} = \mathtt{i}\bar u(p_\Lambda)\frac{g}{m}&\epsilon^{\mu\nu\alpha\beta}k_\alpha(p_\Lambda - p)_\beta\\ &\times\frac{\left(-g_{\nu\sigma} + (p-p_\Lambda)_\nu(p-p_\Lambda)_\sigma/m^2_{K^*}\right)}{t - m^2_{K^*} + \mathtt{i}m_{K^*}\Gamma_{K^*}}\\ &\times\left[f_V\gamma^\sigma + \frac{f_T}{m_\Lambda + m_p}(\not p_\Lambda - \not p)\gamma^\sigma\right]\varepsilon_\mu u(p).\end{aligned} \tag{A.56}$$

The scalar amplitudes are given as

$$\mathcal{A}_1 = \frac{G_V(m_\Lambda + m_p) + G_T\, t/(m_\Lambda + m_p)}{t - m_{K^*}^2 + \mathtt{i} m_{K^*}\Gamma_{K^*}}, \tag{A.57a}$$

$$\mathcal{A}_2 = \frac{2k\cdot p_\Lambda\, G_T}{(m_\Lambda + m_p)(t - m_{K^*}^2 + \mathtt{i} m_{K^*}\Gamma_{K^*})}, \tag{A.57b}$$

$$\mathcal{A}_3 = \frac{-2k\cdot p\, G_T}{(m_\Lambda + m_p)(t - m_{K^*}^2 + \mathtt{i} m_{K^*}\Gamma_{K^*})}, \tag{A.57c}$$

$$\mathcal{A}_4 = \frac{G_V - G_T(m_\Lambda - m_p)/(m_\Lambda + m_p)}{t - m_{K^*}^2 + \mathtt{i} m_{K^*}\Gamma_{K^*}}, \tag{A.57d}$$

$$\mathcal{A}_5 = \frac{G_V + G_T(m_\Lambda - m_p)/(m_\Lambda + m_p)}{t - m_{K^*}^2 + \mathtt{i} m_{K^*}\Gamma_{K^*}}, \tag{A.57e}$$

with $G_{V,T} = g f_{V,T}/m$. As in the pseudovector case, the mass m is arbitrarily chosen to be 1 GeV.

A.8 Non-Born u Channel: $Y^*(1/2^\pm)$ Exchange

The non-Born amplitude for the $Y^*(1/2^\pm)$ exchange is

$$\begin{aligned}\mathbb{M}_{NBu}^{Y^*(1/2)} = {} & \mathtt{i}\bar{u}(p_\Lambda)\frac{\kappa_{\Lambda R}}{m_\Lambda + m_R}\sigma^{\mu\nu}k_\nu\Gamma \\ & \times \frac{\not{p}_\Lambda - \not{k} + m_R}{u - m_R + \mathtt{i} m_R\Gamma_R} g_{K\Lambda^* p}\gamma_5\Gamma\varepsilon_\mu u(p),\end{aligned} \tag{A.58}$$

with Γ defined as in (A.30). The scalar amplitudes $\mathcal{A}_j$ are then

$$\mathcal{A}_1 = \frac{g_{K\Lambda^* p}}{u - m_R^2 + \mathtt{i} m_R\Gamma_R}\frac{m_R \pm m_\Lambda}{m_R + m_\Lambda}\kappa_{\Lambda R}, \tag{A.59a}$$

$$\mathcal{A}_5 = \pm\frac{g_{K\Lambda^* p}}{u - m_R^2 + \mathtt{i} m_R\Gamma_R}\frac{2\kappa_{\Lambda R}}{m_\Lambda + m_R}, \tag{A.59b}$$

$$\mathcal{A}_6 = \frac{1}{2}\mathcal{A}_5, \tag{A.59c}$$

where the upper (lower) sign corresponds with the positive (negative) parity of the resonance.

A.9 Non-Born u Channel: $Y^*(3/2^\pm)$ Exchange

Interaction Lagrangians for strong and electromagnetic vertices for the exchange of spin-3/2 hyperon resonance in the u channel are adopted from Ref. [90]. The Lagrangian of the strong vertex has in the u channel the following form

$$\mathcal{L}_S = \frac{f}{m_R m_K}\epsilon_{\mu\nu\lambda\rho}(\partial^\mu\bar{\psi}^\nu)\gamma_5\gamma^\lambda\psi_p(\partial^\rho\phi_K)\Gamma \tag{A.60}$$

and the vertex factor is then easily derived as

$$V_\nu^S = \frac{f}{m_R m_K}\Gamma\epsilon_{\mu\nu\lambda\rho}\gamma_5\gamma^\lambda q^\mu p_K^\rho. \tag{A.61}$$

The Lagrangian of the electromagnetic vertex can be recast as

$$\begin{aligned}\mathcal{L}_{EM} &= -\frac{g}{m_R(m_R+m_\Lambda)}\bar\psi_\Lambda\Theta_{\alpha\beta,\mu\nu}G^{\alpha\beta}F^{\mu\nu}\gamma_5\Gamma \\ &= -\frac{1}{m_R(m_R+m_\Lambda)}[g_1\bar\psi_\Lambda(\partial_\mu\psi_\nu)F^{\mu\nu}\gamma_5 + g_2\bar\psi_\Lambda\gamma_\beta\gamma^\sigma G^{\beta\alpha}F_{\alpha\sigma}\gamma_5]\Gamma,\end{aligned} \tag{A.62}$$

where $\Theta_{\alpha\beta,\mu\nu} = g_{\alpha\mu}g_{\beta\nu} + a_1 g_{\alpha\mu}\gamma_\beta\gamma_\nu$. The corresponding vertex factor reads

$$\begin{aligned}V_\beta^{EM} = &\frac{g_1}{m_R(m_R+m_\Lambda)}q^\alpha(k_\alpha\varepsilon_\beta - k_\beta\varepsilon_\alpha) \\ &+ \frac{g_2}{m_R(m_R+m_\Lambda)}[\not q(k_\beta\not\varepsilon - \varepsilon_\beta\not k) - \gamma_\beta(q\cdot k\not\varepsilon - q\cdot\varepsilon\not k)]\gamma_5\Gamma.\end{aligned} \tag{A.63}$$

The amplitude for the $Y^*(3/2^\pm)$ exchange in the u-channel reads

$$\begin{aligned}\mathbb{M}_{NBu}^{Y^*(3/2)} = &\ \bar u(p_\Lambda)\,\Gamma\,\gamma_5\,\frac{1}{m_R(m_R+m_\Lambda)}\Big[g_1\,q^\alpha\,F_{\alpha\beta} + g_2\Big(\not q F_{\beta\alpha}\gamma^\alpha - \gamma_\beta\,q^\alpha\,F_{\alpha\rho}\,\gamma^\rho\Big)\Big] \\ &\times\frac{\not q + m_R}{u - m_R^2 + \mathtt{i}m_R\Gamma_R}\left(g^{\beta\nu} - \frac{1}{3}\gamma^\beta\gamma^\nu\right)\Gamma\frac{\mathtt{i}f}{m_R m_K}\,\epsilon_{\mu\nu\lambda\rho}\,\gamma_5\gamma^\lambda q^\mu p_K^\rho\,u(p).\end{aligned} \tag{A.64}$$

Casting the amplitude to the compact form, the scalar amplitudes are given as

$$\begin{aligned}\mathcal{A}_1' = &-\frac{1}{3}G_1 q\cdot k\,(\pm m_R m_p + q\cdot p) + \frac{1}{3}G_2[\pm 5m_R m_p\,q\cdot k \pm 2m_R m_p u \\ &+ 2q\cdot p\,q\cdot k \pm 2m_R m_\Lambda\,q\cdot p + 2u\,q\cdot p + 2m_\Lambda m_p u + 3u\,p\cdot k],\end{aligned} \tag{A.65a}$$

$$\mathcal{A}_2' = G_1 q\cdot k\,(\pm m_R m_\Lambda - u) + G_2(2q\cdot k\,u - uk^2 \mp 4m_R m_\Lambda\,q\cdot k), \tag{A.65b}$$

$$\begin{aligned}\mathcal{A}_3' = &\ G_1\left\{\frac{1}{3}k^2(\pm m_p m_R + q\cdot p) + p\cdot k\,(u \mp m_R m_\Lambda)\right\} \\ &+ G_2\left[\pm 4m_R m_\Lambda\,p\cdot k \mp \frac{5}{3}m_R m_p k^2 - \frac{2}{3}q\cdot p\,k^2 - 2p\cdot k\,u\right],\end{aligned} \tag{A.65c}$$

$$\mathcal{A}_4' = \mp G_1 m_R\,q\cdot k + G_2[\pm 4m_R\,q\cdot k + u(\pm m_R + m_\Lambda)], \tag{A.65d}$$

$$\begin{aligned}\mathcal{A}_5' = &\ \frac{1}{3}G_1[q\cdot p\,(\pm m_R - m_\Lambda) \mp m_R m_p m_\Lambda + u\,m_p \pm 3m_R\,p\cdot k] \\ &+ G_2\left[\pm\frac{5}{3}m_R m_p m_\Lambda \mp 4m_R\,p\cdot k - \frac{1}{3}u\,m_p + \frac{2}{3}m_\Lambda\,q\cdot p \mp \frac{4}{3}m_R\,q\cdot p\right],\end{aligned} \tag{A.65e}$$

$$\begin{aligned}\mathcal{A}_6' = &\ \frac{1}{3}G_1[q\cdot p\,(\pm m_R - m_\Lambda) \mp m_R m_p m_\Lambda + u\,m_p \pm 3m_R\,p\cdot k] \\ &+ G_2\left[\pm\frac{5}{3}m_R m_p m_\Lambda \mp 4m_R\,p\cdot k \mp 2m_R\,q\cdot p - u\,m_p + \frac{2}{3}m_\Lambda\,q\cdot p\right],\end{aligned} \tag{A.65f}$$

where $G_{1,2}$ are given as in (5.4) with m_p replaced by m_Λ and the upper (lower) sign corresponds with the case of positive (negative) parity of the hyperon resonance. Each amplitude $\mathcal{A}'_i$, $i = 1, \ldots, 6$, has to be multiplied by the propagator denominator

$$\mathcal{A}_i = \frac{1}{u - m_R^2 + \mathtt{i} m_R \Gamma_R} \mathcal{A}'_i. \tag{A.66}$$

Appendix B

Regge Trajectories and Propagators

At the energies of a few GeV and higher, where no individual resonances can be distinguished, the dynamics of the process is governed by the exchange of t-channel Regge trajectories. This choice is motivated by the shape of the $K\Lambda$ photoproduction cross section which is peaked on small $|t|$, *i.e.* on small kaon angles $\theta_K^{c.m.}$. This behaviour indicates a dominant role played by t-channel kaon exchanges.

The Regge trajectories, which are often called after a lightest member (so-called first materialization) of the particular trajectory, connect spin and mass squared of the exchanged particle. When the spins of a set of resonant states are plotted against their mass squared in a Chew-Frautschi plot, see Figure B.1, it is observed that all Regge trajectories can be reasonably well parameterized by means of a linear function

$$\alpha_X(t) = \alpha_{X,0} + \alpha'_X(t - m_X^2), \tag{B.1}$$

with m_X and $\alpha_{X,0}$ the mass and spin of the trajectory lightest member X, respectively. What is more, α'_X, which is the slope of the trajectory, happens to be close to an universal constant for all trajectories and acquires the value of $0.8\,\mathrm{GeV}^2$. It is widely believed that this universal slope of the trajectories reflects the behaviour of the underlying partonic degrees of freedom of the hadronic spectrum. Trajectory equations for $K^+(494)$ and

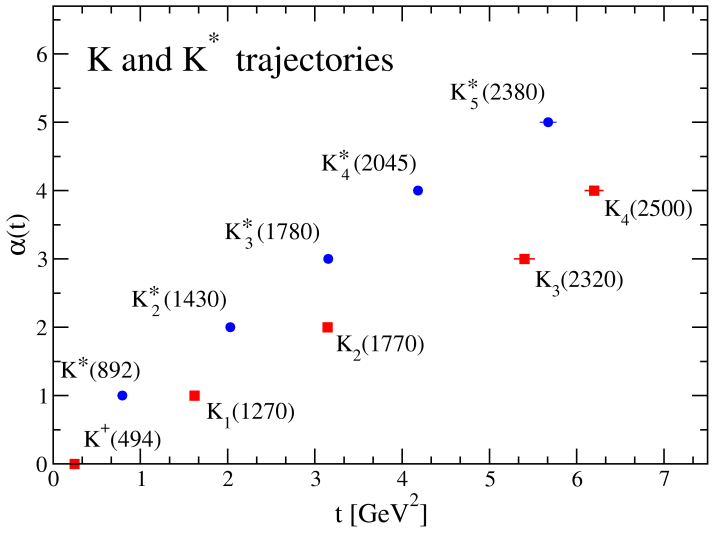

Figure B.1: Chew-Frautschi plot for the two lightest kaon trajectories assumed in our analysis. The squares and dots represent trajectories with parity $+1$ and -1, respectively. Both trajectories are linear to a very good approximation.

$K^{*+}(892)$ read

$$\alpha_{K(494)}(t) = 0.70\,(t - m_K^2), \tag{B.2a}$$

$$\alpha_{K^{*+}(892)}(t) = 1 + 0.85\,(t - m_{K^*}^2), \tag{B.2b}$$

respectively. Note that $t = m_X^2$ can never be reached in the physical region of the process as t is negative in this region.

An efficient way to model trajectory exchanges involves embedding the Regge formalism into a tree-level effective-field model. The amplitude for the t-channel exchange of a linear kaon trajectory $\alpha(t)$ can be obtained from the standard Feynman amplitude by replacing the usual pole-like Feynman propagator of a single particle with a Regge one of the form

$$\mathcal{P}_{Regge}^{\zeta=\pm1}(s,t) = \left(\frac{s}{s_0}\right)^{\alpha(t)} \frac{\pi\alpha'}{\sin(\pi\alpha(t))} \frac{1+\zeta \mathrm{e}^{-\mathrm{i}\pi\alpha(t)}}{2} \frac{1}{\Gamma(\alpha(t)+1)}, \tag{B.3}$$

while keeping the vertex structure given by the Feynman diagrams which correspond to the first materialization of the trajectory.

While deriving the Regge propagator, one has to differentiate between two signature parts of the trajectories, $\zeta = \pm 1$, in order to obey the convergence criteria: $\zeta = +1$ corresponds with the even and $\zeta = -1$ with the odd partial waves. Thus, a summation over this factor is to be done in the propagator. However, the theory does not allow to determine the relative sign between the even and odd parts of the trajectory. Therefore, we end up either with a so-called constant phase, identical to 1, or a rotating phase which gives rise to a complex factor of $\mathtt{exp}(-\mathtt{i}\pi\alpha(t))$:

$$\frac{1+\mathtt{e}^{-\mathtt{i}\pi\alpha(t)}}{2} \pm \frac{1-\mathtt{e}^{-\mathtt{i}\pi\alpha(t)}}{2} = \begin{cases} 1, & \text{constant phase,} \\ \mathtt{e}^{-\mathtt{i}\pi\alpha(t)}, & \text{rotating phase.} \end{cases}$$

In our treatment of $K\Lambda$ photoproduction, we identify the $K^+(494)$ and $K^{*+}(892)$ trajectories as the dominant contributions to the high-energy amplitude. Nonetheless, some groups include into their models also a third kaon trajectory in order to improve the ability of the model to describe the data. In this regard, there are two candidates considered: the axial-vector $K_1(1400)$ and the vector $K^*(1410)$ trajectories [117].

The corresponding propagators for the $K^+(494)$ and $K^{*+}(892)$ trajectories have the following form [29]

$$\mathcal{P}^{K(494)}_{Regge}(s,t) = \frac{(s/s_0)^{\alpha_K(t)}}{\sin(\pi\alpha_K(t))} \frac{\pi\alpha'_K}{\Gamma(1+\alpha_K(t))} \left\{ \begin{array}{c} 1 \\ \mathtt{e}^{-i\pi\alpha_K(t)} \end{array} \right\}, \tag{B.4a}$$

$$\mathcal{P}^{K^*(892)}_{Regge}(s,t) = \frac{(s/s_0)^{\alpha_{K^*}(t)-1}}{\sin(\pi\alpha_{K^*}(t))} \frac{\pi\alpha'_{K^*}}{\Gamma(\alpha_{K^*}(t))} \left\{ \begin{array}{c} 1 \\ \mathtt{e}^{-i\pi(\alpha_{K^*}(t)-1)} \end{array} \right\}. \tag{B.4b}$$

As can be seen from the definition of the Regge propagators, there are poles at non negative integer values of $\alpha_X(t)$, which correspond to the zeroes of the sine function which are not compensated by the poles of the Γ function. Here comes the interpretation of the Regge propagator effectively incorporating the exchange of all members of the $\alpha_X(t)$ trajectory. In the physical region of the process under study (with $t < 0$), these poles cannot be reached.

The separation of the Regge amplitude into two different signatures is a theoretical request to ensure convergence, experimentally both trajectories shown in (B.2) coincide with one another. The residue for the lowest materialisation is, therefore, assumed to be used for the combined trajectory of both odd and even parity. This assumption is then

called degeneracy. Whether a trajectory should be treated as degenerate or non degenerate, depends less on the trajectory equations themselves than on the process studied. It is the structure of the observed cross section that gives a hint whether the degeneracy is a valid supposition for a given channel or not. Non degenerate trajectories leads to peaks in the differential cross section because they exhibit so-called wrong-signature zeroes (these are zeroes of the Regge propagator corresponding to poles of the Γ function which are not removed by the sine function). On the other hand, a smooth differential cross section indicates degenerate trajectories [28]. Since no obvious structure is present in the $p(\gamma, K^+)\Lambda$ cross-section data for $E_\gamma^{lab} \geq 4\,\mathrm{GeV}$, both the $K^+(494)$ and $K^{*+}(892)$ trajectories are supposed to be degenerate [29].

Appendix C

The Gauge-Invariance Restoration in Isobar Models

The condition of gauge invariance, which is intimately connected with the conservation of electric charge, belongs to the most important properties of every physical theory dealing with electromagnetic interactions. In order to fulfil the gauge-invariance condition, the amplitude as the whole shall obey the current-conservation condition

$$k_\mu \mathbb{M}^\mu = 0 \tag{C.1}$$

which holds for every process involving either real or virtual photon with a four momentum k and polarization vector $\varepsilon(k)$.

If we do not include hadron form factors to account for the fact that nucleons are not pointlike objects, the full amplitude constructed with the help of effective Lagrangians is gauge invariant (note that the same holds for, *e.g.* pion photoproduction off the nucleon [49]). Resonant amplitudes are separately gauge invariant; the Born terms are gauge invariant as well, except for contributions of the s and t channel, where gauge non invariant terms of the form $g_{K\Lambda p}(k \cdot \varepsilon)/k^2$ appear, see Equations (A.20) and (A.24). These terms, however, vanish in the sum of s- and t-channel contributions.

With the introduction of hadron form factors the gauge non-invariant terms in the s- and t-channel Born contributions no longer cancel each other and the gauge invariance is lost. In order to restore it, a contact term of the form

$$\begin{aligned}\mathbb{M}_{contact} = &- g_{K\Lambda p}\bar{u}_\Lambda(p_\Lambda)\gamma_5\left[\frac{2p^\mu + \not{k}\gamma^\mu}{s - m_p^2}(\hat{F}_{DW} - F_s)\right. \\ &\left. + \frac{2p_K^\mu}{t - m_K^2}(\hat{F}_{DW} - F_t)\right]u_p(p)\varepsilon_\mu,\end{aligned} \tag{C.2}$$

is introduced. For $\hat{F}_{DW}$ the form

$$\hat{F}_{DW} = F_s(s) + F_t(t) - F_s(s)F_t(t), \tag{C.3}$$

introduced by Davidson and Workman [33] is used. In the definition (C.3) it holds $F_s(s = m_p^2) = F_t(t = m_K^2) = 1$ and $\hat{F}_{DW}(s = m_p^2, t) = \hat{F}_{DW}(s, t = m_K^2) = 1$ which prevents the poles in the contact-term contribution (C.2) from being reached.

In the past, a shape of hadron form factor

$$\hat{F}_H = a_s F_s(s) + a_t F_t(t) + a_u F_u(u), \tag{C.4}$$

proposed by Haberzettl was used [49]. The coefficients in Equation (C.4) fulfil the relation $a_s + a_t + a_u = 1$. The most democratic choice for the coefficients is $a_s = a_t = a_u = 1/3$.

Appendix D

Available Experimental Data

In general, 16 different quantities can be extracted experimentally in the pseudoscalar meson photoproduction. These are the unpolarized differential cross section, 3 single-polarization observables, and 12 double-polarization observables. The spin observables are not independent, but are constrained by various identities which can be further used to check the consistency of various measurements.

Many collaborations have measured observables of the processes $K^+\Lambda$ and $K^+\Sigma^0$ in a large kinematical region even though the number of data is still lower than in the pion-production channels. A great number of experimental data were published from the turn of the century by LEPS [51, 108], GRAAL [66, 67], MAMI [61], and particularly CLAS [17, 18, 82, 83] collaborations. Apart from data published in the last decade, there are also older high-energy data, *e.g.* SLAC [16] data, at one's disposal. Nowadays, one therefore has around 7000 $p(\gamma, K^+)\Lambda$ data at hand, an overview of which is given in Table D.1. Besides a name of the collaboration, year when the data were published, and number of data in the given set, Table D.1 shows also energy and angular ranges where the data are available.

If it is possible to determine a polarization of a given particle, one can measure the asymmetry of the cross section regarding this polarization. Provided there is one particle

polarized, we define single-polarization observables, which are hyperon polarization P, beam asymmetry Σ and target asymmetry T with polarized hyperon, photon and proton, respectively. Double-polarization observables, which demand information about the spin of two particles, can be divided into three types referred to as beam-target, beam-recoil, and target-recoil with photon and proton, photon and hyperon, and proton and hyperon polarized, respectively.

For a measurement of the hyperon polarization P in kaon photoproduction experiments, a "self-analyzing" property of the Λ hyperon is very useful. The Λ hyperon decays by means of weak interaction to $\pi^- p$. Since the proton is preferentially emitted along the polarization direction of the Λ, the Λ polarization can then be determined from the angular distribution of its decay products.

The precise measurement of beam asymmetry Σ was accomplished utilizing photon beams with a high degree of linear polarization in experiments at LEPS [108] and GRAAL [66] which provided the coverage of the energy range from the threshold up to 1.5 GeV. Another beam-asymmetry data set was published by CLAS collaboration [92], giving almost three times as many data as the results of the GRAAL collaboration which serves for a finer structure resolution.

Values for the target asymmetry T have been extracted by the GRAAL collaboration [67] even without a polarized target since this observable can be determined also by measuring the equivalent double-polarization observable which demands a linarly polarized photon and hyperon aligned perpendicular to the reaction plane [9].

For the photoproduction of K^+Y, the most accessible double-polarization observables are the ones which represent polarized photon and recoiling hyperon. Exact measurements of both C_x and C_z have been accomplished by the CLAS collaboration [18]. The O_x and O_z data have been published by the GRAAL collaboration [67].

For adjusting free parameters of the models, we do not use SAPHIR cross section data since they show discrepancies in comparison with CLAS and LEPS cross section data, which are consistent with each other as well as internally consistent. Cross-section data measured by the SAPHIR collaboration are systematically lower than CLAS [82] and LEPS cross section data, especially in the forward angle region. Simultaneous fitting on the CLAS and SAPHIR data is possible only if a normalization function depending on energy is introduced [97].

There are two different ways of computing the total error. The total systematic error may be assembled from several partial systematic errors (or the data may stem from several experiments with various systematic errors). If it is composed of more than ten partial errors (or if the data set is put together from more than ten different experiments), the total error is then given

$$\sigma_{tot} = \sqrt{\sigma_{stat}^2 + \sigma_{sys}^2}.$$

On the other hand, if the total systematic error is determined by one factor (one data set) only, we simply add the statistical and systematic errors

$$\sigma_{tot} = \sigma_{stat} + \sigma_{sys}.$$

In general, it is possible to determine systematic errors σ_{sys} as a sum of partial systematic errors σ_{sys}^i squared coming from different sources. Since various sources of systematic errors do not follow the normal distribution, this approach may lead to underestimate the total systematic error. There is also an opposite approach which consists in adding partial systematic errors linearly.

Adjusting the Parameters of Isobar Model

For the determination of free parameters of isobar model, we have selected around 3400 data points originating from CLAS and LEPS collaborations and replenished them with several tens of data collected by Adelseck and Saghai in their work [3]. To be precise, we used the CLAS 2005 [17], CLAS 2010 [82], and LEPS [108] cross-section data, CLAS 2010 [82] hyperon-polarization data, and LEPS [108] beam-asymmetry data. Since the isobar model works well in the resonance region only, we have restricted the CLAS 2010 data sets to the energy range up to 2.355 GeV and 2.225 GeV for the cross-section and hyperon-polarization data, respectively.

As the CLAS and SAPHIR [44] data are not consistent with each other, particularly in the forward-angle region which is of paramount interest, we decided not to use the SAPHIR cross-section data in the analysis. Unfortunately, even the CLAS 2005 [17] and CLAS 2010 [82] data sets show inconsistency with each other of about one or two standard deviations in the threshold region for kaon angle less than approximately 60°.

Observable	No. of data	E_γ^{lab} [GeV]	θ_K [°]	Collaboration	Year
σ	14	(0.95; 2.60)	-	ABBHHM [1]	1969
	24	(0.92; 1.95)	-	SAPHIR [110]	1998
	36	(0.92; 2.60)	-	SAPHIR [44]	2004
	78	(0.95; 2.91)	-	CLAS [17]	2006
$d\sigma/d\Omega$	55	5, 8, 11, 16	(1; 45)	SLAC [16]	1969
	91	(0.93; 1.39)	(30; 132)	Adelseck [3]	1990
	90	(0.90; 2.00)	(25; 154)	SAPHIR [110]	1998
	720	(0.90; 2.60)	(0; 180)	SAPHIR [44]	2004
	1377	(0.94; 2.95)	(25; 143)	CLAS [17]	2006
	54	(1.53; 2.38)	(18; 32)	LEPS [108]	2006
	19	(1.50; 2.37)	(0; 36)	LEPS [51]	2007
	2066	(0.94; 3.81)	(27; 120)	CLAS [82]	2010
	1341	(0.93; 1.44)	(66; 143)	MAMI [61]	2014
Σ	9	16	(3; 20)	SLAC [94]	1979
	45	(1.50; 2.40)	(0; 53)	LEPS [121]	2003
	30	(1.55; 2.30)	(13; 49)	LEPS [108]	2006
	4	(1.72; 2.20)	(0; 36)	LEPS [51]	2007
	66	(0.98; 1.47)	(30; 140)	GRAAL [66]	2007
T	3	(1.10; 1.30)	90	Bonn [5]	1978
	66	(0.98; 1.47)	(30; 140)	GRAAL [67]	2008
P	7	5	(17; 41)	DESY [118]	1972
	12	(0.91; 2.00)	(30; 150)	SAPHIR [110]	1998
	30	(0.91; 2.60)	(0; 180)	SAPHIR [44]	2004
	233	(0.93; 2.33)	(25; 136)	CLAS [83]	2004
	66	(0.98; 1.47)	(30; 140)	GRAAL [66]	2007
	1707	(0.94; 3.81)	(27; 120)	CLAS [82]	2010
C_x, C_z	324	(1.03; 2.74)	(31; 138)	CLAS [18]	2007
O_x, O_z	132	(0.98; 1.47)	(31; 143)	GRAAL [67]	2008

Table D.1: An overview of available experimental data for the $p(\gamma, K^+)\Lambda$ process. The symbols σ, $d\sigma/d\Omega$, Σ, T and P denote total cross section, differential cross section, beam asymmetry, target polarization and hyperon polarization, respectively. C_x, C_z, O_x, and O_z are double-polarization observables.

Tuning the RPR-model Parameters

While fitting the free parameters of the Regge-plus-resonance model, we were not restricted to the resonance region only and we have, therefore, exploited much more data in comparison with the fitting procedure of the isobar model. Basically, we have used the same data sets but we utilized all data available therein (*i.e.* CLAS 2005 [17] and CLAS 2010 [82] data up to $E_\gamma^{lab} = 2.95\,\text{GeV}$ and $W = 2.835\,\text{GeV}$), which gave us around 5300 data in total.